ALMA MATER STUDIORUM · UNIVERSITY OF BOLOGNA

School of Science
Department of Physics and Astronomy
Master Degree in Physics

Quasi-random systems: duality transformations and numerical simulations

Supervisor:
Dr. Davide Vodola

Submitted by:
Vito Giardinelli

Co-supervisor:
Prof. Elisa Ercolessi

Academic Year 2020/2021

Abstract

For classical systems, the concept of thermalization, introduced by Boltzmann in the 19th century, is the main instrument for explaining the equilibrium thermodynamics. For quantum systems, although the Schrodinger unitary evolution is deterministic and invertible, it is possible to extend the thermalization concept by considering a subsystem that thermalizes with the rest of the system. However, as in the classical case, there is a class of systems that violate the ergodic principle and do not thermalize. This phenomenon of egodicity breaking is present in models with disorder introduced by P.W. Anderson in 1958. In chapter 1 of our work, we present the class of quasi-random systems, showing their most important features like the ergodicity breaking, the self-duality and the presence of mobility edges. In chapter 2, as original work, we found the phase transition lines of the superconducting Aubry-André model using the analytical tool of the duality transformations. Moreover, we investigate directly the many body localization performing simulations of several quantities like the IPR, the imbalance and the fidelity to detect the many body localization. In the last chapter, we analyse the Jordan-Wigner and Bravy-Kitaev transformations for the quantum simulation of our fermionic systems.

Contents

Introduction

The concept of thermalization, on which the classical equilibrium thermodynamics is built, can also be extended to the quantum case [1, 2, 3, 4]. Here, the unitary evolution of the Schrodinger equation is actually deterministic and invertible, so, apparently, there is no possibility of thermalization. Nevertheless, considering a subsystem of the whole quantum system taken in exam, a definition of thermalization can be implemented because the subsystem uses the rest as a thermal bath with which it can thermalize [5, 6, 7]. On the other hand, there are some quantum systems that show a non-ergodic behaviour in the presence of the many body localization [8]. This phenomenon is actually present in models with quasi-random disorder, as theorized by P.W. Anderson in 1958 [9].

The relative branch of condensed matter physics, in the later years, is developing on the experiments side [10] as well as on the side of analytical results and numerical simulations [3]. The majority of experiments conducted on this field is based on cold atoms. In fact, in this physical situation it is easier to isolate the system and control the disorder or the interactions, as it has been done for instance in the remarkable experiment described in [11]. This experiment aims at studying the Hubbard Hamiltonian in a system made with cold atoms whose interactions are controlled with Feshbach resonances and whose disorder is reproduced by two laser beams with incommensurate frequencies. This experiment is the first where many-body localization in an interacting model has been observed. Another experiment, conducted with trapped ions of ytterbium, revealed the many-body localization of an Ising model with long range interaction and random external field [12]. Moreover, the many-body localized states are also proposed as a possible candidates to store quantum information [13]. In fact, in the localized phase, the non-thermalization of the system can be used to store information [14] as well as the many body dephasing can be used as purification resource [15].

On the other hand, there are also open problems about the physics of those systems. For example, what is the role played by the disorder [16] in the many-body localization or by the symmetries in the phase transition [17]. Also the phase diagrams themselves are often determined only approximately or numerically [18, 19, 11]. So, the physics of the quasi-random quantum systems is a field of research that has increased its importance in the last years.

In our work we do a review of the most important fermionic quasi-random models and provide a set of numerical and analytical results about this class of systems.

In chapter 1, we describe the Anderson model that historically introduced the disorder in condensed matter systems [9]. Then, after having introduced the Anderson localization, we explored several variants of the aforementioned model. In particular, we present the Aubry-André model [20] and a duality transformation based on a Fourier transform that allows us to compute the critical lines of the model. We present also non-dual models that show a mobility edge [21] as well as interacting versions that show an ergodicity breaking and scar states [11].

In chapter 2, we present all the results of our numerical and analytical simulations. We consider a generalized Aubry-André model both with superconducting and interacting terms and we perform numerical simulations to detect the aforementioned phenomena like Anderson localization and ergodicity breaking. In particular, we used different quantities to detect these phenomena and introduced a new one independent from time. Moreover, we introduce a novel duality transformation for the superconducting Aubry-André model. With this transformation we are able to obtain the exact position of the critical lines of the phase diagram.

Then, in chapter 3, we investigate two methods to implement fermionic simulations on quantum computers. Usually, this operation is done with the Jordan-Wigner transformations. In the work of Bravy and Kitaev [22] a new kind of transformations to pass from a fermionic Hilbert space to a spin one is introduced. Today these transformations could be used to improve the efficiency of quantum computation [23]. In our work we compare the computational efficiency of Bravy-Kitaev and the Jordan-Wigner transformations.

Chapter 1

Quasi-Random Systems

The world of quasi-periodic quantum systems have to be explored in large part yet. Until now, different approaches were tried to analytically integrate or to simulate numerically these models. In particular, with respect to the periodic or random counterpart, the quasi-periodic systems show some intermediate features [24]. To understand better the effects of quasi-periodicity we can look at the Aubry-Andrè model and its generalizations. All those models, that contain a quasi periodic term, show a particular phase transition due to the phenomenon of the Anderson localization.

1.1 Anderson localization

The Anderson localization is a physical phenomenon that was introduced by P.W.Anderson in 1958 [9]. He introduced it in the scope of condensed matter to study the conductance of metals. In his article "On the absence of diffusion in certain random lattices", Anderson investigated the properties of lattices with a random potential applied to the reticular sites. He tried to explain the behaviour of some kinds of materials that showed a metal-insulator phase transition when the density of impurities overcome a certain limit. This particular insulator phase transition is due to the diffusion that falls to 0. In particular, materials like metallic alloys have that behaviour [25]. Without impurities they are metals because the density of states at the Fermi level is finite. When the disorder induced by the impurities overcomes a certain critical value, they become insulators. This kind of phase transition give rise to Anderson insulators. The vanishing diffusion is due to the fact that electron eigenstates at the Fermi level have been localized by the random impurity potential [26]. In fact, the impurities induce a perturbation to the Bloch waves that turn out to be a quantum destructive interference. This interference is the cause of the exponential decaying of the electronic wave functions. This phenomenon is called Anderson localization. Moreover, in the localized phase, states close by in energy are far away spatially and vice versa. Changing dimension, the phase transition is different. In fact in 3D, given a low density of impurities, the perturbative approach allow to compute the scattering time to whom the conductivity is proportional to. On the other hand if the the density of impurities overcome the critical value the perturbation series does not converge anymore and the phase transition occurs. Instead in 2D and 1D the series does not converge at all, regardless of the disorder strength, and the states become all localized.

Now we explore the 1D case. Anderson used a random potential with a different value on each site to model the impurities, then added an hopping term:

$$H = \sum_{j=1}^{N} t_1 \left(f_j f_{j+1}^\dagger + f_{j+1}^\dagger f_j \right) + V_j f_j^\dagger f_j \tag{1.1}$$

Here, the t_1 is the coupling of the hopping term while V_j is a uncorrelated and bounded random potential depending the occupation of the jth site. This is the simplest formulation of our family of tight binding models and it can be analytically solved. Here it can be shown that in $d = 1$ every eigenstate of the system is localized for any non-zero value of the potential strength. But how to measure the localization of a certain eigenstate? The tool we will use is the Inverse Participation Ratio, briefly IPR. This quantity is defined for the ith eigenstate and for q fixed as:

$$\mathrm{IPR}_q^i = \frac{\sum_n |u_n^i|^{2q}}{(\sum_n |u_n^i|^2)^q} \tag{1.2}$$

Where u_n^i are the projections of the ith eigenstate on the n-th state of the configuration basis. The values of this quantity belong to the interval $[0, 1]$. It tends to 0 if the state is not localized, while has a finite value in localized states. Moreover, the value of IPR(q) numerator increase like $\xi^{-d(q-1)}$, where ξ is the correlation length, for localized states and $L^{-d(q-1)}$, where L is the length of the system, for extended states [26].

1.2 Ergodicity Breaking and quantum scars

Another aspect of our systems that can be studied is the behaviour of the observables during the time. To do that, we have to step back and return to the classical theory of ergodicity. The ergodic hypothesis was formulated in the end of 18^{th} century by Ludwig Boltzmann. This hypothesis states that in a chaotic ensemble, like particles interacting by collisions, the system will visit all the phase space PS and the observables O relax in few time and reach a thermal value stable in time.

Mathematically this allow to exchange the temporal mean of the observable with that on the phase space, avoiding the computation of the phase flux, i.e. solving the equation of motion:

$$O_\infty = \lim_{T\to\infty} \frac{1}{T} \int_0^T O(x(t),p(t))\,dt \longrightarrow \frac{1}{V} \int_{V(PS)} O(\vec{x},\vec{p})\,d\vec{x}d\vec{p} \tag{1.3}$$

Now there is a need to translate this concept to quantum systems. Fundamentally the phase space is replaced by the Hilbert space $\mathcal{H}$, while the observable O is replaced by an operator $\hat{O}$. So, given a basis of states $|k\rangle$, we can rewrite the previous expression as:

$$\langle O\rangle_\infty = \lim_{T\to\infty} \frac{1}{T} \int_0^T \left\langle \psi(t)|\hat{O}|\psi(t)\right\rangle\,dt \longrightarrow \int |\left\langle \psi_0|k\right\rangle|^2 \left\langle k|\hat{O}|k\right\rangle\,dk \tag{1.4}$$

To maintain a formal continuity with the classical formula we have assumed a continuous spectrum of eigenvectors, but it in the discrete case the same relation is valid with the integral replaced by a sum. Moreover, the so called ”Eigenstate Thermal Hypothesis” implies that that the time average of a quantum observable is a function of the energy independently from the initial conditions. To be a thermalizing observable O must also have certain features: its off diagonal terms in the energy base of eigenvectors must decay exponentially $\left\langle \epsilon_k|\hat{O}|\epsilon_j\right\rangle \propto e^{|\epsilon_k-\epsilon_j|}$, and the magnitude of its diagonal elements varies smoothly with the length of the system $\left\langle \epsilon_j|\hat{O}|\epsilon_j\right\rangle - \left\langle \epsilon_{j-1}|\hat{O}|\epsilon_{j-1}\right\rangle = \Delta_i \propto e^{-N}$. So, now we can look at the systems that do not respect, at least partially, this statement. The two kinds of mechanisms that we can distinguish are the strong and the weak loss of ergodicity. In the strong loss of ergoditity all the eigenstates do not termalize and there is no subsystem in which the ETH holds. On the other hand, with the weak mechanism only a part of the Hilbert space has lost the ergodicity while the rest continues to thermalize.

Another concept that can be useful for our purposes is that of the quantum scars. Those quantum scars were first introduced in [27], in the scope of the single-particle chaotic billiards. Practically, in the solution of the Schrodinger equation of a free single particle with boundary condition of a stadium billiard emerged that the pattern of classical unstable periodic orbits was conserved in the quantum case. For this reason the states that do not thermalize are called quantum scar states in analogy with the classical case [5]. In the next sections we will explore quantum scars of our systems and will try to understand their behaviour.

1.2.1 An example of Ergodicity Breaking: PXP model

Often, quantum scars are associated to a model coming from condensed matter physic: the PXP model [28]. The model comes from a simplification of the real situation of a platform of Rydberg atoms that strongly repel between each other when they are excited. This system can be modeled considering Rydberg atoms like two-state spins and preventing the possibility to find two neighbors both excited. Starting from the microscopic Hamiltonian:

$$H = \sum_{j=1}^{N} \left(\frac{\Omega}{2} \sigma_j^x - \Delta q_j \right) + \sum_{i<j}^{N} V_{i,j} q_i q_j \tag{1.5}$$

where Ω is the Rhabi frequency, Δ is the detuning parameter and $V_{i,j}$ is the van der Waals interaction that goes like $\propto |i-j|^6$. The operator $q_i = (1-\sigma_j^z)/2$ counts the excitation in the site j, so the term $q_i q_j$ take in account the excitations of all possible couple of sites. Now we can assume strong repulsion and stop the interaction on first neighbors, then we assume zero detuning $\Delta = 0$ and the limit $V >> \Omega$. The asintotic Hamiltonian turn out to be:

$$H = \sum_{i=1}^{N} q_i q_{i+1} + \epsilon \sum_{i=1}^{N} \sigma_x^j \tag{1.6}$$

and ϵ is the vanishing parameter $\frac{\Omega}{2V}$. The paramagnet part become relevant only in the subspace without neighbor excitations, so introducing the projectors $P_j = \frac{1-\sigma_j^z}{2}$ we can write the effective PXP Hamiltonian:

$$H = \sum_{i=1}^{N} P_{j-1} \sigma_x^j P_{j+1} \tag{1.7}$$

This Hamiltonian shows quantum scars with opportunely built observables. For example, the observable $O^z = (1/L) \sum_{j=1}^{L} \sigma_j^z$ is one of them. Moreover, with PBC and the induced translation symmetry, the observable O^z is equal to $\langle \sigma_1^z \rangle = \langle Z_1 \rangle$, i.e. the occupation of the first site. To test if the system is ergodic with respect to the previous observable, the operator associated to it have to fulfill the Sredniki ansaz. The following ansaz is about the form of the matrix elements of the operator in the eigenstates basis:

$$O_{ab} = O'(E)\delta_{ab} + e^{-S(E)/2} f(E,\omega) R_{ab} \tag{1.8}$$

where $E = (E_a + E_b)/2$ and $\omega = E_a - E_b$. Then, O' is a smooth function of E, S is the the thermodynamic entropy and f is a smooth function of E and ω. In the end the coefficients R_{ab} are random numbers with 0 mean. This ansaz divides the canonical ensemble prediction corresponding to the diagonal part of the operator from the off-diagonal elements that are exponentially dumped by the entropy and whose mean vanishes. The canonical prediction is computed from the Gibbs states defined by the density matrix $\rho \propto e^{-\beta \hat{H}}$.

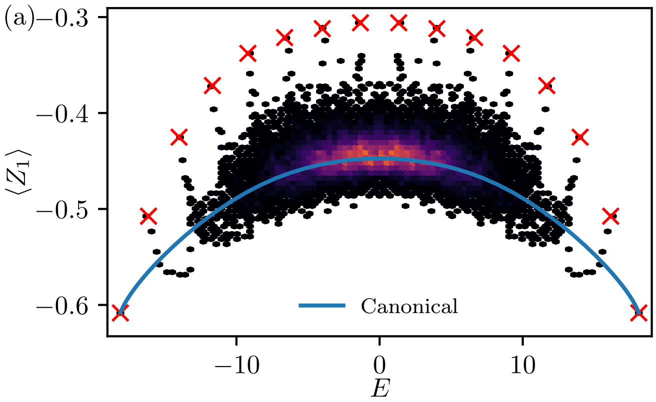

Figure 1.1: Here we can see the mean value of the observable $\langle Z_1 \rangle$ for each eigenstate as function of the energy. The colorscale indicates the density of points. The computed expectation value can be compared with the canonical ensemble prediction. As we can see the majority of the states have an expectation value around the canonical one. Picture take from [28]

The simulations of the expectation value of $\langle Z_1 \rangle$ show that for several states the expectation value is significantly different from the canonical ensemble prediction (fig 1.1). These states form a peculiar states tower structure. Although the greater part of the eigenstates has an expectation value near to the canonical one, these states are an example of quantum scars.

1.3 The Aubry-André model

The concept behind the Anderson model is largely generalized to models with an incommensurate potential. Here we present the Aubry-André model, that is the most simple generalization of the Anderson model. Next we see other models with different terms in the Hamiltonian that show phenomena like mobility edges, critical phases and ergodicity breaking.

1.3.1 Self-Duality

The Aubry-André Hamiltonian is the following:

$$H = \sum_{j=1}^{N} t_1 \left(f_j f_{j+1}^\dagger + f_{j+1}^\dagger f_j \right) + V \cos(2\pi j \phi + \alpha_0) f_j^\dagger f_j \tag{1.9}$$

The difference with the pure Anderson model is the form of the random potential. Here, V_j has the form of a quasi-periodical random number: $V_j = V \cos(2\pi j\phi + \alpha_0)$

where V is the amplitude of the incommensurate potential, $\phi = \frac{1+\sqrt{5}}{2}$ is the golden ratio and α_0 is the actual random parameter, uniformly distributed in the interval $[0, 2\pi]$. Now we will focus on results obtained with a single realization of α_0.

So, also for this model all the eigenstates are either localized or extended. This happens if $V > 2t_1$, where t_1 is the coupling constant of the hopping term [20]. This behaviour arises because this model has a so called "self duality" in the point of the phase diagram $V = 2t_1$. This self duality is recovered through the following transformations:

$$u_n = \sum_m w_m e^{im(2\pi\phi n+\alpha_0)} e^{i\alpha_0 n} \tag{1.10}$$

This transformation exchanges localized states with extended states. In few words, for every localized block function u_n in the phase $V > 2t$, there exists another one w_n in the extended regime $V < 2t$.

It is interesting to show how the self-duality is reached. From the Hamiltonian (1.1), we have the following Schrodinger equation:

$$Eu_n = t_1(u_{n-1} + u_{n+1}) + V_n u_n \tag{1.11}$$

where $V_n = V\cos(2\pi n\phi + \alpha_0)$. Now, applying the transformations (1.10), we want an equation for the w_m. First of all, work out the form of the left hand side of equation (1.9):

$$Eu_n = \sum_m e^{im(2\pi\phi n+\alpha_0)} e^{i\alpha_0 n} E w_m \tag{1.12}$$

On the other hand, the shifted hopping terms assume the following form:

$$t_1 u_{n+1} = \sum_m e^{im(2\pi\phi(n+1)+\alpha_0)} e^{i\alpha_0(n+1)} t_1 w_m = \sum_m e^{im(2\pi\phi n+\alpha_0)} e^{i\alpha_0 n} [t_1 w_m e^{im2\pi\phi+\alpha_0}] \tag{1.13}$$

$$t_1 u_{n-1} = \sum_m e^{im(2\pi\phi(n-1)+\alpha_0)} e^{i\alpha_0(n-1)} t_1 w_m = \sum_m e^{im(2\pi\phi n+\alpha_0)} e^{i\alpha_0 n} [t_1 w_m e^{-im2\pi\phi-\alpha_0}] \tag{1.14}$$

Then, the hopping term carries out a cos-like factor:

$$t_1(u_{n+1} + u_{n-1}) = \sum_m e^{im(2\pi\phi n+\alpha_0)} e^{i\alpha_0 n} t_1 w_m [e^{+im2\pi\phi+\alpha_0} + e^{-im2\pi\phi-\alpha_0}] = \tag{1.15}$$

$$= \sum_m e^{im(2\pi\phi n+\alpha_0)} e^{i\alpha_0 n} t_1 w_m [2\cos(2\pi m\phi + \alpha_0)] \tag{1.16}$$

Notice that the hopping term corresponds to a potential of the same form of V_n in the w_m space. Now, we have to transform the original potential. If the duality is respected, we expect that the potential V_n give rise to a hopping term in the w_m space. The calculation goes as follow:

$$V\cos(2\pi n\phi+\alpha_0)u_n=\sum_m e^{im(2\pi\phi n+\alpha_0)}e^{i\alpha_0 n}Vw_m[\cos(2\pi n\phi+\alpha_0)]= \tag{1.17}$$

$$=\sum_m e^{im(2\pi\phi n+\alpha_0)}e^{i\alpha_0 n}\frac{V}{2}w_m[e^{+in2\pi\phi+\alpha_0}+e^{-in2\pi\phi-\alpha_0}]= \tag{1.18}$$

$$=\sum_m e^{im(2\pi\phi n+\alpha_0)}e^{i\alpha_0 n}\frac{V}{2}w_m[e^{+in2\pi\phi+\alpha_0}]+\sum_m e^{im(2\pi\phi n+\alpha_0)}e^{i\alpha_0 n}\frac{V}{2}w_m[e^{-in2\pi\phi-\alpha_0}]= \tag{1.19}$$

$$=\sum_l e^{i(l+1)(2\pi\phi n+\alpha_0)}e^{i\alpha_0 n}\frac{V}{2}w_l+\sum_k e^{i(k-1)(2\pi\phi n+\alpha_0)}e^{i\alpha_0 n}\frac{V}{2}w_k \tag{1.20}$$

Notice tat in the last passage we renamed the indexes. Now, we can shift the first sum setting $m=l+1$ and the second one setting $m=k-1$ to get the final result:

$$V\cos(2\pi n\phi+\alpha_0)u_n=\sum_l e^{i(l+1)(2\pi\phi n+\alpha_0)}e^{i\alpha_0 n}\frac{V}{2}w_l+\sum_k e^{i(k-1)(2\pi\phi n+\alpha_0)}e^{i\alpha_0 n}\frac{V}{2}w_k= \tag{1.21}$$

$$=\sum_m e^{im(2\pi\phi n+\alpha_0)}e^{i\alpha_0 n}\frac{V}{2}[w_{m+1}+w_{m-1}] \tag{1.22}$$

Clearly, we have to assume the termodynamic limit to shift the sum. The last step is to put together all the pieces and extract the Schrodinger equation for w_m:

$$\sum_m e^{im(2\pi\phi n+\alpha_0)}e^{i\alpha_0 n}\left[\frac{V}{2}(w_{m+1}+w_{m-1})+2t_1\cos(2\pi m\phi+\alpha_0)w_m-Ew_m\right]=0 \tag{1.23}$$

We can immediately find the relations between the coefficients in the two representations comparing with the original equation (1.11) the term in the square brackets in (1.23). The result is:

$$\begin{pmatrix}V'\\ t_1'\end{pmatrix}=\begin{pmatrix}0&2\\ \frac{1}{2}&0\end{pmatrix}\begin{pmatrix}V\\ t_1\end{pmatrix} \tag{1.24}$$

From the mathematical properties of this transformation, we can extract some physical information. First of all, its eigenvalues are ±1, so that exists a dual vector on which the transformations acts like the identity, while there is another that is reflected with respect to the origin. Those two vectors $\lambda_\pm$ are the following:

$$\lambda_+=\begin{pmatrix}2\\ 1\end{pmatrix}\quad\lambda_-=\begin{pmatrix}2\\ -1\end{pmatrix} \tag{1.25}$$

In the plane $t - V$ these two vectors corresponds to the straight lines $V = 2t$ and $V = -2t$. Given that the transformation is dual on the line $V = 2t_1$ because $V' = V$ and $t'_1 = t_1$ that implies u_n and w_m satisfy the same equation. On the other hand the other eigenvector tells us that the transformations exchange the localization of the wave function. In fact, taking t_1 and V greater than 0, the transformation maps points in the half-plane $V < 2t_1$ to the region $V > 2t_1$. It can be shown in a few passages:

$$\begin{gathered}
\text{We can take a point in the space of couplings} \quad (V_0, t_0) \\
\text{in the extended phase where} \quad V < 2t_1 \\
\text{Given} \begin{cases} V' = 2t_0 \\ t' = V_0/2 \end{cases} \quad \text{we can write the following inequality:} \\
V' = 2t_0 > V_0 = 2t' \quad \text{that implies} \quad V' > 2t' \\
\text{so, the point} \quad (V', t') \quad \text{falls in the localized phase}
\end{gathered}$$

This means that while u_n respects a Schrodinger equation in the localized phase, w_m evolution is governed by an equation laying in the extended one and vice versa.

1.3.2 Mobility Edges

What is interesting now is to look at its generalizations to see the emergence of a "mobility edge". The mobility edge is nothing but a net division in the spectrum between localized and extended states.

In a few words, the localized states tend to be less energetic with respect to these extended and there exists a critical boundary over which this happens. To understand better all the theory behind the mobility edge and the Aubry-André model is instructive to observe its mathematical structure [8]. Diddle and Sarma studied a generalization of the Aubry-André model. This model has an infinite sum of hopping terms whose coupling decays exponentially.

$$H = \sum_{j=1}^{N} \left[\sum_{i \neq j} t_1 e^{-p|i-j|} \left(f_i f_j^\dagger + f_j^\dagger f_i \right) \right] + V \cos(2\pi j \phi + \alpha_0) f_j^\dagger f_j \tag{1.26}$$

In the Hamiltonian (1.26) p, can be considered the correlation length of the hopping interaction. The associated Schroedinger equation has the form:

$$E u_i = \sum_{i \neq j} t e^{-p|i-j|} u_j + V \cos(2\pi j \phi + \alpha_0) u_i \tag{1.27}$$

For this model with a exponentially dumped long range hopping, a self duality in the Aubry-André model form does not hold. Nevertheless, with a proper formulation, there is a generalized self duality that help us to find the mobility edge.

Defining ω as:

$$\omega = \sqrt{p(E+t_1)^2 - V^2} \tag{1.28}$$

We can derive the following relation:

$$T_j = \frac{\cosh(p_0) - \cos(2\pi j\phi + \alpha_0)}{\sinh(p_0)}, \tag{1.29}$$

where T_j is equal to the next espression, introducing the parameter p_0:

$$(E+t_1) - V\cos(2\pi j\phi + \alpha_0) = \omega T_j, \tag{1.30}$$

Putting together these equations we can we obtain that:

$$\frac{E+t}{V} = \cosh(p_0) \tag{1.31}$$

Now, substituting T_n in the Schrodinger equation we get the equation:

$$\omega T_j u_j = \sum_m t_1 e^{-p|m-j|} u_m \tag{1.32}$$

that turn out to be dual under the transformations given by:

$$w_i = \sum_m e^{im(2\pi\phi j + \alpha_0)} T_m u_m \tag{1.33}$$

It can be shown [8] that the so formulated Schroedinger equation (1.32), after the aforementioned transformation (1.33), become the following equation:

$$\omega \tilde{T}_i w_i = \sum_m t_1 e^{-p_0|m-j|} w_m \tag{1.34}$$

with $\tilde{T}_i$ equal to:

$$\tilde{T}_i = \frac{\cosh(p) - \cos(2\pi i\phi + \alpha_0)}{\sinh(p)}, \tag{1.35}$$

Now, the duality condition where (1.34) and (1.32) are exactly the same equation is $p = p_0$. The request of duality take to the following condition:

$$V = \frac{E+t_1}{\cosh(p)} \tag{1.36}$$

So, we have an equation for the Anderson localization phase transition line $V(t)$ parametrized also by E and p. It means that if a state is localized does not depend only on the coupling constants V and t_1 but also on the value of the exponential dumping p and the energy of the state E. Now, for all states whose value of $p > p_0$

are localized and vice versa for $p < p_0$. The fact that $V = V(t_1, E, p)$ allow the existence of a mobility edge.

Basically, in figure 1.2, we can observe the localization of the single particle states for a chain 500 sites long. Here the color indicates the value of the IPR of the states. We can see for four different values of the parameter p the mobility edge theoretically predicted versus the actual IPR of the states. In particular it has a form of a straight line in the plane $\frac{E}{t_1}$ - $\frac{V}{t_1}$. In this case $\cosh(p)$ is the slope of the mobility edge line. To make a comparison between this model and the pure AA model we have the two duality conditions:

$$\begin{cases} \frac{V}{t_1} = 2 & \text{for the Aubry-André model} \\ \frac{E}{t_1} = \frac{V}{t_1}\cosh(p) + 1 & \text{for the exponential dumping model} \end{cases} \tag{1.37}$$

The first one is a vertical line in the plane $\frac{E}{t_1}$ - $\frac{V}{t_1}$, while the second, as said before, is a straight line of slope $\cosh(p)$. If we perform the limit $p \to \infty$ we recover a vertical line, but its equation become $\frac{V}{t_1} = 0$ that means that there are only localized states. In fact, in the limit $p \to \infty$ all the hopping terms in the Hamiltonian (1.32) vanish.

1.4 Non-dual tight binding models

Here we explore other variants of Aubry-André model that do not have a duality at all. Those models cannot be approached theoretically. An attempt to approximate them can be done with the exponential model, whose mobility edge can be solved exactly. We will show the different behaviours of several kinds bindings. The first case we analyze is a model with second order hopping term. Then we explore a Gaussian short range hopping and a power law long range dumping [21]. In these models we have profoundly different situations compared to the exponential dumping one. So, the approximations can be done if the hopping falls enough rapidly with the distance $|i - j|$.

1.4.1 Second order binding

The model with the second order hopping, also called t1-t2 model, has the following Hamiltonian:

$$H_{t_1-t_2} = \sum_{j=1}^{N} t_1\left(f_i f_{i+1}^{\dagger} + f_i^{\dagger} f_{i+1}\right) + t_2\left(f_i f_{i+2}^{\dagger} + f_i^{\dagger} f_{i+2}\right) + V cos(2\pi j\phi + \alpha_0)(f_j^{\dagger} f_j) \tag{1.38}$$

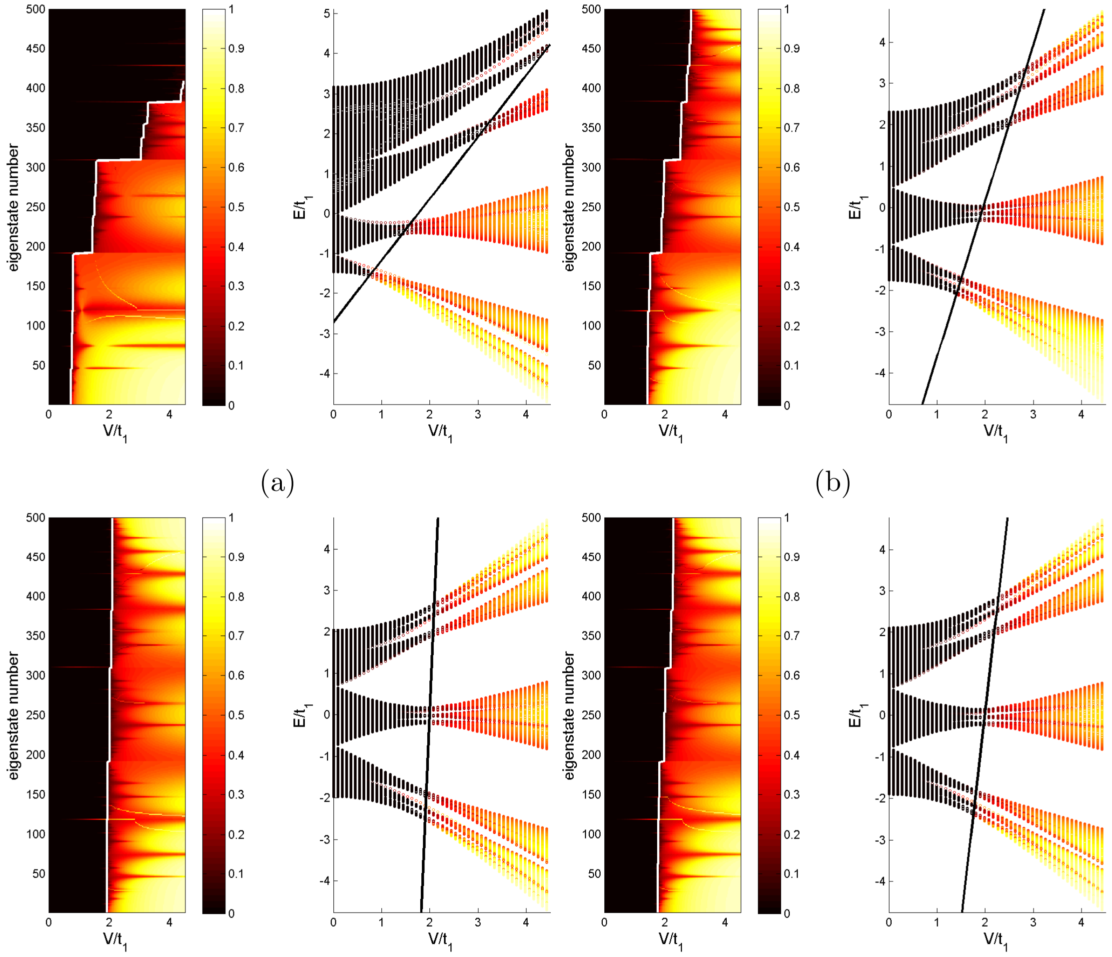

(a)

(b)

(c)

(d)

Figure 1.2: In this figure we can see the single particle eigenstates of the exponential binding model 500 sites long for different values of the parameter p: (a) p = 1, (b) p = 2, (c) p = 3, (d) p = 4. On every graph, on the left the for increasing V the value of IPR for each eigenstate and on the right the IPR for each eigenvalue. The straight lines $\frac{E}{t_1} = cosh(p)\frac{V}{t_1} + 1$ show the boundary between spatially localized and spatially extended states. We can see that cosh(p) is the slope of the curve. For small values of p the mobility edge is more pronounced. Picture taken from [21]

with the following Schrodinger equation:

$$Eu_n = t_1(u_{n+1} + u_{n-1}) + t_2(u_{n+2} + u_{n-2}) + Vcos(2\pi j\phi + \alpha_0)u_n \tag{1.39}$$

In this case we have two couplings for the hopping terms t_1 and t_2 and they have to put in relation with the exponential dumping $te^{(-p|i-j|)}$. This can be done in the limit $t_2 << t_1$. In fact, in this case the second order dumping is governed by the ratio t_1/t_2. Imposing the two following relation we get the approximate version of the exponential model:

$$\begin{cases} p = \ln(t_1/t_2) \\ t = t_1 e^p \end{cases} \tag{1.40}$$

In figure 1.3 we can see the plot of the eigenvalues ordered with increasing energy and in the plane E/t_1- V/t_1. The color stands for the value of the IPR. The different plots are done with different values of the ratio t_2/t_1. We can observe that when $\frac{t_2}{t_1} < 0.3$ the mobility edge is compatible with the solid line made using the equation (1.36) using $p = \ln(t_2/t_1)$.

1.4.2 Gaussian decaying binding

The Gaussian tight-binding model Hamiltonian has the following form:

$$H_{gau} = \sum_{j=1}^{N} \left[\sum_{i\neq j} e^{-\sigma|i-j|^2}(f_i f_j^\dagger + f_j^\dagger f_i) \right] + Vcos(2\pi j\phi + \alpha_0)(f_j^\dagger f_j) \tag{1.41}$$

with the associated Schrodinger equation:

$$Eu_n = \sum_{j\neq n} e^{-\sigma|n-j|^2} u_j + V\cos(2\pi j\phi + \alpha_0)u_n \tag{1.42}$$

Here the Gaussian dumping is parametrized by σ. We have to find a relation between σ and the correlation length of the exponential decaying model p. Again, we can consider the first two terms of the Gaussian dumped hopping that corresponds to the couplings of the first and the second order hopping terms:

$$\begin{cases} t_1 = e^{-\sigma} & \text{for } j = n+1 \\ t_2 = e^{-4\sigma} & \text{for } j = n+2 \end{cases} \tag{1.43}$$

Then using the relations (1.40) we get:

$$\begin{cases} p = 3\sigma \\ t = e^{-\sigma} e^p \end{cases} \tag{1.44}$$

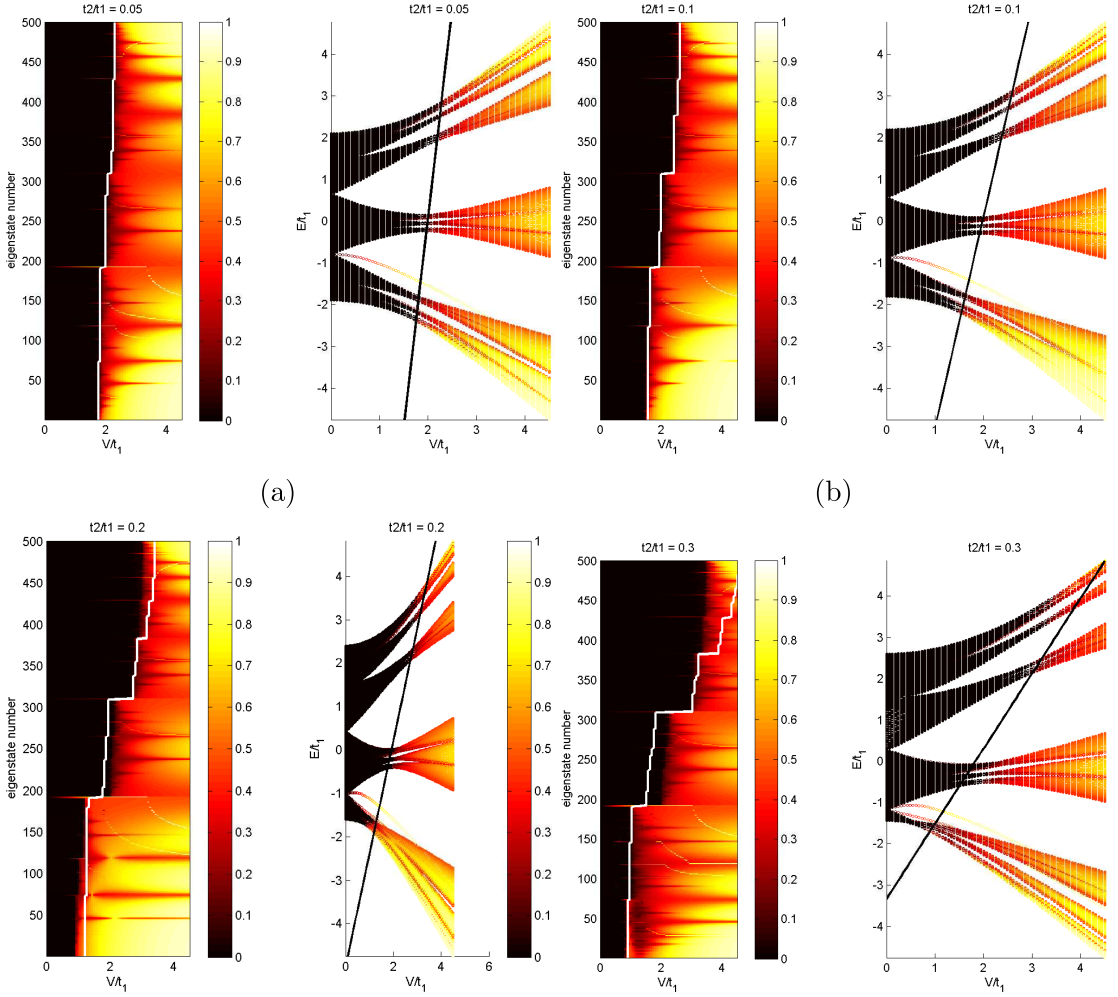

(a) (b)

(c) (d)

Figure 1.3: In this figure we can see the single particle eigenstates in the $t1 - t2$ model 500 sites long for different values of the parameter $t2/t1$: (a) $t2/t1 = 0.05$, (b) $t2/t1 = 0.1$, (c) $t2/t1 = 0.2$, (d) $t2/t1 = 0.3$. On every graph, on the left the for increasing V the value of IPR for each eigenstate and on the right the IPR for each energy eigenvalue. The straight lines are the mobility edge boundaries approximated with exponential binding model using $p' = log(\frac{t_1}{t_2})$. Pictures taken from [21]

As we know, the approximation holds for small values of $t_2/t_1 << 1$, so that now this condition translates into $\sigma >> 1$.

In figure 1.4 we have the plots of the IPR of the ordered eigenvalues for the increasing energy. The IPR value is indicated by the color. The solid lines show the predicted mobility edges made with the with the previous approximation. As we expected, the approximation holds well for larger values of σ.

1.4.3 Long range power-law binding

The last case we took in exam is the long range power-law binding. Its Hamiltonian is the following:

$$H = \sum_{j=1}^{N}\left[\sum_{i\neq j}|i-j|^{-r}(f_i f_j^\dagger + f_j^\dagger f_i)\right] + V cos(2\pi j\phi + \alpha_0)(f_j^\dagger f_j) \tag{1.45}$$

with the Schroedinger equation:

$$Eu_n = \sum_{j\neq n}|j-n|^{-r}u_j + V\cos(2\pi j\phi + \alpha_0)u_n \tag{1.46}$$

With the same arguments used for the first two cases of tight binding one can write t_1 and t_2 as:

$$\begin{cases} t_1 = 1 & \text{for } j = n+1 \\ t_2 = 2^{-r} & \text{for } j = n+2 \end{cases} \tag{1.47}$$

and the analogous values of p and t for the exponential model:

$$\begin{cases} p = r\ln(2) \\ t = e^p \end{cases} \tag{1.48}$$

Then the validity of the approximation is guaranteed for $t_2/t_1 << 1$, so that we have to request $r >> 1$. In figure 1.5 we have the same kind of graphs we had for the second order and the Gaussian binding. The color indicates the IPR of the states in the plane E/t_1-V/t_1 and in the graphs with energy ordered eigenvalues. For different values of r we have the predicted mobility edges using our approximation versus the actual IPR of the states. As expected the prediction holds for greater values of r.

1.5 Further extensions of the Aubry-André model

Now we investigate two extensions of the Aubry-André model with a p-wave superconducting term and an interacting term.

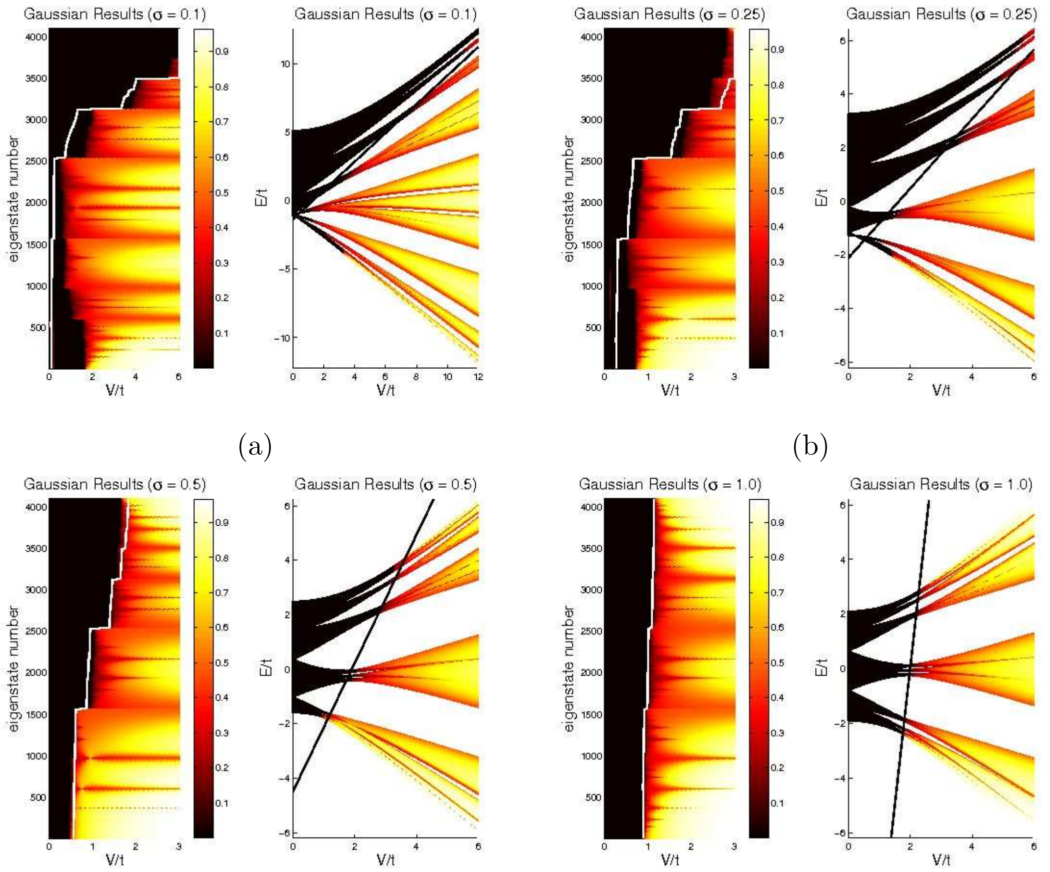

(a) (b)

(c) (d)

Figure 1.4: In this figure we can see the single particle eigenstates in the gaussian binding model for different values of the parameter σ: (a) $\sigma = 0.1$, (b) $\sigma = 0.25$, (c) $\sigma = 0.5$, (d) $\sigma = 1$. On every graph, on the left for increasing V the value of IPR for each eigenstate and on the right the IPR for each energy eigenvalue. The straight lines are the mobility edge boundaries approximated with exponential binding model using $p' = 3\sigma$. Picture taken from [21]

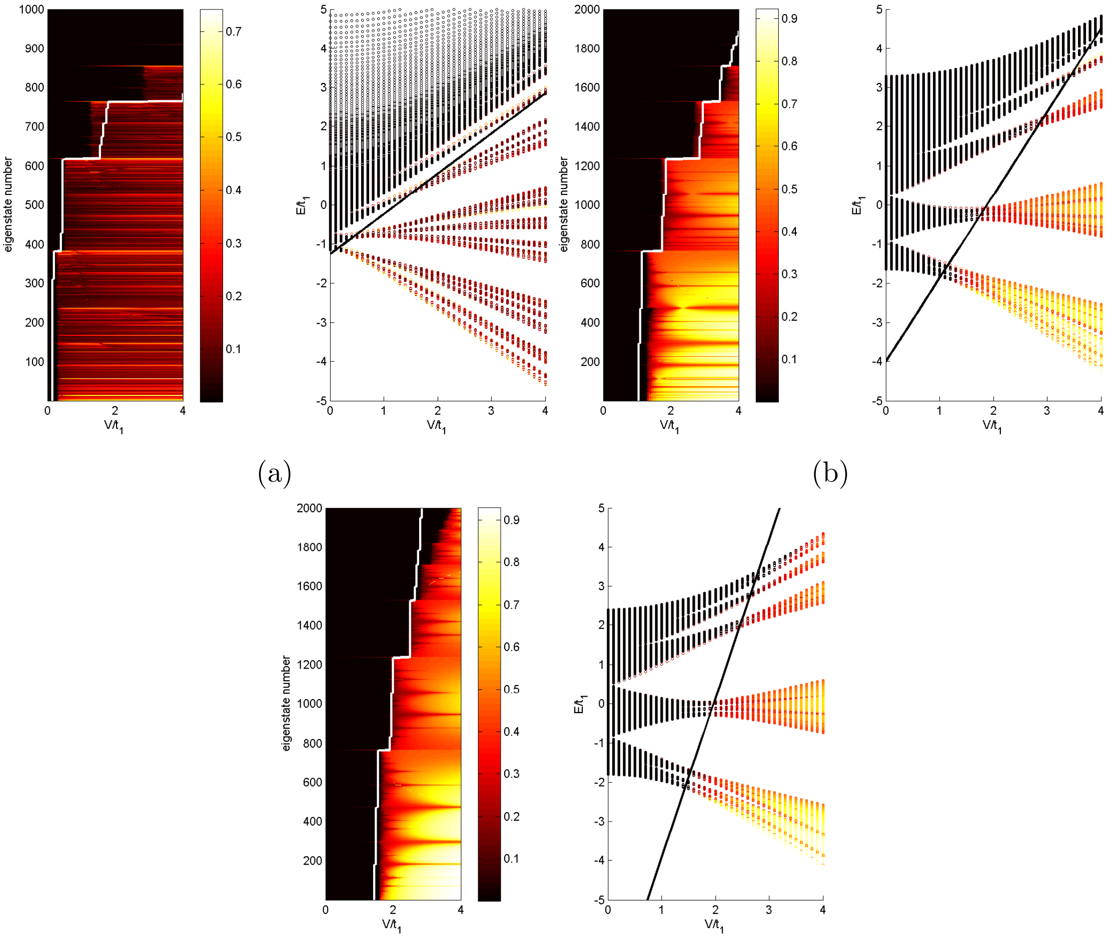

(a) (b)

(c)

Figure 1.5: In this figure we can see the single particle eigenstates in the polynomial binding model for different values of the parameter r: (a) r = 0.3, (b) r = 2, (c) r = 3. On every graph, on the left for increasing V the value of IPR for each eigenstate and on the right the IPR for each energy eigenvalue. The straight lines are the mobility edge boundaries approximated with exponential binding model using $p' = rln(2)$. Picture taken from [21]

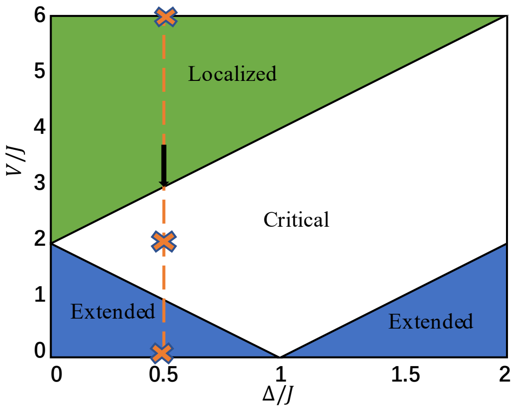

Figure 1.6: This figure show the phase diagram of Aubry-André with p-wave superconductor model. There are three phases corresponding to the degree of localization of eigenstates. In the critical phase eigenfunctions assume a multifractal behaviour. Picture taken from [29]

1.5.1 Aubry-André Model with superconducting term

This model is the extension of the Aubry-André model with a p-wave superconducting term [29]. Its Hamiltonian looks like:

$$H = \sum_{j=1}^{N} -J(f_j^\dagger f_{j+1} + f_{j+1}^\dagger f_j) + \Delta(f_{j+1}^\dagger f_j^\dagger + f_{j+1} f_j) - V cos(2\pi j\phi + \alpha_0) f_j^\dagger f_j \quad (1.49)$$

Where J is the coefficient of the hopping term, Δ is the coefficient of the p-wave superconducting term and V is the amplitude of the incommensurate potential. It is interesting to look at its phase diagram to understand its features figure 1.6. As showed in [18], its phase space is rich and well defined. The phase transition curves are $V = 2|1+\Delta|$ and $V = 2|1-\Delta|$. We have an extended phase for $V < 2|1-\Delta|$ a localized phase for $V > 2|1+\Delta|$ and a critical behaviour in between. In this model we will not see mobility edges because there are no long range hopping terms. This system can be diagonalized with Bogoliubov transformations imposing:

$$\eta_n^\dagger = \sum_{j}^{N} (u_{n,j} f_j^\dagger + v_{n,j} f_j)$$

where n label stands for the n-th eigenstate of the Hamiltonian, while $u_{n,j}$ and $v_{n,j}$ are the Bogoliubov modes chosen to be real. The result is an Hamiltonian like this:

$$H = \sum_{j=1}^{N} E_j(\eta_j^\dagger \eta_j - \frac{1}{2})$$

While, expressing the wave function in the following way:

$$\langle\psi_n| = [u_{n,1}, v_{n,1}, u_{n,2}, v_{n,2}, ..., u_{n,N} u_{n,N}]^T \tag{1.50}$$

We have the following Schroedinger equation for u_j and v_j:

$$Eu_j = -J(u_{j+1} + u_{j-1}) - \Delta(v_{j+1} - v_{j-1}) - V_j u_j \tag{1.51}$$

$$Ev_j = J(v_{j+1} - v_{j-1}) + \Delta(u_{j+1} - u_{j-1}) + V_j v_j \tag{1.52}$$

Now we can explicit some symmetries of that model [18]: there is a particle- hole symmetry and a duality symmetry . The first one means that for every solution with energy $E > 0$ we have a symmetric solution with $E \leq 0$. This happen because changing $f_j \rightarrow f_j^\dagger$ does not affect the definition of η_n, given that $u_{n,j}$ and $v_{n,j}$ are chosen to be real. The other symmetry is linked with the substitution to the k_j ladder operators $f_j \rightarrow k_j$ if j is even and $f_j \rightarrow -k_j^\dagger$ if j is odd. In fact, doing those substitutions plus $\alpha_0 \rightarrow \alpha_0 + \frac{1}{2}$, the Hamiltonian does not change form, but the role of J and Δ is exchanged. This means that the Hamiltonian is self-dual in $\Delta = J$. Clearly, exist also a form of Aubry-André duality between localized and extended states, but its analytical expression is not in a simple form.

1.5.2 Aubry-André model with interactions

This model, whose behaviour is discussed in [11], shows the ergodicity breaking. The model has the Hamiltonian (1.53).

$$H = \sum_{j,\sigma}^{N} t\left(f_{j,\sigma} f_{j+1,\sigma}^\dagger + f_{j,\sigma}^\dagger f_{j,\sigma}\right) + V cos(2\pi j\phi + \alpha_0) f_{j,\sigma}^\dagger f_{j,\sigma} + \sum_{j,\sigma}^{N} U n_{j,\sigma} n_{j+1,\sigma} \tag{1.53}$$

Where $n_{j,\sigma}$ is the number operator and $\sigma \in \{\uparrow, \downarrow\}$ is the value of the spin. We can now focus on the behaviour of our system. As we can expect, when $U = 0$ we fall into the Aubry-André model, of which we know that the localized phase subsists when $V > 2t$. In the regime with $U > 0$ there is an interaction that tends to move away the particles, so that the configurations with two adjacent sites are energetically inconvenient. Now to study the Anderson localization, we can use another observable that characterize the system: the imbalance.

$$\mathcal{I} = \frac{N_e - N_o}{N_e + N_o} \tag{1.54}$$

In its definition (1.54) N_e and N_o are the number of particles in even and odd sites respectively. This observable is very relevant in Néel states like $|\mathbb{Z}_2\rangle = |\bullet\circ\bullet\circ\dots\rangle$ and its complementary. In fact, these are the states with the maximum number of

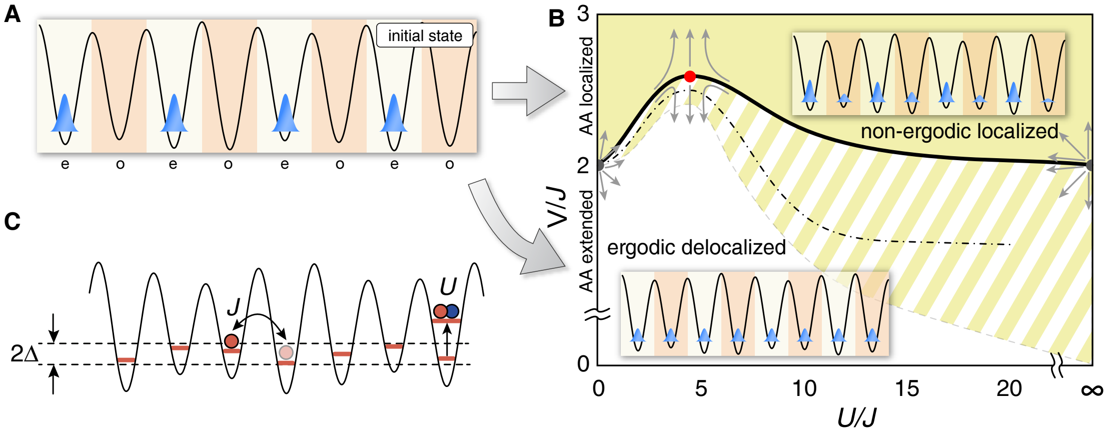

Figure 1.7: Here is explained the function of the various terms in the Aubry-André model with interactions. On the left there is a representation **A** of a charge density wave corresponding to the Neèl state. In image **C** there is a visual representation of the three terms of the Hamiltonian (1.53). On the right **B** there is a phase diagram that shows if the imbalance of the aforementioned state falls to 0 or has a finite value. In the striped area the transition depends on number of doblons, while over the black solid line the no doblons are allowed. The grey lines indicate the renormalization flow. Notice that in the regimes $U = 0$ and $U = \infty$ the phase transition is governed by the Aubry-André renormalization points in $V = 2$. The red dot stays for the many body localization transition point. Picture taken from [11]

particles and imbalance $\mathcal{I} = \pm 1$. The ergodicity breaking can be easily detected looking at the value of imbalance evolving the system during the time. In fact an extended phase will spread the initial state among all the others, so that the imbalance will fall to zero immediately. On the other hand, if we are in a localized phase, the imbalance stays at a fixed value different from zero. This is a clear example of an observable that in a certain regime do not thermalizes.

Chapter 2

Simulation of generalized Aubry-Andrè model

As original work, we want to explore deeply using simulations our class of systems. Firstly, we introduce the a generalized Aubry-Andrè model, then we analyze the submodels contained in it performing simulations on the inverse participation ratio, on the fidelity and the time evolution to detect phase transitions. The study of the different Hamiltonians belonging to the various submodels is made also visualizing the matrix elements of the Hamiltonian itself and of the observables taken in exam. In the end, the most remarkable result we got is the reformulation of the phase diagram of the superconducting Aubry-Andrè model. We achieved this result generalizing the duality transformations showed in 1.3.1. Moreover, our proposal of phase diagram seems to have more consistent limits of the coupling constants, thing that reinforces its possible validity.

2.1 Interacting Aubry-André model with p-wave superconducting term

We can now introduce our model that is a hybrid model between the superconducting Aubry-André model and the Aubry-André model with interactions. Its Hamiltonian is the following:

$$H = \sum_{j=1}^{L} -J(f_j^\dagger f_{j+1} + f_{j+1}^\dagger f_j) + \Delta(f_{j+1}^\dagger f_j^\dagger + f_{j+1} f_j) + V\cos(2\pi j\phi + \alpha_0) n_j + U n_j n_{j+1} \tag{2.1}$$

where $n_j = f_j^\dagger f_j$. In the Hamiltonian H we have the nearest neighbor hopping term, the p-wave superconductive one, the incommensurate potential and the first neighbor interaction. The incommensurate potential is made by an irrational parameter ϕ, and a random phase α_0 chosen from the uniform distribution in the range $[0, 2\pi]$. In our model the original interaction term of equation (1.53) has been substituted by a nearest neighbor interaction, because we want to study spinless fermions.

2.2 Aubry-Andrè model

To start our analysis we can focus on the Aubry André model. It is obtained from our model setting $\Delta = U = 0$. Without loss of generality we can also put $J = 1$, so that the only independent parameter is now V. Now we present wide range results obtained on this model, looking at different quantities that characterize its behaviour.

2.2.1 The incommensurate potential

The first aspect of our model that can be studied is the effect of the incommensurate parameter $\phi = \frac{1+\sqrt{5}}{2}$. In figure 2.1 we can see the different behaviour of the spectrum for an 8-sites chain. We performed the computation with $\alpha_0 = 0$ because we want to focus on the parameter ϕ. The color indicates the IPR, while on the x-axis there is the value of the magnitude V of the potential. The cases represented are: a constant potential on the various sites $V_j = V$(a), two strictly periodic potentials $V_j = V\cos(\pi j)$ (b) and $V_j = V\cos(\pi j/2)$ (c), and the incommensurate potential $V_j = V\cos(2\pi j\phi)$ (d).

The differences in terms of IPR, defined in (1.2), between different forms of potential are very deep. In fact for $V = V_0$ the depth of the potential well is equal for all sites. So, the IPR is practically always 0 because the particles do not have favourite sites to stay. In the periodic cases the IPR is significantly different from 0 only in several eigenstates. This happens because now the depth of the potential wells is periodic on the sites. Finally, the incommensurate case is profoundly different from the others because we can see that IPR is different from 0 in all eigenstates when $V > 2$ as predicted by the theory behind the Aubry-André model 1.3.1. To emphasize the two different regimes of localization, we can do a mean of the IPR over many different realization of the starting phase α_0. In figure 2.2 we can see the result of the mean over 100 different values of α_0 uniformly distributed in the interval $[0, 2\pi]$. We can see a more gradual transition and a soother change of IPR with increasing V.

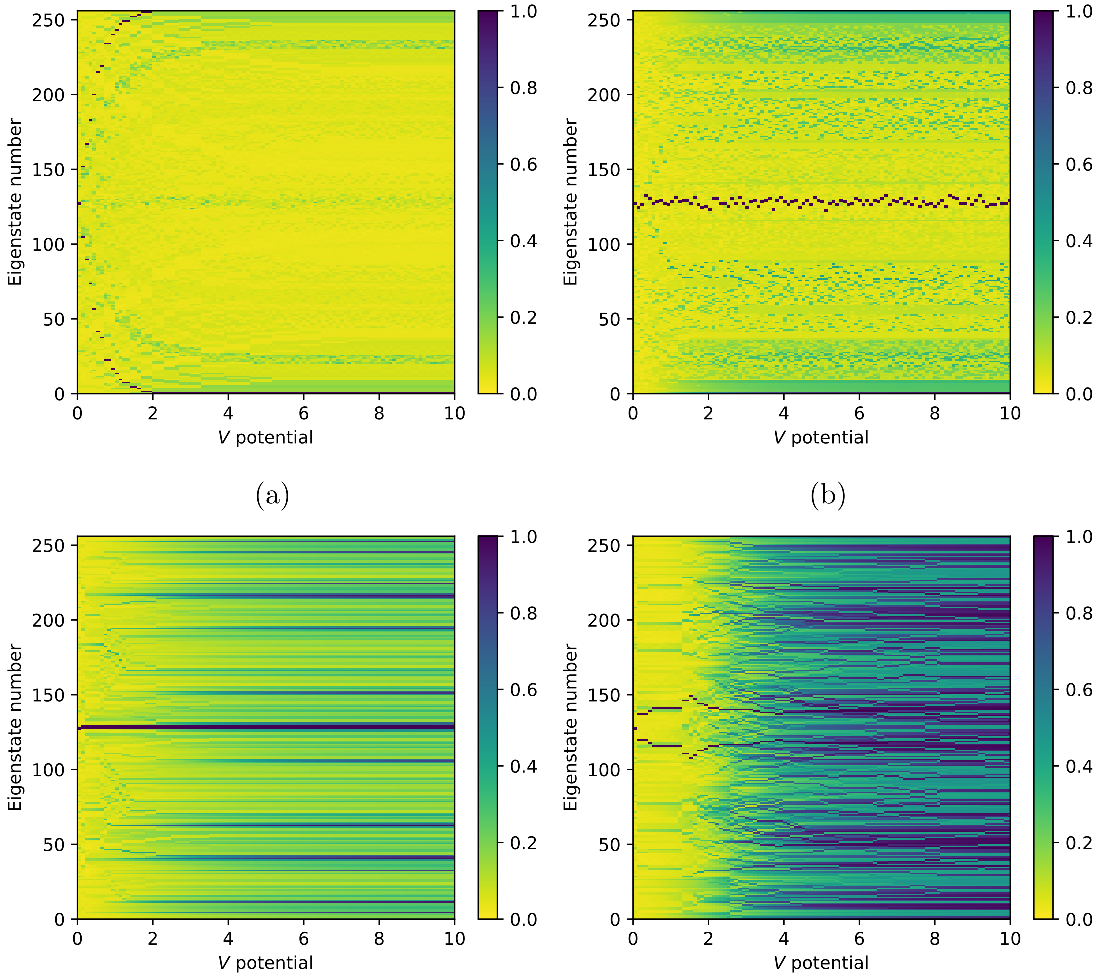

(a) (b) (c) (d)

Figure 2.1: In this figure there is the plot of the IPR for every eigenstate in Aubry-André model. We took in exam 8 sites and 100 values of V equally spaced between 0 and 10. The different plots belong to different form of potential: (a) constant potential $V = V_0$, (b) periodic $V cos(\pi j)$, (c) periodic $V cos(\pi j/2)$, (d) incommensurate potential $V cos(2\pi j \phi)$.

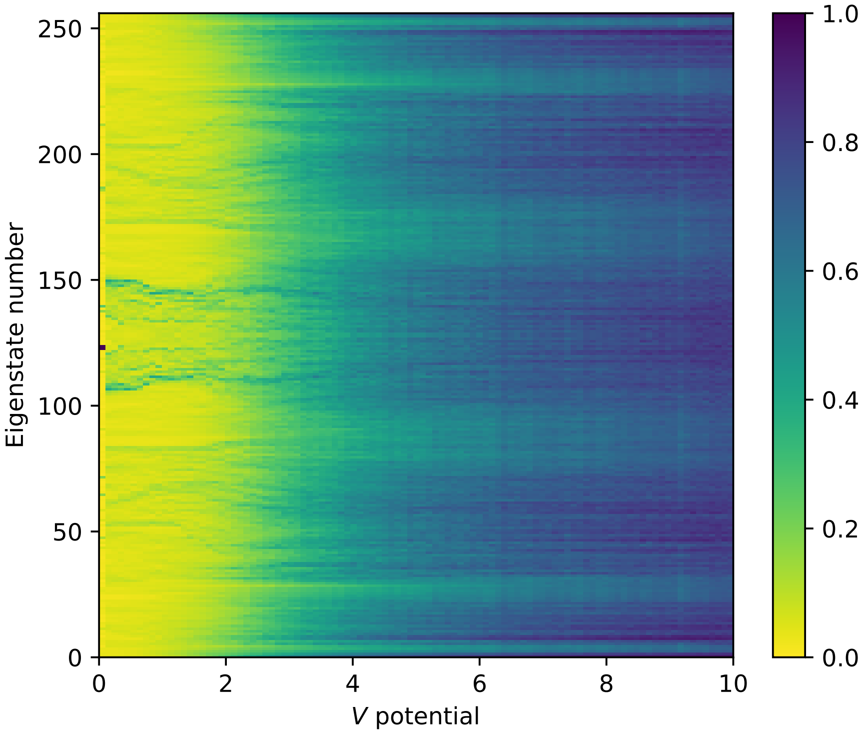

Figure 2.2: Here we can see the map of the IPR for every eigenstate with 101 values of V taken from 0 to 10. For every initialization of V, the IPR is the mean of 100 realizations of the value α_0. Clearly, the transition between low IPR states and high IPR states is more smooth and the IPR fluctuations in the spectrum are smaller than the single realization case in figure 2.1

.

2.2.2 Time evolution of localized and extended states

In the previous sections 1.1 we have already seen localized and extended phase of our Aubry-Andrè model. To understand better what effectively it means, we can look at fig 2.3. Here we computed the time evolution:

$$|c(t)\rangle = e^{-i\hat{H}t}\,|c\rangle_0 \tag{2.2}$$

of the initial state of the configuration basis $|c\rangle_0 = |10101010\rangle$ with the following Aubry-Andrè Hamiltonian:

$$H = \sum_{j=1}^{L} -J(f_j^\dagger f_{j+1} + f_{j+1}^\dagger f_j) + V\cos(2\pi j\phi + \alpha_0) f_j^\dagger f_j \tag{2.3}$$

and plotted the modulus of projection of the evolved state on all the states of the configuration basis:

$$|\alpha_k| = |\,\langle c_k|c(t)\rangle\,| \quad \text{with} \quad k = 1\ldots 2^L \tag{2.4}$$

The two pictures correspond to two different values of V with $L = 8$. In the figure 2.3 (a) V is set to 1, so that we are in the extended phase. It can be seen because the projections on other states become immediately significantly different from 0 and the projection on the initial state falls around 0.2. On the contrary the figure 2.3 (b) show a totally different situation. Here $V = 8$ and the most significant component of the evolved state is represented by the initial state during all the evolution.

Hamiltonian visualization and state ordering

Another way to visualize the phase transition is throughout the Hamiltonian operator and the basis change between the eigenstates basis and the number basis. In the previous chapters, we encountered different kinds of state basis to describe our systems. For example, the Hilbert space represented in the configuration basis $\mathcal{H}_c$ is the most intuitive one, and is built acting with the creation operators $f_j^\dagger$ on the vacuum $|0\rangle$. The order in which the states are arranged is arbitrary, because it does not affect the physics of the system. Nevertheless, it is important to visualize the system properties. For this reason, an instructive view is to represent our Hamiltonian in the basis of the number operator. The number operator $\hat{N}$ is given by:

$$\hat{N} = \sum_{j=0}^{L} f_j^\dagger f_j \tag{2.5}$$

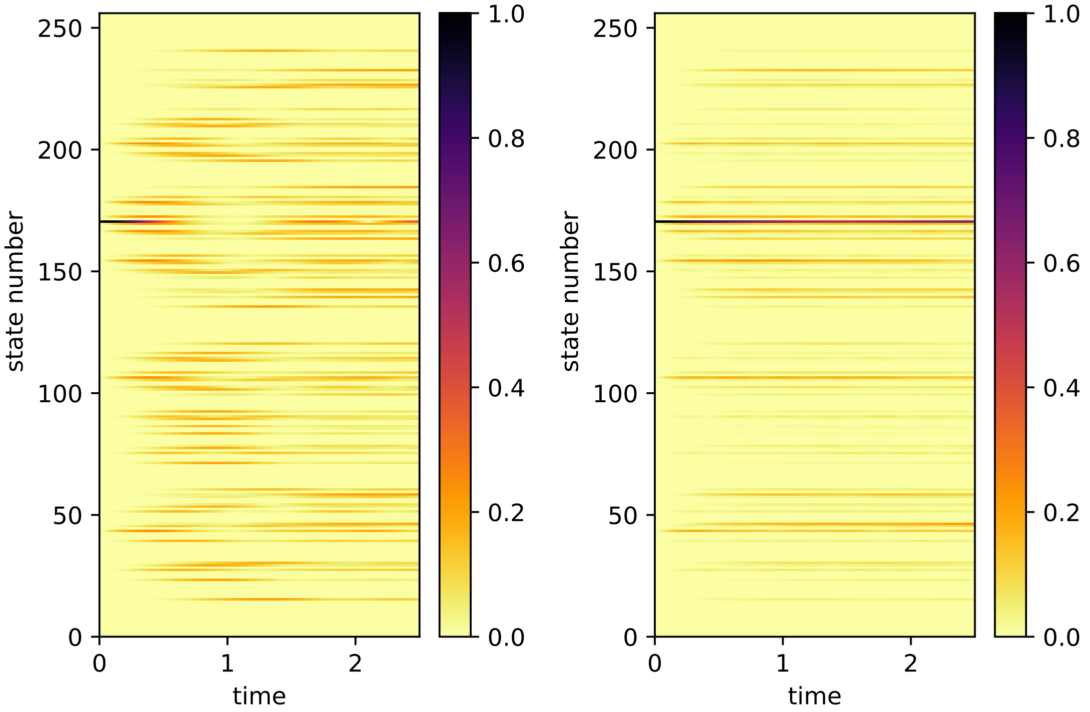

(a)

(b)

Figure 2.3: Here we can see the evolution of the projection of the initial state on the configuration basis. The initial state is the neel state $|10101010\rangle$ that corresponds to the state 169. On the left the evolution with $V = 1$, on the right $V = 8$. During the time in the extended phase it spreads on other states (a) while on the localized phase (b) the greater part of the evolved state remains on the initial state. Here the color indicates the modulus of the projection of the evolved state on the entire configuration basis. The plot is realized with 20 realization of the noise with 100 time steps.

with the Hilbert space $\mathcal{H}_n$, built on the eigenstates of the number operator. The configuration basis is also a basis of eigenvectors for $\hat{N}$, but this time is sorted following increasing number of particles. For example, for a 4-particle system we would have:

$$\begin{aligned}
&|0000\rangle && \text{subspace with 0 particles}\\
&|1000\rangle, |0100\rangle, |0010\rangle, |0001\rangle && \text{subspace with 1 particles}\\
&|1100\rangle, |0110\rangle, |0011\rangle, |1010\rangle, |1001\rangle, |0101\rangle && \text{subspace with 2 particles}\\
&|1110\rangle, |0111\rangle, |1101\rangle, |1011\rangle && \text{subspace with 3 particles}\\
&|1111\rangle && \text{subspace with 4 particles}
\end{aligned} \tag{2.6}$$

For a generically large system of L spinless fermions the subspace $\mathcal{H}_m$ with m particles has dimension equal to the corresponding binomial coefficient:

$$dim(\mathcal{H}_m) = \frac{L!}{(L-m)!m!} = \binom{L}{m} \tag{2.7}$$

The basis change transformation used to pass from the configuration basis to that of the number operator corresponds to what called mathematically a *permutation* matrix. A permutation matrix Π is defined as a permutation of the identity matrix columns. For example, the permutation for the 4-sites long chain that maps the configuration basis to the number operator one is the following :

$$\Pi_4 = \begin{pmatrix}
1&0&0&0&0&0&0&0&0&0&0&0&0&0&0&0\\
0&1&0&0&0&0&0&0&0&0&0&0&0&0&0&0\\
0&0&1&0&0&0&0&0&0&0&0&0&0&0&0&0\\
0&0&0&0&1&0&0&0&0&0&0&0&0&0&0&0\\
0&0&0&0&0&0&0&0&1&0&0&0&0&0&0&0\\
0&0&0&1&0&0&0&0&0&0&0&0&0&0&0&0\\
0&0&0&0&0&1&0&0&0&0&0&0&0&0&0&0\\
0&0&0&0&0&0&1&0&0&0&0&0&0&0&0&0\\
0&0&0&0&0&0&0&0&0&1&0&0&0&0&0&0\\
0&0&0&0&0&0&0&0&0&0&1&0&0&0&0&0\\
0&0&0&0&0&0&0&0&0&0&0&0&1&0&0&0\\
0&0&0&0&0&0&0&1&0&0&0&0&0&0&0&0\\
0&0&0&0&0&0&0&0&0&0&0&1&0&0&0&0\\
0&0&0&0&0&0&0&0&0&0&0&0&0&1&0&0\\
0&0&0&0&0&0&0&0&0&0&0&0&0&0&1&0\\
0&0&0&0&0&0&0&0&0&0&0&0&0&0&0&1
\end{pmatrix} \tag{2.8}$$

A generic operator A transforms following the equation:

$$A' = \Pi A \Pi^{-1} \tag{2.9}$$

Moreover it can be also considered as a unitary transformation when it acts on Hermitian operators. Now we can look at the Hamiltonian operator written in the number basis.

In figure 2.4, we can see the matrix elements of the Hamiltonian of the AA model for different values of V. Given two states in the configuration basis $\langle c_i|$, $\langle c_j|$, in the figure we show the magnitude of the matrix element $|\langle c_i| H |c_j\rangle|$ for a 6-sites system that has 64 states. Immediately it is visible a block structure in low V cases. This is due to the hopping term that mixes only states with the same number of particles. So, in this case the number of particle is conserved. In fact, every block corresponds to subspaces with 0,1,2,3,4,5 and 6 particles. Clearly, because of combinatorics, the middle subspaces are that with the higher dimensionality. On the other hand when V increases the hopping part of the Hamiltonian disappears and only the diagonal part survives.

Another proof of the conservation of the number of particles is given in figure 2.5. Here we have the same evolution of figure 2.3, but this time the states are ordered following the number basis. We can clearly see that the evolution is confined on the subspace with 4 particles, even in the extended phase.

Moreover, can be useful visualization is that of the unitary matrix $\mathcal{U}_{e\mapsto n}$ that maps the eigenstates basis $\mathcal{H}_e$, ordered with increasing values of the relative eigenenergies, into the number basis $\mathcal{H}_n$. It is directly connected with the IPR. Moreover, increasing V can be detected the phase transition. In figure 2.6 we can see the modulus of the matrix elements of the basis change. Practically, element β_{ij} is the projection of the eigenstate $|e_i\rangle$ on the states of number operator basis $|n_j\rangle$:

$$|\beta_{ij}| = |\langle e_i|n_j\rangle| \tag{2.10}$$

The link with the IPR is the following: if we raise to the fourth power every element of the matrix taken singularly, the IPR of the j-th eigenstate would be the sum of j-th row elements. From this point of view, for $V < 2$ we are considering an highly non-local transformation. In fact, qualitatively, one can understand from the figure that the projection of whatever eigenstate spread out onto many different states of number basis. On the other hand, when V starts to increase, the entire basis change falls in a simple permutation transformation governed by the incommensurate potential. In this regime the eigenstates of the hamiltonian tend to be the same of the number operator, with a corresponding increment of the IPR. But, in both cases, the transformation mixes states with the same number of particles. It can be seen from the column structure of the transformations.

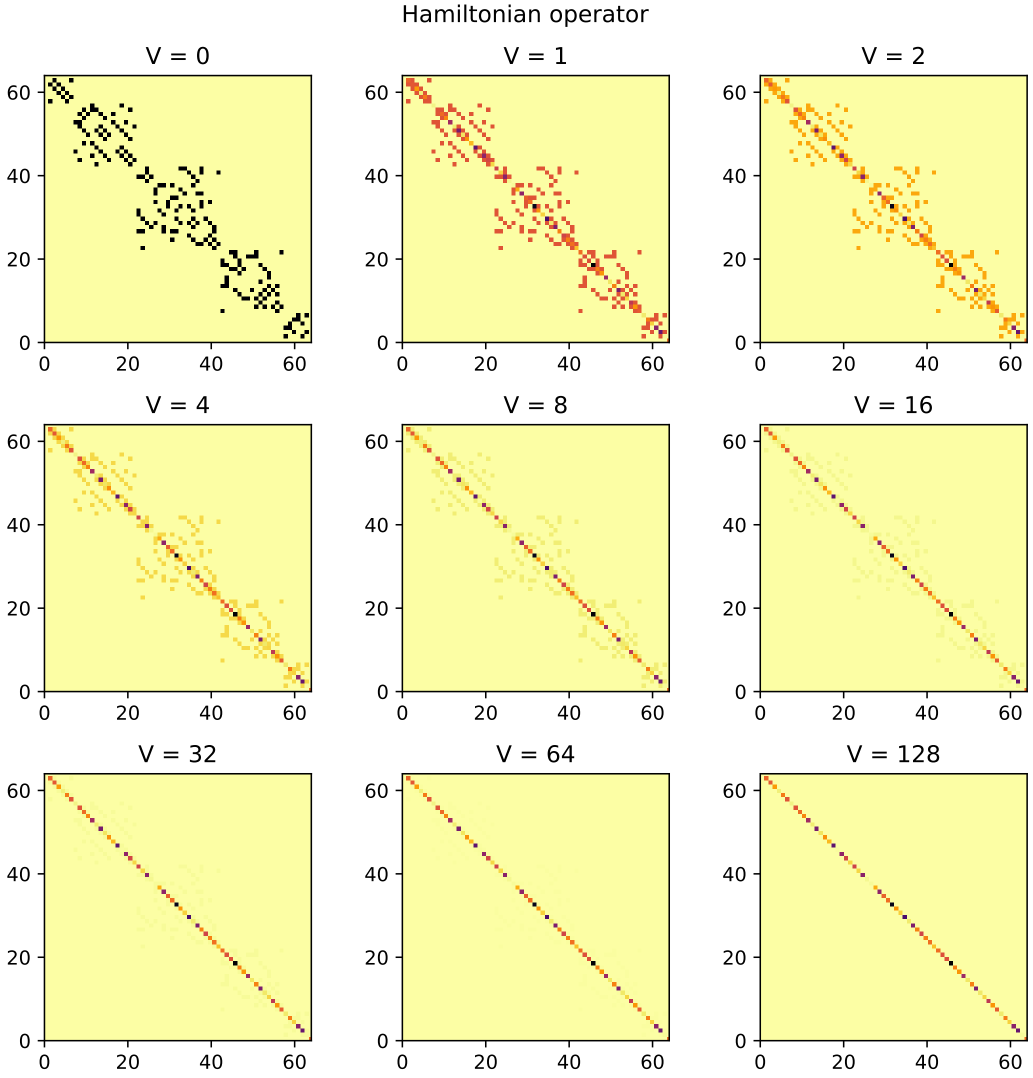

Figure 2.4: Here we can see nine figures of the modulus of matrix elements $\langle c_i | H | c_j \rangle$ of the Hamiltonian operator written in the number operator basis for different values of the incommensurate potential depth V. We can see that for small values of V he Hamiltonian has a block structure given by the conservation of number of particles. While V increases the matrix elements hopping terms tends to be neglected and the Hamiltonian get a diagonal form given by the lonely incommensurate potential. Here the we have a qualitative colorscale in which the background color indicates values equal to 0.

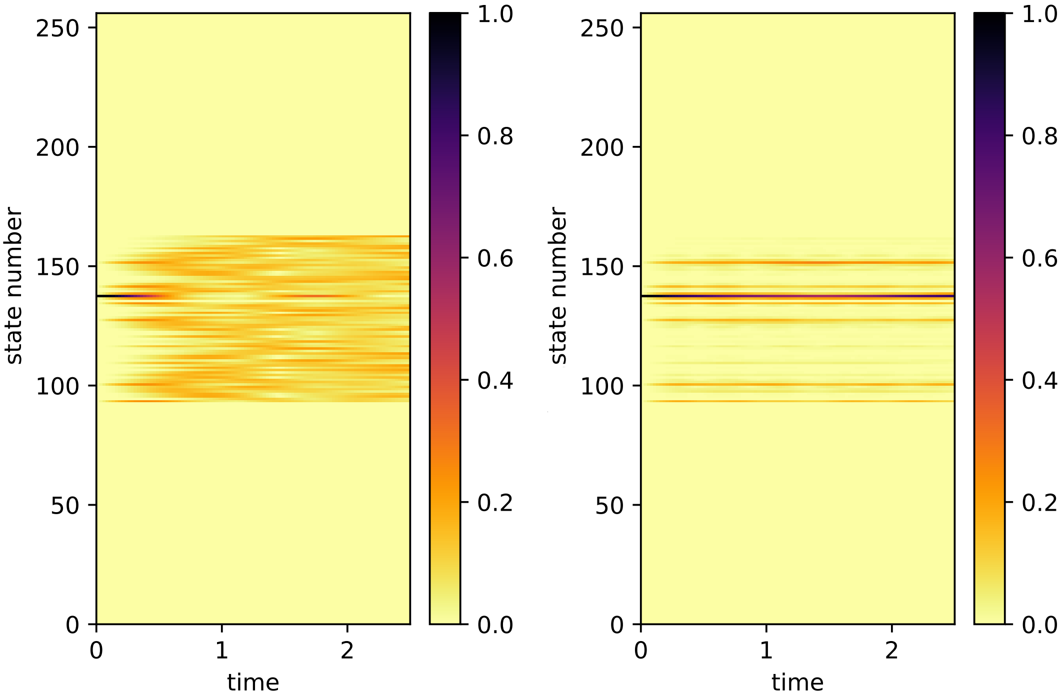

Figure 2.5: Here we can see the evolution of the projection of the initial state on the configuration basis. The initial state is the state $|10101010\rangle$. As we can see the evolution is confined on the subset of states with 4 particles. The plot is realized with 20 realization of the noise with 100 time steps.

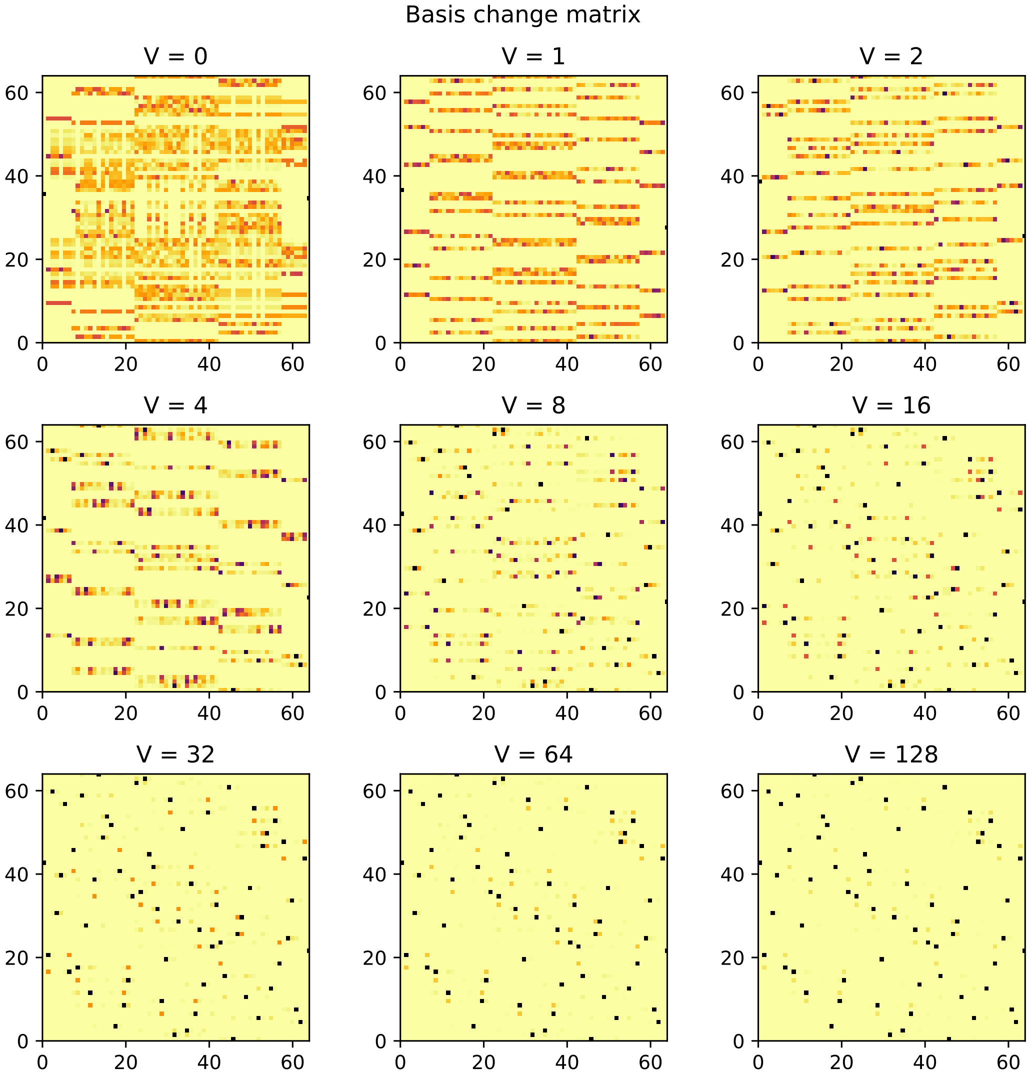

Figure 2.6: Here we can see the basis change matrix $\mathcal{U}_{e\mapsto n}$ between the energy eigenstates basis and the number eigenstates basis for a 6-sites long system. For different values of V we observe a radical change. Especially when $V < 2$ we have an highly non-local transformation. When V is much greater than 2 we fall in a permutation because the hopping term become a perturbation of the incommensurate potential. Nevetheless, also in extended regime we can recover the conserved number of particles because are distinguishable some subsets of columns that do not comunicate with each other. Here we have a qualitative colorscale in which the background color indicates values equal to 0.

2.3 Aubry-Andrè model with interactions

In this section we study the interacting version of the Aubry-Andrè model:

$$H = \sum_{j=1}^{L} -J(f_j^\dagger f_{j+1} + f_{j+1}^\dagger f_j) + V\cos(2\pi j\phi + \alpha_0)n_j + Un_j n_{j+1} \tag{2.11}$$

We want to investigate the ergodicity breaking of that system. To do it, for every state of the configuration basis we can build a diagram that shows if the ergodicity breaking happens or not. This diagrams are build given an initial configuration state $|c\rangle_0$, choosing an observable $\hat{O}$ and plotting its asymptotic value varying the coupling constants U and V:

$$\lim_{t\to\infty} \langle c(t)|\hat{O}|c(t)\rangle_{U,V} = \gamma(U,V) \tag{2.12}$$

The time evolution is implied to be done with the Hamiltonian (2.11). The aim of these diagrams is using the expectation value of the observable to detect different phases depending on the value of the couplings. In our case we have to choose an observable to detect the ergodicity breaking due to the Anderson localization. For example, we can take the imbalance operator defined as:

$$\hat{I} = \frac{1}{\hat{N}} \sum_{j=0}^{L-1} (-1)^j f_j^\dagger f_j \tag{2.13}$$

We can use it as an indicator of the phase localized or extended of the system. Roughly speaking the imbalance is the number of particles in even sites minus the number of particles in odd sites normlaized with the total number of particles. It has a value equal to 1 or -1 in the states whose the particles lies in all even (I=1) or odd sites (I=1). If the system is in an extended phase, an initial state with an high value of the imbalance, due to the diffusion of the particles, evolves in as state whose expectation value of the imbalance falls to 0. Otherwise, if the system is in a localized phase, the expectation value of imbalance holds a finite value because the most significant projection on of the evolved state is made by that on the initial state. Notice that the imbalance cannot detect the phase transition in these states whose initial expectation value is 0. This is due to the fact that even in the localized phase its value does not change.

We can see that time evolution of the expectation value of the imbalance can have for the same initial state different behaviours depending on the value of α_0, fig 2.7. To regularize the results and decrease the fluctuations, we can take a mean on the realizations that we will call mean-imbalance. We have shown the results obtained doing a mean over many realizations of the parameter α_0 in figure 2.8.

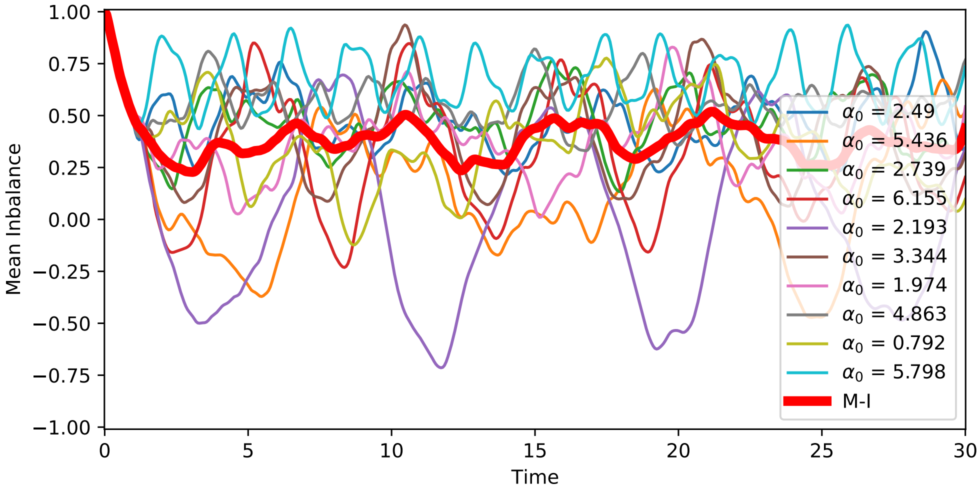

Figure 2.7: We can see here 10 different realizations of the noise α_0. Because of for different values of it we can have that imbalance fluctuations are more or less intense, it is useful perform a mean to make more smooth the behaviour of the observable during the time. As initial state we used the 4-alternate particle state.

In the end the true indicator of the ergodicity breaking is the asymptotic value of the mean-imbalance.

Now we can look at the results of our simulations. We have taken in exam four initial configuration states: $|1000000\rangle$ single particle state, $|10100000\rangle$ 2-alternate particle state, $|10101000\rangle$ 3-alternate particle state and the Néel state $|10101010\rangle$. This choice of states is made because they are the states with maximum imbalance with a given number of particles. All the other states with $I \neq 0$ show an intermediate behaviour respect to that of our states. On the other hand, states with an initial value of imbalance equal to 0 do not show any trace of localization, as we have explained before. In figure 2.9 we can see the results. Here, for each value of U and V, we evolved the mean-imbalance I with a mean on 50 values of α_0. Then we took the expectation value of the imbalance for 50 values of time equally spaced between 20 and 30 time units. We did a temporal mean because we want to avoid the fluctuations in the asymptotic value. We can observe that for the single particle there is no dependence from the coefficient U and we recover the Aubry-André transition when $V > 2$. When the number of particle increases there is a straight line pattern that emerges, while the Aubry-André extended phase band become less marked. In particular, the extended phase disappear totally for 4-alternate particles state when $U > 5$ it is confined around the straight oblique line $V \simeq \frac{1}{2}U$.

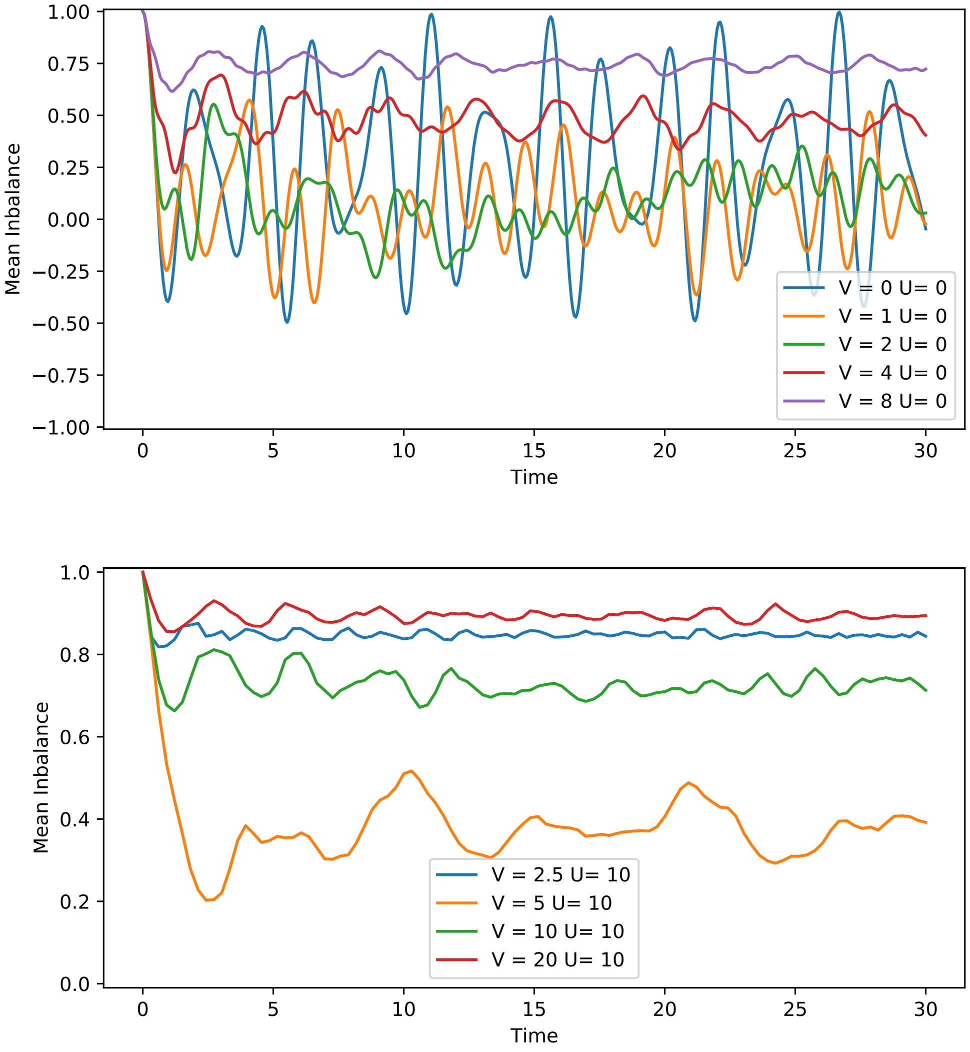

Figure 2.8: Here is shown the evolution of the expectation value of the imbalance through the time. For every value of U and V the mean imbalance is the mean on 50 realizations of the noise. We can see that with $U = 0$ the amplitude of the fluctuations is greater, especially in the extended phase. In the bottom figure we investigated the line $U = 10$. Here the imbalance stabilizes always on non-zero values. Moreover, the imbalance seems to be smaller when $V/U = \frac{1}{2}$. We always used the 4-alternate particle state as initial state.

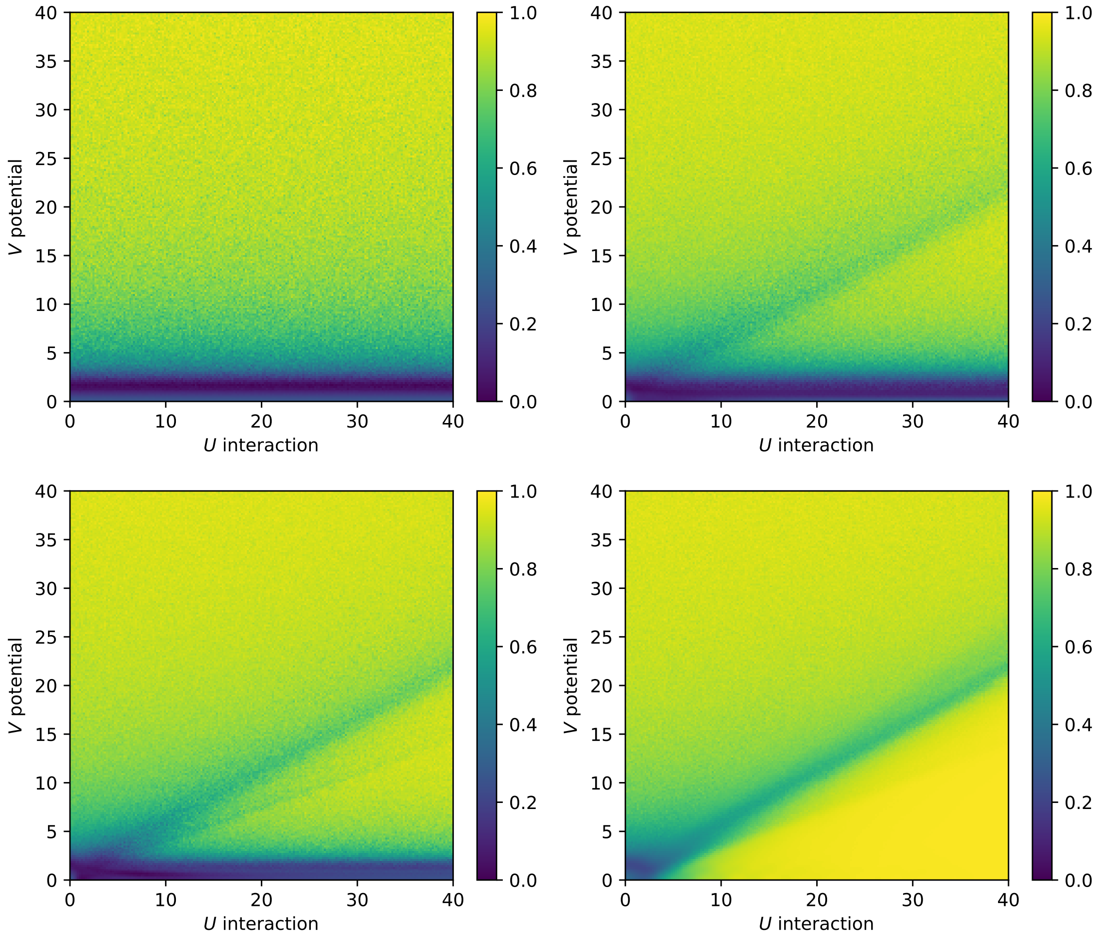

Figure 2.9: This figure represents the phase space of four different initial states in terms of Imbalance. Practically, we took the mean evolution over 50 noise realizations of the imbalance I of the initial state and took a mean of it after a certain time. The initial states studied are a single particle $|10000000\rangle$ state, two alternate particle state $|10100000\rangle$, three alternate particle state $|10101000\rangle$ and the Nèel state $|10101010\rangle$. In the first three cases we considered the mean on 50 values of imbalance from 20 to 30 time units. For the last case we performed the mean on 5 values taken between 20 to 22 time units. This different sampling strategy is referred to the fact that the fluctuations in the last case are significantly less. The values of U and V are 200 equally spaced between 0 and 40.

We can also see our diagrams from the point of the standard deviation σ of the samplings taken in the time interval. In this way we want to investigate if the imbalance is constant during the time or it oscillate, so that only its temporal mean is constant. From figure 2.10 we can observe clearly that the areas belonging to the extended phase in figure 2.9 now are those with a greater deviation from the mean. We can conclude that the states with a greater localization are also those with a more regular behaviour of the imbalance during the time.

Fidelity as ergodicity breaking indicator

Until now we have described the various phases using the imbalance I. Another quantity that can detect the various phases is the fidelity F. The concept of fidelity is built on the density matrices formalism.

Next to the bra/ket formalism the entire quantum mechanics can be reformulated using density matrices. A density matrix ρ, given a basis of states $\psi_i \dots \psi_n$, is defined in the following way:

$$\rho = \sum_i^n p_i \left|\psi_i\right\rangle \left\langle\psi_i\right| \tag{2.14}$$

where p_i are the probabilities of finding the system in the state i. There is a bijective correspondence between states and density matrices. Moreover the density matrices are Hermitian operators and have some peculiar properties:

- ρ has a trace always equal to 1
- ρ is semi positive defined

Moreover, the density matrix can be defined also for classical statistics mixtures. In other words, a density matrix can be written also in a deterministic case in which the uncertainty is not given by a superposition of states but from our ignorance on the state of the system. Furthermore, the classical mixture does not have off-diagonal interference terms. However, in our case the density matrices are referred to quantum states which do not include the classical mixture. In these cases, ρ has the property to be idempotent: $\rho^2 = \rho$. The states described by these particular density matrices are called pure states. Clearly, the form of ρ depends on the basis chosen. Coming back to the fidelity, it is often used in quantum computation as a notion of distance between different quantum states ϕ_1,ϕ_2. Its definition is given in terms of the relative density matrices ρ_1, ρ_2 :

$$F(\rho_1, \rho_2) = tr\sqrt{\rho_1^{1/2}\rho_2\rho_1^{1/2}} \tag{2.15}$$

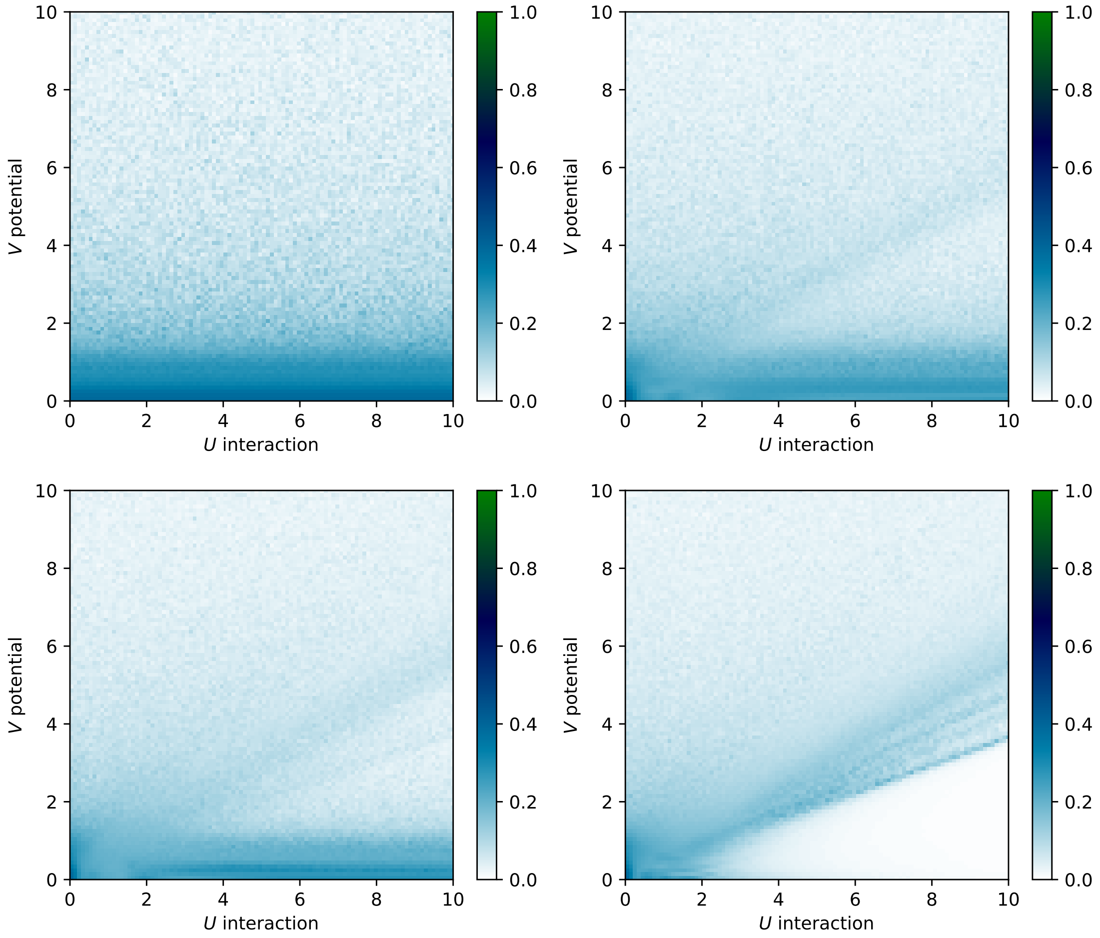

Figure 2.10: In this figure we can observe the standard deviation of the data showed in figure 2.9. The initial states studied are a single particle $|10000000\rangle$ state, two alternate particle state $|10100000\rangle$, three alternate particle state $|10101000\rangle$ and the Néel state $|10101010\rangle$. We considered the mean on 50 values of imbalance from 20 to 30 time units. As we can see the extended phases are those with a greater value of σ. It means that even if the mean imbalance has a temporal 0 mean, it significantly oscillate. The values of U and V are 100 equally spaced between 0 and 10.

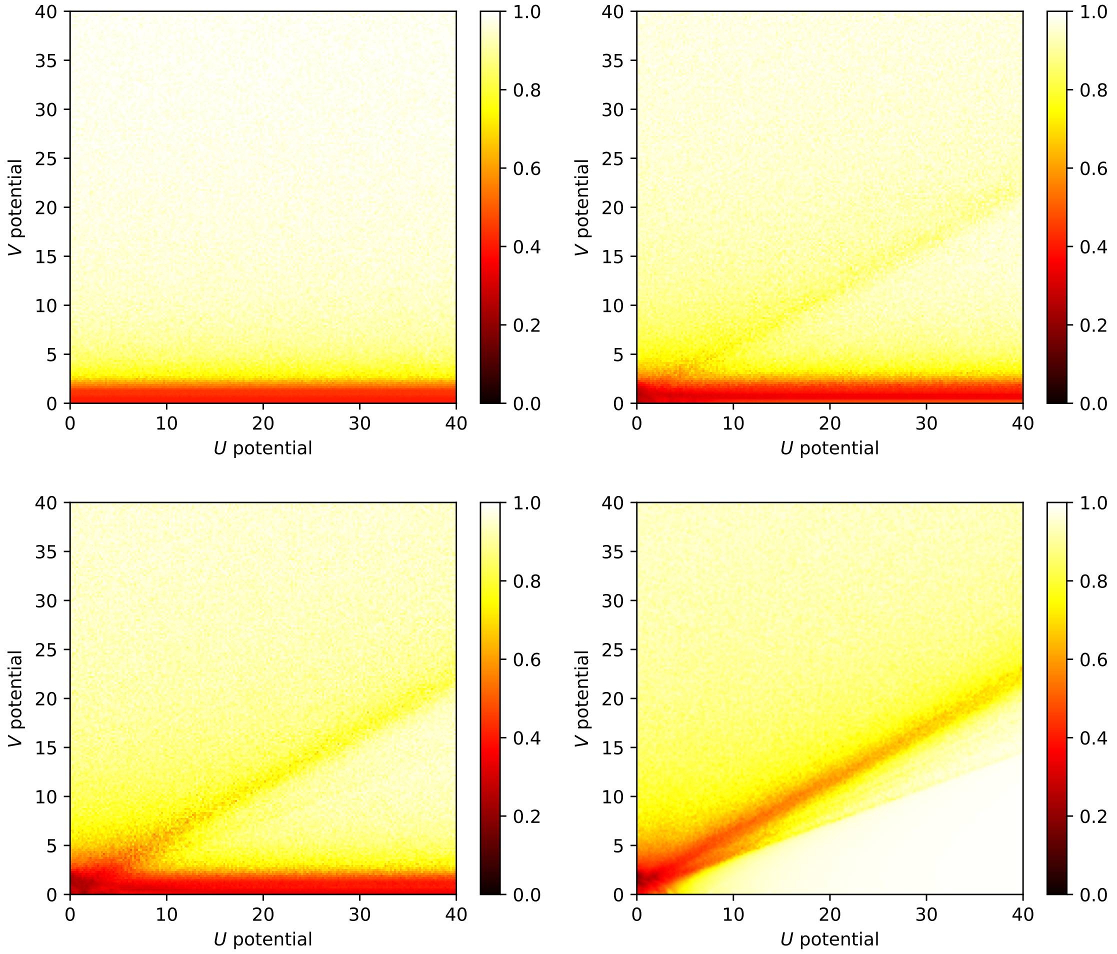

Figure 2.11: This figure was obtained evolving the fidelity F from 20 to 30 time units, taking its asymptotic value with the mean on 50 values taken interpolating the time interval. Then is taken the mean of 20 asymptotic values obtained with different random values of α_0 and . The initial states chosen are the same used for the imbalance. As we can see respect to the imbalance we observe almost perfectly stackable results. The values of U and V are 200 equally spaced between 0 and 40.

We can use this quantity to measure, during the time evolution, what is the probability to find the evolved state in the initial one. In our case, choosing the configuration basis, the initial states that we have considered in previous computations are all pure states. Given that, the fidelity reduces to the simple form of the projection of the evolved state $|\psi(t)\rangle$ on the initial state $|\psi(0)\rangle$:

$$F(\psi(t), \psi(0)) = |\langle\psi(t)|\psi(0)\rangle| \tag{2.16}$$

In particular we can ask how much the expectation value of the imbalance imbalance depends on the permanency in the initial state. The answer is in figure 2.11. Here we have plotted the temporal mean of the fidelity for the same values of U and V. If we compare it with 2.9, the same pattern of localization arise. The regimes with an high imbalance perfectly coincide with a high fidelity. For example, in the Neèl state the imbalance is given almost only by the fidelity because it is the only state with four particles that has imbalance equal to 1. The magnitude differences between the two plots are given by the fact that the fidelity is the modulus of the projection, while the imbalance is proportional to the square modulus of the projection.

2.3.1 The relation between two observables: Hamiltonian and Imbalance

To understand better what is the role played by the Hamiltonian respect to the imbalance, we can look at its form in the imbalance basis $\mathcal{H}_i$, made by the eigenstates of the imbalance ordered with increasing values of I. This time we use the un-normalized imbalance:

$$\hat{I} = \sum_{j=0}^{L}(-1)^j f_j^\dagger f_j \tag{2.17}$$

because the number operator is not completely invertible. In figure 2.12 the Hamiltonian does not have blocks anymore, so that it mixes states with different values of imbalance. This means that the two operators do not commutes. In fact, the off-diagonal terms are those that belong to the hopping term:

$$\hat{J} = \sum_{0}^{L-1}(f_j^\dagger f_{j+1} + f_{j+1}^\dagger f_j) \tag{2.18}$$

This latter, in a system with PBC, acts shifting the site in which the particle lays, so that if the particle was in an even site is shifted in an odd one and vice versa. Given that, the contribution of the particle to the imbalance value change sign after having applied the hopping, so that the imbalance is not conserved.

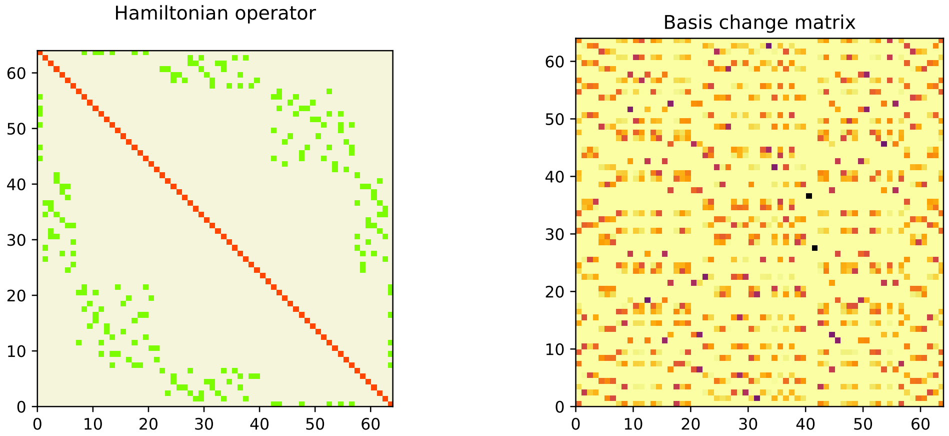
Hamiltonian operator

Basis change matrix

Figure 2.12: Here there are the plots of the Hamiltonian operator in the basis of unnormalized imbalance and the basis change between the eigenstates basis and the imbalance basis with $V = 1$. As we can see, differently from the number operartor, there are no blocks because the Hamiltonian mixes subspaces with different values of imbalance. In particular, in red there are the matrix elements belonging to the potential, while the green dots are the elements belonging to the number operator. Analogously the basis change is very chaotic because there are no distinguishable columns that represent subspaces that have the same number of particles.

2.3.2 Evolution of the IPR

Despite our analysis of extended and localized phase is built on the IPR, we did not talk about this quantity yet. In particular its treatment is not trivial because we have defined this quantity for the eigenstates expressed in the configuration basis, while our simulations until now are based on initial configuration states. A solution can be try to compute the IPR for an evolved state $\mathrm{IPR}(|c(t)\rangle)$. Now we show that it is a quantity that changes during the time.

Given the configuration state $|c\rangle$ we can write it in the eigenstates basis like: $|c\rangle = \sum_j \phi_j^c |e_j\rangle$

then we evolve the state in the eigenstates basis:
$|c(t)\rangle = \exp(-iHt)|c\rangle = \exp(-iHt)\sum_j \phi_j^c \exp(-ie_jt)\phi_j^c = \sum_j \exp(-ie_jt)\phi_j^c |e_j\rangle$
We want the projection on the configuration state $|c_k\rangle$:
$\langle c_k|c(t)\rangle = \sum_{lj} \langle e_l| \mathcal{U}^{\dagger}_{(e\mapsto c)lk} \exp(-ie_jt)\phi_j^c |e_j\rangle$
using the orthonormality of the eigenstate basis we have: $\langle e_l|e_j\rangle = \delta_{lj}$
so that the projection on the state $|c_k\rangle$ is: $\langle c_k|c(t)\rangle = \sum_j \mathcal{U}^{\dagger}_{(e\mapsto c)jk} \exp(-ie_jt)\phi_j^c$
To compute the IPR we have only to sum over k all the projections raised to the 4-th power:

$$\mathrm{IPR}(|c(t)\rangle) = \sum_k |\langle c_k|c(t)\rangle|^4 = \sum_k \left| \sum_j \mathcal{U}^{\dagger}_{(e\mapsto c)jk} \exp(-ie_jt)\phi_j^c \right|^4 \tag{2.19}$$

Moreover, can be shown that the square modulus of the projections $|\langle c_k|c(t)\rangle|^2$ depends on mixed terms like $\cos(t(e_i - e_j))$ that continuously oscillate, such that the projection is not constant.

2.3.3 Building a time independent localization indicator

We can try to build a quantity that is fixed in time using the projections on the eigenstates. First of all, we want to show that the modulus of the projections of a given state of the configurations basis on the eigenstates basis is constant. Taking the state $|c\rangle$ we write it in the eigenstate basis $|c\rangle = \sum_j \phi_j^c |e_j\rangle$ and then we compute the time evolution $|c(t)\rangle = \sum_j \exp(-ie_jt)\phi_j^c |e_j\rangle$ as did before. But now we look for the projection on the eigenstates basis. The result turns out to be, using orthonormality:

$$\langle e_k|c(t)\rangle = \langle e_k| \sum_j \exp(-ie_j t)\phi_j^c \, |e_j\rangle = \exp(-ie_k t)\phi_k^c \tag{2.20}$$

But taking the square modulus the phase depending on time vanish because of the product with its complex conjugate:

$$|\langle e_k|c(t)\rangle|^2 = \Big((\phi_k^c)^* \exp(ie_k t)\Big)\Big(\exp(-ie_k t)\phi_k^c\Big) = |\phi_k^c|^2 \tag{2.21}$$

So that for every eigenstate the projection of the initial state on him has a constant modulus. Given that we can build a quantity that we call Weighted Inverse Participation Ratio WIPR. This quantity is defined in the following way for all the states of the configuration basis:

$$\text{WIPR}(|c\rangle) = \sum_j |\phi_j^c|^2 \text{IPR}(|e_j\rangle) \tag{2.22}$$

In practice, we do a weighted mean of the IPR of the eigenstates using the square modulus of the projections of the configuration state on the eigenstates as weight because it is already normalized. Looking at graphical representations of the two quantities we have just described, we can notice some differences between them. First of all we can analyze the evolved IPR in figure 2.13. Here we see a situation strongly similar to that we have observed for the imbalance and the fidelity. There are some differences given by the fact that the imbalance is an observable acting on the ket vector, so that its value is proportional to the square of the linear combination coefficients $|\langle c_k|c(t)\rangle|^2$, while the fidelity is the modulus of the projection of the evolved state on the initial one $|\langle c(0)|c(t)\rangle|$, so that it represents only the most significant term of the IPR when it is raised to the fourth power. Nevertheless, the phase diagrams show the same behaviour. Slightly different is the situation for the WIPR. In this case, figure 2.14, an anomalous behaviours appear. In particular, we see that with respect to the figure 2.13, in the down right case with 4 particles, the region $V \leq U/2$ seems to be not completely localized. The difference probably lays in the different definition of the two quantities, so that the WIPR can only provide an estimation of the IPR.

2.4 Aubry-André model with p-wave superconducting term

Another regime of the model we presented in section 2.1 that can be studied is when $U = 0$ and $\Delta \neq 0$. We recover the AAH model. Starting from the view of the

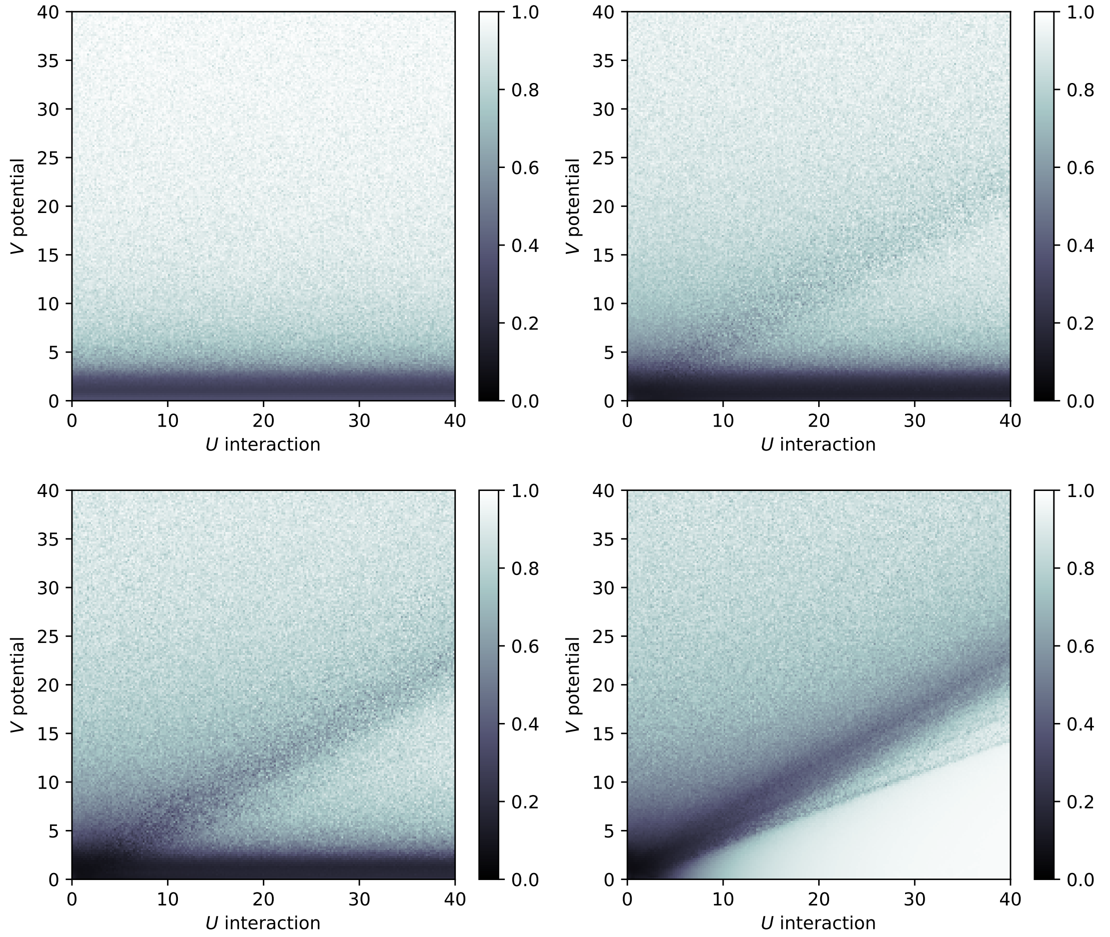

Figure 2.13: This figure represents the phase space of four different initial states in terms of the temporal mean of the IPR of the evolved state. Practically, for every value of U and V we evolved the initial configuration state from 20 to 30 time units and performed the mean of 50 values of the IPR picked up in this interval. Moreover we performed also the mean on 10 realizations of α_0. As we can see, the phase diagram is almost the same of imbalance and fidelity. The values of U and V are 200 equally spaced between 0 and 40.

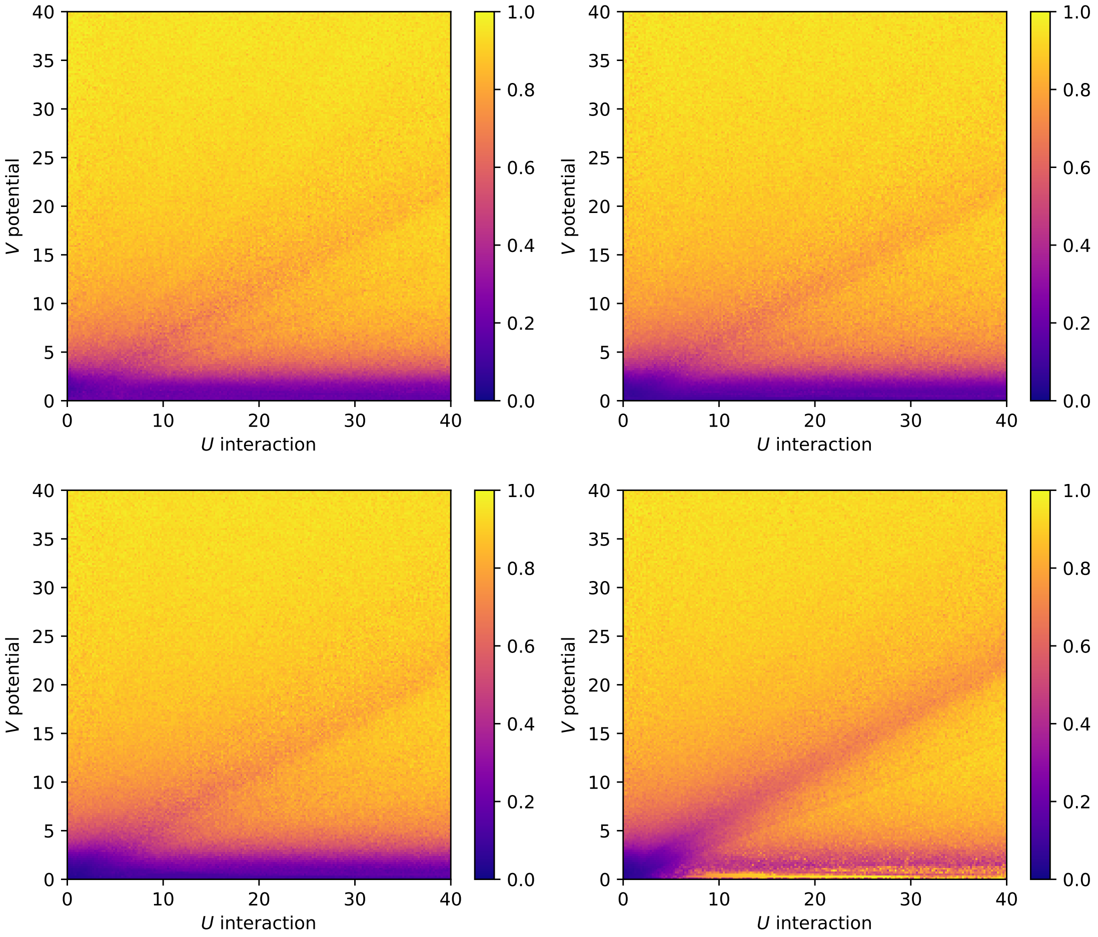

Figure 2.14: This figure represents the phase space of four different initial states in terms of Weighted IPR. Practically, for every value of U and V we performed the weighted mean of the IPR using as weights the square modulus of the projection of the configuration state on the eigenstates. Moreover we performed also the mean on 10 realizations of α_0. As we can see, even with some differences, the form of the phase diagram is the same of imbalance and fidelity. The values of U and V are 200 equally spaced between 0 and 40.

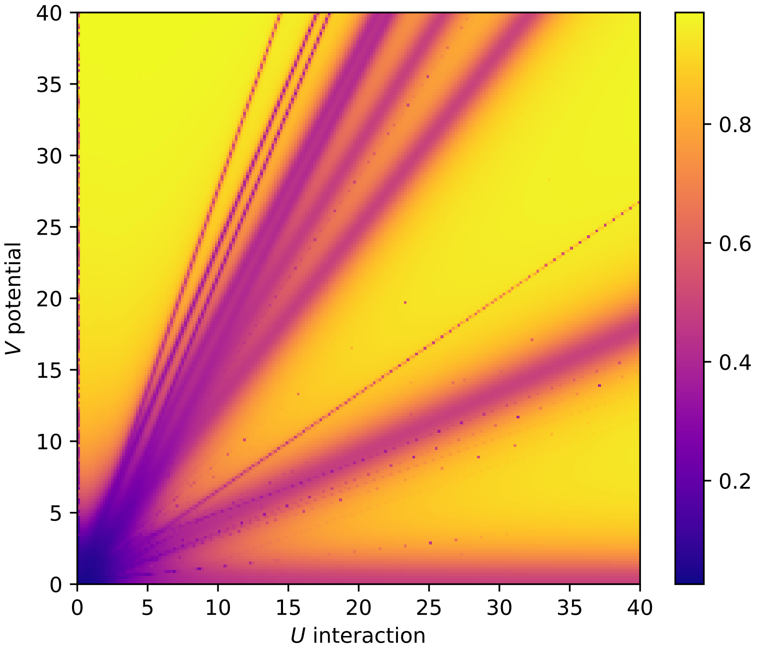

Figure 2.15: Here there is the phase diagram of the the weighted-IPR, WIPR. It is obtained, given values of U and V, computing the IPR for every eigenstate. Then, given a configuration state, is performed a weighted mean of the IPR of the eigenstates using the square modulus of the projections of the configuration state on the eigenstates basis as weight. In this case we can see this operation made for the Néel state with $\alpha_0 = 0$.

Hamiltonian, we can find some new features respect to the previous cases. Here the p-wave superconductor term $\hat{\Delta} = \Delta \sum_0^L (f_j^\dagger f_{j+1}^\dagger + f_j f_{j+1})$ creates/destroy a couple of particle in adjacent sites. This change deeply the properties of our system.

2.4.1 Hamiltonian and Hilbert space description

From figure 2.16 we can observe also graphically that the number of particles is not conserved anymore. This is represented by the off-diagonal blue dots in the upper left image: in the number basis the Hamiltonian is not made only by blocks. On the contrary, the superconductive term inexorably creates one particle in an even site and another in an odd site. This effect leave unchanged the imbalance, but only if it is not normalized with respect to the number of particles. In the end, the only quantity conserved in a system with the hopping term, the potential and the superconductive one is the parity. The parity operator $\hat{\mathcal{P}}$ is defined in the following way:

$$\hat{\mathcal{P}} = \prod_{j=0}^{L-1} (I - 2 f_j^\dagger f_j) \tag{2.23}$$

It has value -1 if the number of particles is odd and 1 if the number of particles is even. So that, the Hamiltonian mixes the states in the subspaces with the same parity of particles.

2.4.2 IPR phase diagrams and time evolution

To study the phase diagram we can start with the evolved IPR. As we can see from figure 2.17, the situation is quite specular to that we observed in the case with U turned on. As we expected, the superconductive term amplifies the extended phase. In fact now the evolved state can spread out on a subspace with dimensionality 2^{L-1}, that is half of the total dimension. So that, we should observe a localized regime approximately when $V \geq 2|\Delta + 1|$, according to the theoretical prediction given in section 1.5.1. Clearly, for an 8-sites simulation we cannot pretend to have a net division between the localized and the extended phase. The same, looking at the evolution of the localization in the initial state we can see that the evolution is confined in the subspace with the same parity 2.18.

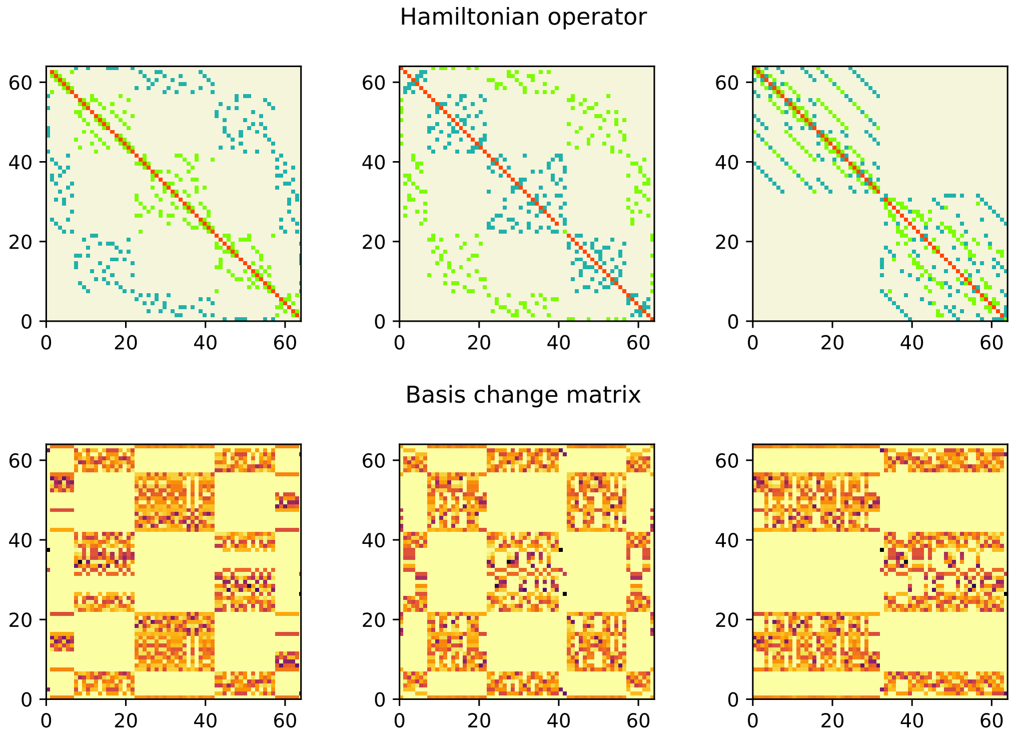

Figure 2.16: Here we can see the AAH Hamiltonian and their basis change respect to other three different basis. On the left we have the relation with the different basis. Now the blue dots are referred to the superconductive term. We can see that in the number operator basis, they break the block diagonality of the operator, because the Hamiltonian put in communication subspaces with the same parity of particles. The same, the basis change projects the eigenvectors on the configuration states with the same parity. At center, we can see the same Hamiltonian in the imbalance basis. Now the superconductive term preserve this quantity, while the hopping one not. In the last case on the right, we have all represented in the parity operator basis, that is the only quantity conserved by the system, in which the Hamiltonian shows 2 blocks belonging to the subspaces with an even ad an odd number of particles.

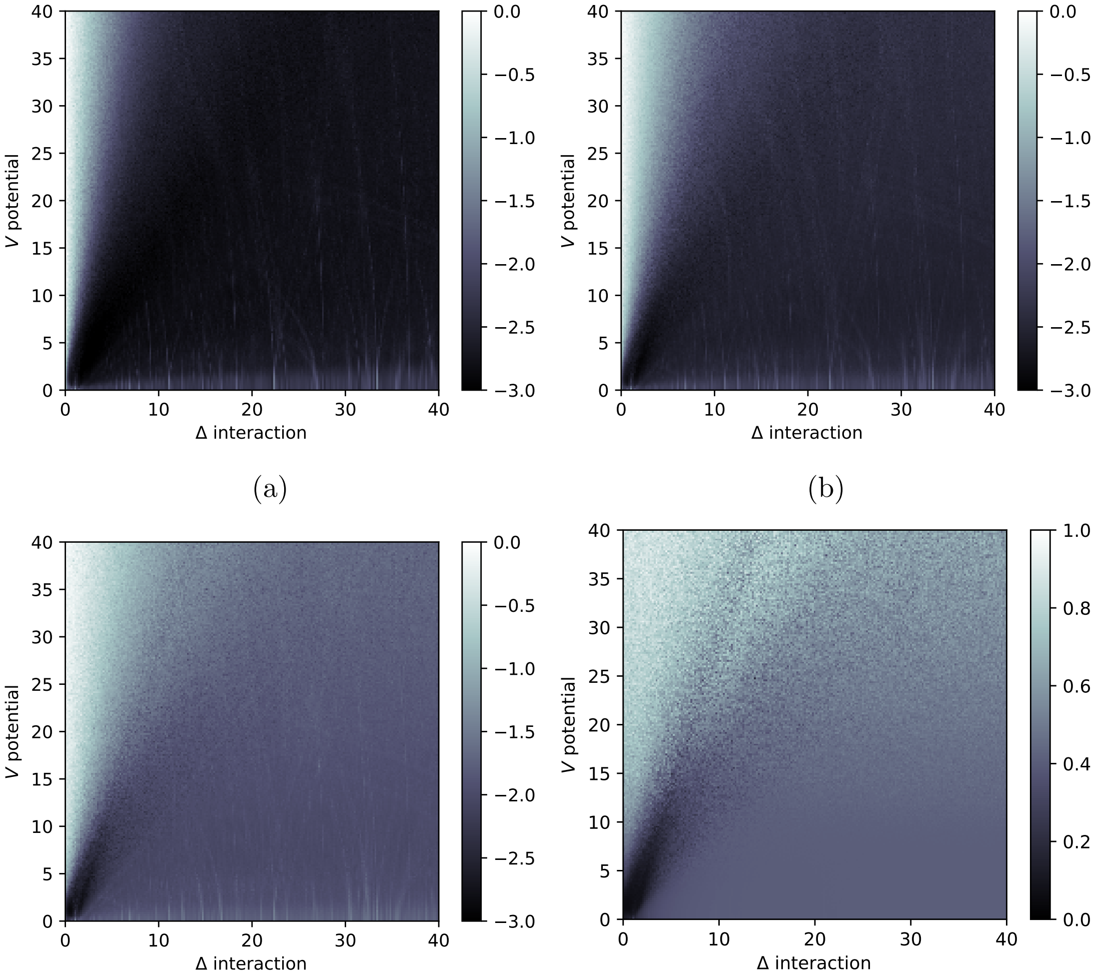

(a)

(b)

(c)

(d)

Figure 2.17: Here we see the phase diagram of the evolved IPR. The sampling strategy used is always taking 50 values in the interval between 20 and 30 time units. Moreover the mean is performed on 10 realizations of the random parameter. Notice that the first three pictures are represented in logarithmic colorscale. The initial states are: the single particle one (a), the two alternate particle (b), the three alternate (c) and the Néel state (d).

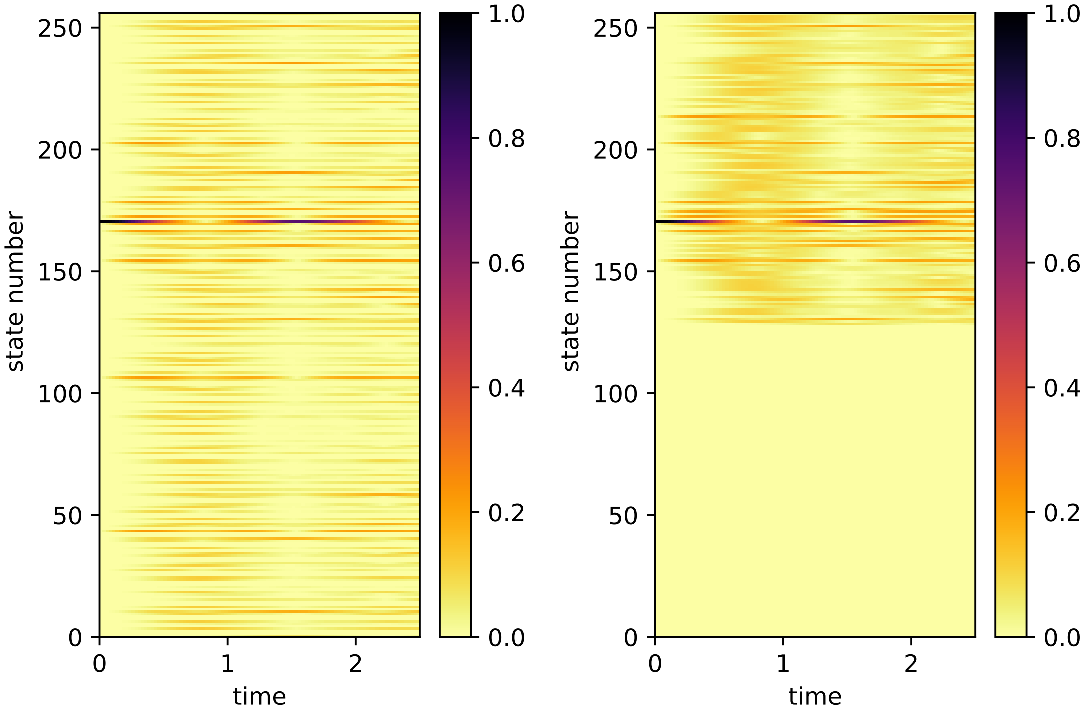

(a) (b)

Figure 2.18: Here we have the evolution of the projections of the Néel state on the configuration states. We have the scheme of the configuration basis (a) and the same evolution (b) made in the parity operator basis. Here we can easily see that our state evolves exploring the half of Hilbert space with the same parity. To perform our evolution we have chosen $V = 1$, $\Delta = 1$ and $J = 1$. Moreover, the simulation is made on 20 realizations of the random parameter.

2.5 Duality transformations for Aubry-André model with p-wave superconductor

We can study the duality of the Aubry-André model with p-wave superconducting term. Until now none explicit expression of the Aubry-André duality for this model is known. The main problem is that we have to absorb the p-wave superconducting term in the Anderson duality transformations (1.10). In section 1.3.1 we have shown all the steps that lead to the duality symmetry in the Aubry-André model. Moreover, we have seen that from the duality symmetry it is possible also recover the phase transition line. We show now how to get a similar result including the p-wave term, obtaining a transformation that maps the Schrodinger equation to another one in the phase space.

First of all, to diagonalize the following Hamiltonian:

$$H = \sum_{j=1}^{N} -J(f_j^\dagger f_{j+1} + f_{j+1}^\dagger f_j) + \Delta(f_{j+1}^\dagger f_j^\dagger + f_{j+1} f_j) - V cos(2\pi j \phi + \alpha_0) f_j^\dagger f_j \tag{2.24}$$

we have to use the Bogoliubov De Gennes transformations. We define a new set of ladder operators η and $\eta^\dagger$ that turn the original Hamiltonian into the canonical one:

$$H = \sum_{j=1}^{N} E_j (\eta_j^\dagger \eta_j - \frac{1}{2})$$

where

$$\eta_j^\dagger = \sum_{n}^{N} (u_{n,j} f_j^\dagger + v_{n,j} f_j)$$

with u and v coefficients of the transformations chosen to be real. Defining the wave function in the following way

$$|\psi_j\rangle = [u_{j,1}, v_{j,1}, u_{j,2}, v_{j,2}, ..., u_{j,N} u_{j,N}]^T \tag{2.25}$$

we can write the Schrodinger equation:

$$E\,|\psi_j\rangle = H\,|\psi_j\rangle \tag{2.26}$$

from this relation we get an equation for the u_n and v_n, hiding the energy level index j:

$$Ev_n = J(v_{n+1} + v_{n-1}) + \Delta(u_{n+1} - u_{n-1}) + V_n v_n \tag{2.27}$$

$$Eu_n = -J(u_{n+1} + u_{n-1}) - \Delta(v_{n+1} - v_{n-1}) - V_n u_n \tag{2.28}$$

As we can see now we have two equation to transform, moreover the Δ terms mixes u_n and v_n. The first task is to write the previous equations in a clearer form. To do this we can put u_n and v_n in a column vector $\vec{\psi}_j = (u_n, v_n)^T$, then the equations reads:

$$E\begin{pmatrix} v_n \\ u_n \end{pmatrix} = J\begin{pmatrix} 1 & 0 \\ 0 & -1 \end{pmatrix}\begin{pmatrix} v_{n+1}+v_{n-1} \\ u_{n+1}+u_{n-1} \end{pmatrix} + \Delta\begin{pmatrix} 0 & 1 \\ -1 & 0 \end{pmatrix}\begin{pmatrix} v_{n+1}-v_{n-1} \\ u_{n+1}-u_{n-1} \end{pmatrix} + V_n\begin{pmatrix} 1 & 0 \\ 0 & -1 \end{pmatrix}\begin{pmatrix} v_n \\ u_n \end{pmatrix} \tag{2.29}$$

Substituting $\vec{\psi}_j$:

$$E\vec{\psi}_n = J\sigma^z(\vec{\psi}_{n+1} + \vec{\psi}_{n-1}) + \Delta i\sigma^y(\vec{\psi}_{n+1} - \vec{\psi}_{n-1}) + V_n\sigma^z\vec{\psi}_n \tag{2.30}$$

We can notice that the Pauli matrices appear in the equation formulated in this way. Now we can write our duality transformations, where the imaginary unit is replaced by the $i\sigma^x$ matrix.

$$\vec{\psi}_n = \sum_m e^{i\sigma^x m(cn+d+\beta)} e^{i\sigma^x n(d-\beta)} \vec{\varphi}_m \tag{2.31}$$

Where we use the Euler formula in the following matrix form:

$$e^{i\sigma^x t} = \mathbb{I}\cos(t) + i\sigma^x \sin(t) \tag{2.32}$$

Then we can proceed as done in the 1.3.1 computing the transformed terms. The right side of equation (2.30):

$$E\vec{\psi}_n = \sum_m e^{i\sigma^x m(cn+d+\beta)} e^{i\sigma^x n(d-\beta)} E\vec{\varphi}_m = \sum_m e^{-i\sigma^x m(cn+d+\beta)} e^{-i\sigma^x n(d-\beta)} E\vec{\varphi}_{-m,-d} \tag{2.33}$$

In the last step we have changed the sign of m and d because the next terms does not commute with the exponential. The index d is implied in the next calculations. On the other hand for the hopping term we have:

$$\begin{aligned} J\sigma^z(\vec{\psi}_{n+1} + \vec{\psi}_{n-1}) &= 2J\sigma^z \sum_m e^{i\sigma^x m(cn+d+\beta)} e^{i\sigma^x n(d-\beta)} \left[\cos(cm+d-\beta)\vec{\varphi}_m\right] = \\ &= \sum_m e^{-i\sigma^x m(cn+d+\beta)} e^{-i\sigma^x n(d-\beta)} 2J\sigma^z \cos(cm+d-\beta)\vec{\varphi}_m \end{aligned} \tag{2.34}$$

Notice that when σ^z passes through the sum the exponential changes sign, due to the anti-commutation of Pauli matrices. The superconductive one instead gives:

$$\begin{aligned} &\Delta i\sigma^y(\vec{\psi}_{n+1} - \vec{\psi}_{n-1}) = \\ &= 2\Delta i\sigma^y \sum_m e^{i\sigma^x m(cn+d+\beta)} e^{i\sigma^x n(d-\beta)} \left[i\sigma^x \sin(cm+d-\beta)\vec{\varphi}_m\right] = \\ &= \sum_m e^{-i\sigma^x m(cn+d+\beta)} e^{-i\sigma^x n(d-\beta)} 2\Delta(-i\sigma^z)\sin(cm+d-\beta)\vec{\varphi}_m \end{aligned} \tag{2.35}$$

Also here the exponential changes sign when σ^y is taken into the sum. Now we can work out the transformations for the incommensurate potential:

$$\begin{aligned}
&\sigma^z V_n \psi_n = \sigma^z V\cos(cn+d) = \\
&= \sigma^z \sum_m e^{i\sigma^x m(cn+d+\beta)} e^{i\sigma^x n(d-\beta)} \frac{V}{2}\left(e^{i\sigma^x (cn+d)} + e^{-i\sigma^x (cn+d)}\right)\vec{\varphi}_m = \\
&= \sigma^z \sum_l e^{i\sigma^x (l+1)(cn+d+\beta)} e^{i\sigma^x n(d-\beta)} e^{-i\sigma^x \beta}\frac{V}{2}\vec{\varphi}_l + \\
&+ \sigma^z \sum_l e^{i\sigma^x (k-1)(cn+d+\beta)} e^{i\sigma^x n(d-\beta)} e^{-i\sigma^x \beta}\frac{V}{2}\vec{\varphi}_k
\end{aligned} \tag{2.36}$$

Now, doing the same trick we used in the Anderson transformation, we can translate the sum indexes and reorder the various terms:

$$\begin{aligned}
&\sigma^z V_n \psi_n = \sigma^z \sum_m e^{i\sigma^x m(cn+d+\beta)} e^{i\sigma^x n(d-\beta)} \frac{V}{2}(\vec{\varphi}_{m+1} e^{-i\sigma^x \beta} + \vec{\varphi}_{m-1} e^{i\sigma^x \beta}) = \\
&= \sigma^z \sum_m e^{i\sigma^x m(cn+d+\beta)} e^{i\sigma^x n(d-\beta)} \frac{V}{2} \times \\
&\times \left[\cos(\beta)(\vec{\varphi}_{m+1} + \vec{\varphi}_{m-1}) - i\sigma^x \sin(\beta)(\vec{\varphi}_{m+1} - \vec{\varphi}_{m-1})\right]
\end{aligned} \tag{2.37}$$

Then we can take σ^z into the sum:

$$\begin{aligned}
&\sigma^z V_n \psi_n = \\
&= \sum_m e^{-i\sigma^x m(cn+d+\beta)} e^{-i\sigma^x n(d-\beta)} \frac{V}{2} \times \\
&\times \left(\sigma^z \cos(\beta)(\vec{\varphi}_{m+1} + \vec{\varphi}_{m-1}) + \sigma^y \sin(\beta)(\vec{\varphi}_{m+1} - \vec{\varphi}_{m-1})\right)
\end{aligned} \tag{2.38}$$

we can write the equation for ϕ_m reintroducing the d index:

$$\begin{aligned}
E\vec{\varphi}_{-m,-d} =& \frac{V}{2}\sigma^z \cos(\beta)(\vec{\varphi}_{m+1,d} + \vec{\varphi}_{m-1,d}) + \frac{V}{2}\sigma^y \sin(\beta)(\vec{\varphi}_{m+1,d} - \vec{\varphi}_{m-1,d}) + \\
&+ 2J\sigma^z \cos(cm+d-\beta)\vec{\varphi}_{m,d} - 2i\Delta\sigma^z \sin(cm+d-\beta)\vec{\varphi}_{m,d}
\end{aligned} \tag{2.39}$$

Now, we want a complete equivalence with (2.30), so we have to manipulate two terms of (2.39) to get :

$$\begin{aligned}
&2J\sigma^z \cos(cm+d-\beta)\vec{\varphi}_m - 2i\Delta\sigma^z \sin(cm+d-\beta)\vec{\varphi}_m = \\
&= 2J\sigma^z \left(\cos(cm+d-\beta) - i\frac{\Delta}{J}\sin(cm+d-\beta)\right)
\end{aligned} \tag{2.40}$$

Clearly, the choice to put in evidence J is arbitrary. It can be done also with Δ, but the result is the same. We can pose, $\frac{\Delta}{J} = -i\tan(\beta)$. Then we have:

$$\begin{aligned}
&2J\sigma^z\Big(\cos(cm+d-\beta) - \tan(\beta)\sin(cm+d-\beta)\Big) = \\
&= \frac{2J}{\cos(\beta)} 2J\sigma^z\Big(\cos(\beta)\cos(cm+d-\beta) - \sin(\beta)\sin(cm+d-\beta)\Big) = \\
&= \frac{2J}{\cos(\beta)}\sigma^z cos(cn+d-\beta+\beta) = \frac{2J}{\cos(\beta)}\cos(cn+d) = \frac{2J_n}{\cos(\beta)}
\end{aligned} \tag{2.41}$$

Now the equation for $\vec{\varphi}$ is the following:

$$E\vec{\varphi}_{-m,-d} = \frac{V\cos(\beta)}{2}\sigma^z(\vec{\varphi}_{m+1,d}+\vec{\varphi}_{m-1,d}) + \frac{V\sin(\beta)}{2}\sigma^y(\vec{\varphi}_{m+1,d}-\vec{\varphi}_{m-1,d}) + \frac{2J_n}{\cos(\beta)}\sigma^z\vec{\varphi}_{m,d} \tag{2.42}$$

Now we have the same functional form of (2.30) for the Schrodinger equation of and we can explicit the duality relations:

$$\begin{cases} V \longrightarrow 2J/\cos(\beta) \\ J \longrightarrow V\cos(\beta)/2 \quad \text{with} \quad \frac{\Delta}{J} \longrightarrow -i\tan(\beta) \\ \Delta \longrightarrow -iV\sin(\beta)/2 \end{cases} \tag{2.43}$$

Notice that the condition we $\frac{\Delta}{J} = -i\tan(\beta)$ implies that β is an imaginary angle. So that the circular $\cos(\beta)$ and $\sin(\beta)$ become respectively $\cosh(|\beta|)$ and $i\sinh(|\beta|)$. We can express them writing $\sin(\beta)$ and $\cos(\beta)$ as functions of the tangent:

$$\begin{cases} \cos(\beta) = \frac{1}{\sqrt{1-(\Delta/J)^2}} \\ \sin(\beta) = i\frac{\Delta/J}{\sqrt{1-(\Delta/J)^2}} \end{cases} \tag{2.44}$$

In the square root $\tan(\beta)^2 = -(\Delta/J)^2$. As expected they are the expression of the hyperbolic sine and cosine as function of the hyperbolic tangent. We get a form with an explicit dependence from J and Δ:

$$\begin{cases} V \longrightarrow 2J\sqrt{1-(\Delta/J)^2} \\ J \longrightarrow V\frac{1}{2\sqrt{1-(\Delta/J)^2}} \\ \Delta \longrightarrow V\frac{\Delta/J}{2\sqrt{1-(\Delta/J)^2}} \end{cases} \tag{2.45}$$

Notice that these transformations are completely real when Δ is less than J. In the end, we get an explicit expression for the transformations that map the initial constants to new constants. The new constants that identify another system laying in the opposite Anderson phase with respect to the previous one (extended or localized)

2.5.1 Properties of the duality transformations

Now we can analyze the transformations and try to check if they are consistent with the Aubry-André limit and if they share the same properties.

We can rewrite our transformations with the explicit dependence from J and Δ. They can be put in a matrix $\mathbb{D}$ and looks as follow:

$$\begin{pmatrix} V' \\ J' \\ \Delta' \end{pmatrix} = \begin{pmatrix} 0 & 2\sqrt{1-(\Delta/J)^2} & 0 \\ \frac{1}{2\sqrt{1-(\Delta/J)^2}} & 0 & 0 \\ \frac{\Delta/J}{2\sqrt{1-(\Delta/J)^2}} & 0 & 0 \end{pmatrix} \begin{pmatrix} V \\ J \\ \Delta \end{pmatrix} \tag{2.46}$$

As we can see they are highly non-linear transformations, but some result can be achieved. Moreover, one can check that also for the other component of $\vec{\psi}$ the transformations have the same form. The first counter-proof to check the self-consistency of our transformations is looking at their limits. The limit for $\Delta \to 0$ is immediately done:

$$\lim_{\Delta\to 0} \begin{pmatrix} 0 & 2\sqrt{1-(\Delta/J)^2} & 0 \\ \frac{1}{2\sqrt{1-(\Delta/J)^2}} & 0 & 0 \\ \frac{\Delta/J}{2\sqrt{1-(\Delta/J)^2}} & 0 & 0 \end{pmatrix} = \begin{pmatrix} 0 & 2 & 0 \\ \frac{1}{2} & 0 & 0 \\ 0 & 0 & 0 \end{pmatrix} \tag{2.47}$$

As we can see, it is exactly the matrix we got for the Aubry-André duality. On the contrary, this formulation is not suitable for the limit $J \to 0$ because the term $\sqrt{1+(\Delta/J)^2}$ diverges on the first row. This is not a problem because can be developed equivalent transformations, putting in evidence Δ instead of J in the equation (2.40). They turn out to be:

$$\mathbb{D}_{AA} = \begin{pmatrix} 0 & 0 & 2\frac{J}{\Delta}\sqrt{1-(\Delta/J)^2} \\ \frac{1}{2\sqrt{1-(\Delta/J)^2}} & 0 & 0 \\ \frac{\Delta/J}{2\sqrt{1-(\Delta/J)^2}} & 0 & 0 \end{pmatrix} \tag{2.48}$$

Whose limit $J \to 0$ is not well defined because it is imaginary. Nevertheless, it suggests a duality for the subsystem made by the incommensurate potential plus the superconductive term:

$$\lim_{J\to 0} \begin{pmatrix} 0 & 0 & 2\frac{J}{\Delta}\sqrt{1-(\Delta/J)^2} \\ \frac{1}{2\sqrt{1-(\Delta/J)^2}} & 0 & 0 \\ \frac{\Delta/J}{2\sqrt{1-(\Delta/J)^2}} & 0 & 0 \end{pmatrix} = \begin{pmatrix} 0 & 0 & 2i \\ 0 & 0 & 0 \\ -i/2 & 0 & 0 \end{pmatrix} \tag{2.49}$$

Notice that in the third row: $\lim_{J\to 0} \frac{\Delta/J}{\sqrt{1-(\Delta/J)^2}} = i$.

Another property that we want to show is the idempotence, that is iterating two times the transformations gives the identity. For example when we studied the Anderson duality for the AA model, we get a matrix $\mathbb{D}$ whose square was the identity. Now the same procedure can be done getting the following result:

$$\begin{pmatrix} V' \\ J' \\ \Delta' \end{pmatrix} = \begin{pmatrix} 1 & 0 & 0 \\ 0 & 1 & 0 \\ 0 & \frac{\Delta}{J} & 0 \end{pmatrix} \begin{pmatrix} V \\ J \\ \Delta \end{pmatrix} = \begin{pmatrix} 1 & 0 & 0 \\ 0 & 1 & 0 \\ 0 & 0 & 1 \end{pmatrix} \begin{pmatrix} V \\ J \\ \Delta \end{pmatrix} \tag{2.50}$$

The non-linearity is crucial to get explicitly the identity. In fact, when we multiply the last row of the first matrix we get exactly Δ, so that we can rewrite the identity in the canonical way. Another important feature of our transformations is that they are homogeneous. In fact, if we do the replacement:

$$\begin{cases} V \longrightarrow kV \\ \Delta \longrightarrow k\Delta \\ J \longrightarrow kJ \end{cases} \tag{2.51}$$

where k could be also a function $k(V, J, \Delta)$. we can see that the transformation does not change their form, because it depends non-linearly only by the ratio Δ/J. So, we can conclude that in the space of couplings holds $\mathbb{D}(k\vec{V}) = k\mathbb{D}(\vec{V})$. This result can be generalized because these transformations are completely linear in V. In fact, as long as the ratio Δ/J is fixed, they are linear. Roughly speaking, the following relation holds:

$$\mathbb{D}\left(\begin{pmatrix} aV_1 \\ aJ \\ a\Delta \end{pmatrix} + \begin{pmatrix} bV_2 \\ bJ \\ b\Delta \end{pmatrix}\right) = a\mathbb{D}\begin{pmatrix} V_1 \\ J \\ \Delta \end{pmatrix} + b\mathbb{D}\begin{pmatrix} V_2 \\ J \\ \Delta \end{pmatrix} \tag{2.52}$$

From a geometrical point of view, once fixed the ratio $\Delta/J = m$, we have linear transformations in the plane spanned by the ax V and the line of equation $\Delta = mJ$ in the plane J-Δ. In a few words, we have a family of transformations labeled by the ratio m.

2.5.2 Finding duality

Our goal is to find a plane in which the transformation acts like the identity. Given that surface, we immediately can conclude that the transformations maps the system over that surface, determining the Anderson transition. In the Aubry-André duality, this corresponds to the eigenvector belonging to the eigenvalue +1. In that case it was simple to do it because the transformation was a linear application. Now, we cannot repeat the same procedure, but an analogous of eigenvectors and eigenvalues can be found. In fact, given the structure of our transformations, we should have two eigenvectors for every value of the ratio Δ/J, because we have seen that once fixed this ratio the transformations are linear. For example we can look at the parametrization given by $\vec{\lambda}_1 = \left(\Delta, J, 2J\sqrt{1-(\frac{\Delta}{J})^2}\right)^T$ and look in what vector is mapped by $\mathbb{D}$:

$$\begin{pmatrix} 0 & 2\sqrt{1-(\Delta/J)^2} & 0 \\ \frac{1}{2\sqrt{1-(\Delta/J)^2}} & 0 & 0 \\ \frac{\Delta/J}{2\sqrt{1-(\Delta/J)^2}} & 0 & 0 \end{pmatrix} \begin{pmatrix} 2J\sqrt{1-(\frac{\Delta}{J})^2} \\ J \\ \Delta \end{pmatrix} = \begin{pmatrix} 2J\sqrt{1-(\frac{\Delta}{J})^2} \\ J \\ \Delta \end{pmatrix} \tag{2.53}$$

surprisingly this vector is mapped into itself, so we can consider it as an eigenvector with eigenvalue $+1$. A similar computation can be done for the eigenvector $\vec{\lambda}_{-1} = \left(\Delta, -J, 2J\sqrt{1-(\frac{\Delta}{J})^2}\right)^T$ that is mapped into its opposite, with eigenvalue -1. Notice that for every eigenvector we have a multiple choice of $\pm\Delta$, but we are interested in the region with positive constants. Now we have formalized the dual surface as the variety given by the equation:

$$V = 2\sqrt{J^2 - \Delta^2} \tag{2.54}$$

The homogeneity of the transformations tell us that if a point Q is on the critical surface, also all the points that lies in the line passing through the origin O and the point Q are in the critical surface. So that the space of couplings is perfectly divided in an extended phase and in a localized phase. Then, we can use the argument used for Aubry-André duality to show that our transformations map points from one side to the other side of the surface:

Given $\begin{cases} V' = 2J\sqrt{1-(\Delta/J)^2} \\ \Delta' = -V\Delta/2J\sqrt{1-(\Delta/J)^2} \\ J' = V/2\sqrt{1-(\Delta/J)^2} \end{cases}$, we can take a point in the extended phase.

Then, this point fulfills the following inequality: $V < 2J\sqrt{1-(\Delta/J)^2}$

We can write the following chain of inequalities:

$V' = 2J\sqrt{1-(\Delta/J)^2} > V = 2J'\sqrt{1-(\Delta/J)^2}$

that implies $V' > 2J'\sqrt{1-(\Delta'/J')^2}$

(2.55)

Notice that in the last expression $\Delta'/J' = \Delta/J$ because the transformations leave unchanged the ratio. So, we have showed that our transformations map a point under the surface $V = 2J\sqrt{1-(\Delta/J)^2}$ to another one over that surface. This is what concerned the sector $\Delta < J$.

2.5.3 Extension of duality

The transformations we got can be extended to recover the entire phase diagram like that shown in fig 1.6. In the previous section we have derived the following critical surface:

$$V^2 = 2J^2 - 2\Delta^2 \tag{2.56}$$

and the following transformations:

$$\begin{cases} V \longrightarrow 2\sqrt{J^2 - \Delta^2} \\ J \longrightarrow V\frac{J}{2\sqrt{J^2-\Delta^2}} \\ \Delta \longrightarrow V\frac{\Delta}{2\sqrt{J^2-\Delta^2}} \end{cases} \tag{2.57}$$

that are real in the region $\Delta < J$. So, looking at figure 2.19 (a), in the plane V-Δ we have transformations that map points in the red zone inside the ellipse $V^2 + 2\Delta^2 = 2J^2$ to points in the black zone outside the ellipse. Clearly the blue line fixes the limit of validity of the transformations. On the other hand, we can manipulate the equation 2.30 to get the extension on the values $\Delta > J$. This extension can be obtained adding a phase with the following transformation:

$$\psi_n = e^{i\sigma^y \frac{\pi}{2}} \psi'_n \tag{2.58}$$

applied on 2.30. Then one applies the transformations 2.31 and again 2.58. The result is the following:

$$E\vec{\varphi}_{m,d} = \frac{V\cos(\beta)}{2}(\vec{\varphi}_{m+1,d} + \vec{\varphi}_{m-1,d}) - \frac{V\sin(\beta)}{2} i\sigma^x(\vec{\varphi}_{m+1,d} - \vec{\varphi}_{m-1,d}) + \frac{2\Delta_n}{\cos(\beta)}\vec{\varphi}_{m,d} \tag{2.59}$$

Where we imposed:

$$\frac{J}{\Delta} = i\tan(\beta) \tag{2.60}$$

instead of $\frac{\Delta}{J} = i\tan(\beta)$. The result is that the extended transformations are real for $\Delta > J$:

$$\begin{cases} V \longrightarrow \pm 2\sqrt{\Delta^2 - J^2} \\ J \longrightarrow \pm V\frac{J}{2\sqrt{\Delta^2-J^2}} \\ \Delta \longrightarrow \pm V\frac{\Delta}{2\sqrt{\Delta^2-J^2}} \end{cases} \tag{2.61}$$

Notice that the sign ± arise because the two components are decoupled by the transformations. Nevertheless, the physics of the system does not change. In fact, the critical surface is the same for both the component of $\vec{\varphi}_m$:

$$V^2 = 2\Delta^2 - 2J^2 \tag{2.62}$$

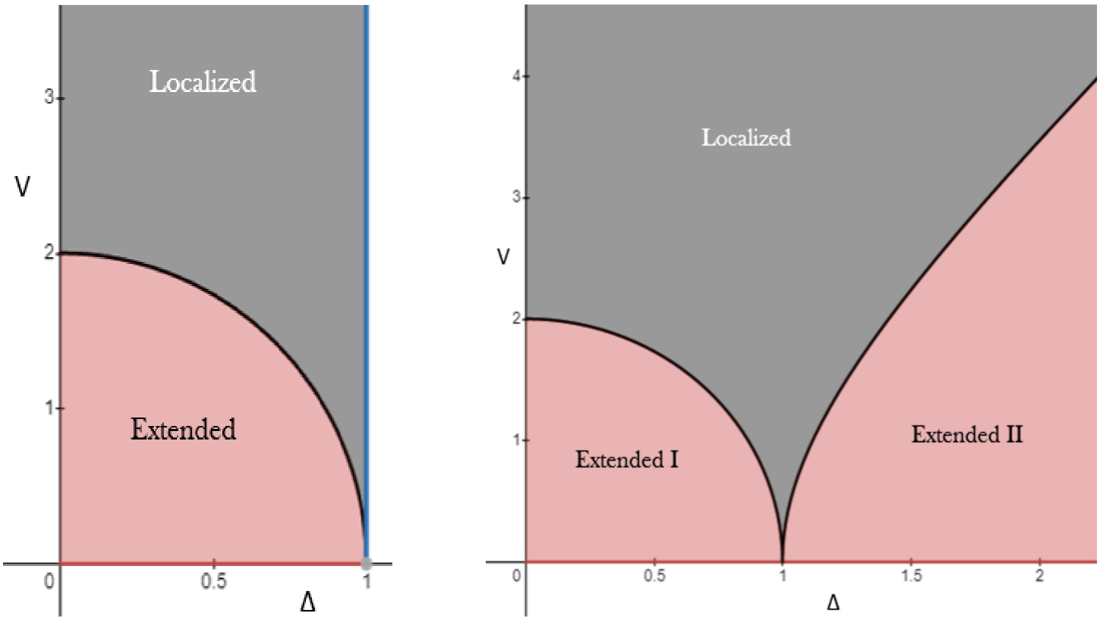

(a) (b)

Figure 2.19: Here we can see the partial phase diagram made with the transformations 2.57 and 2.65 for $J = 1$. In (a) we have the partial critical surface represented by the black solid line. Our transformations map points in the red region with points in the black region. On the critical surface, instead, the points are mapped into themselves. The blue line indicates the maximum value of Δ for which the transformations are real. In (b) we can see the phase diagram with the extended duality. Geometrically, we added to the ellipse $V^2 + 2\Delta^2 = 2J^2$ a branch of the hyperbola $V^2 - 2\Delta^2 = 2J^2$. This give rise to two extended zones: Extended I and Extended II. Now, also the points in the region Extended II are mapped in the localized phase by the duality transformations.

For those transformations, all the properties we have showed in section 2.5.1 are conserved, except the limits that are exchanged. Now the limit $J \to 0$ is real:

$$\lim_{J\to 0}\begin{pmatrix} 0 & 0 & 2\sqrt{1-(J/\Delta)^2} \\ \frac{J/\Delta}{2\sqrt{1-(J/\Delta)^2}} & 0 & 0 \\ \frac{1}{2\sqrt{1-(J/\Delta)^2}} & 0 & 0 \end{pmatrix} = \begin{pmatrix} 0 & 0 & 2 \\ 0 & 0 & 0 \\ 1/2 & 0 & 0 \end{pmatrix} \tag{2.63}$$

While the limit $\Delta \to 0$ is imaginary:

$$\lim_{J\to 0}\begin{pmatrix} 0 & 2\frac{\Delta}{J}\sqrt{1-(J/\Delta)^2} & 0 \\ \frac{J/\Delta}{2\sqrt{1-(J/\Delta)^2}} & 0 & 0 \\ \frac{1}{2\sqrt{1-(J/\Delta)^2}} & 0 & 0 \end{pmatrix} = \begin{pmatrix} 0 & 2i & 0 \\ -i/2 & 0 & 0 \\ 0 & 0 & 0 \end{pmatrix} \tag{2.64}$$

Now we can write the complete version of the transformations putting together the two real branches:

$$\begin{cases} V \longrightarrow 2\sqrt{|J^2-\Delta^2|} \\ J \longrightarrow V\frac{J}{2\sqrt{|J^2-\Delta^2|}} \\ \Delta \longrightarrow V\frac{\Delta}{2\sqrt{|J^2-\Delta^2|}} \end{cases} \tag{2.65}$$

With the extended critical surface given by:

$$V^2 = 2|J^2-\Delta^2| \tag{2.66}$$

In figure 2.19 (b) we can see the phase diagram for the two branches: now there are two different extended regions.

Moreover there is a further extension using the following transformations:

$$\vec{\psi}_n = \sum_m e^{i\sigma^y m(cn+d+\beta)} e^{i\sigma^y nd} \vec{\varphi}_m \tag{2.67}$$

Notice the difference with respect to 2.31: the matrix σ^x is replaced with σ^y. Applying these transformations directly on 2.30 we get the following transformations:

$$\begin{cases} V \longrightarrow 2\sqrt{J^2+\Delta^2} \\ J \longrightarrow V\frac{J}{2\sqrt{J^2+\Delta^2}} \\ \Delta \longrightarrow V\frac{\Delta}{2\sqrt{J^2+\Delta^2}} \end{cases} \tag{2.68}$$

setting $\Delta/J = \tan(\beta)$. So, in this case β is real parameter. The critical surface for these transformations is:

$$V^2 = 2\Delta^2 + 2J^2 \tag{2.69}$$

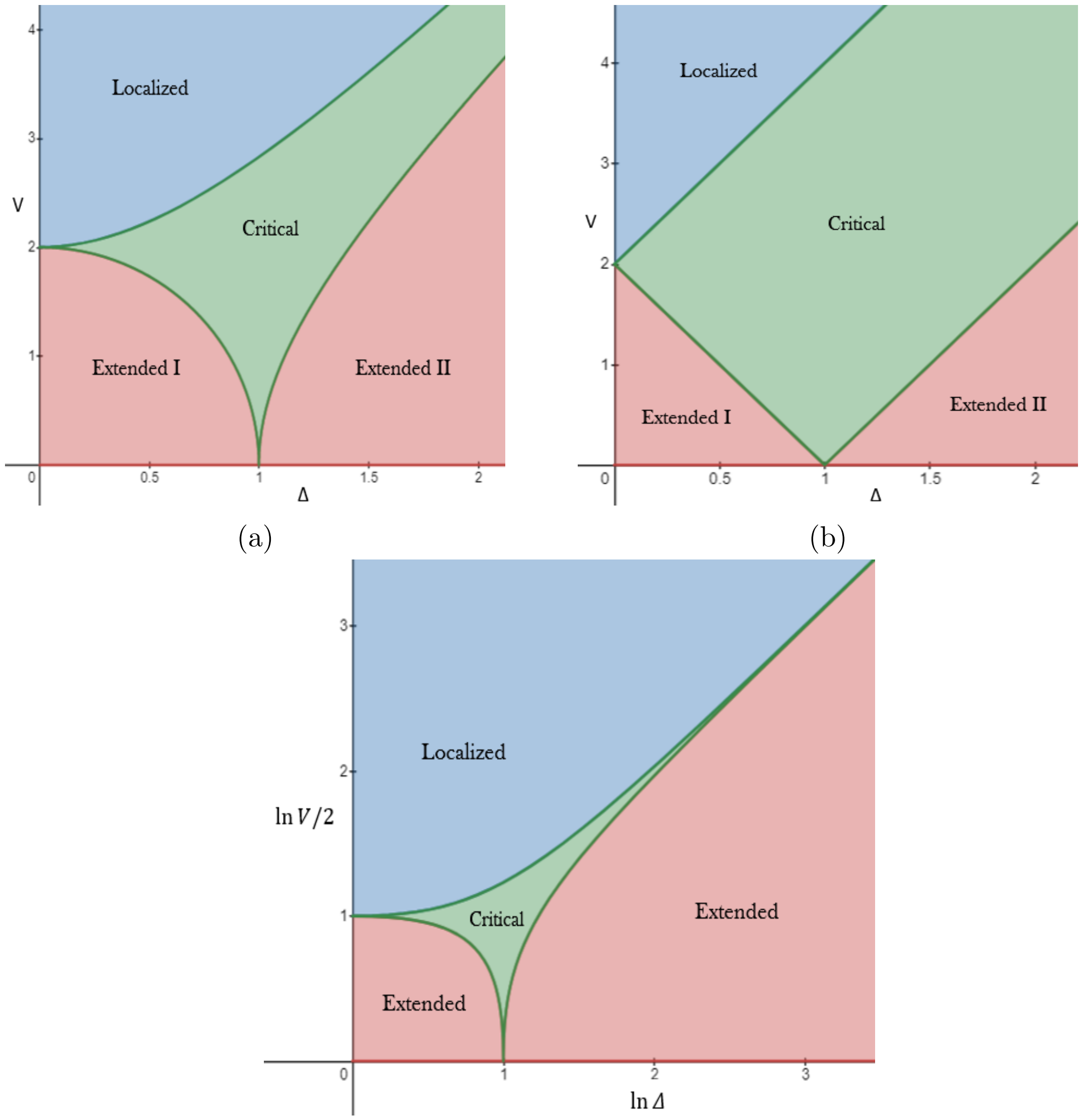

(a)

(b)

(c)

Figure 2.20: Here we can see the complete phase diagram obtained with duality transformations (a) and the phase diagram currently accepted (b). Our phase diagram is obtained combining the critical surfaces $V^2 = 2\Delta^2 + 2J^2$ and $V^2 = 2|\Delta^2 - J^2|$. By analogy with (b) we assigned to the four regions the label of the corresponding phase. We can see that the topology of the two phase diagrams is the same, but their limits are different. In fact in (a) the critical phase disappear when $V, \Delta \to \infty$, while in (b) persists. In fact, in (c) we see again our phase diagram obtained with the duality transformations in the plane V-Δ in logarithmic scale for $J = e$. Now is manifest that the critical region disappear for $\Delta, V >> J$, so that we recover the critical line $V = 2\Delta$

This last equation complete the phase space, showed in figure 2.20 (a). Here we have three different regions that can be associated, by analogy, to the extended, critical and localized phases of the diagram 2.20 (b) belonging to the theoretical prediction given by the works [18], [30],[31]. We can see that the result of our computations in significantly different from the currently accepted prediction. In fact we have:

$$\begin{cases} V_1 = 2|J^2 + \Delta^2|^{1/2} \quad \text{vs} \quad V_1 = 2|J + \Delta| \\ V_2 = 2|J^2 - \Delta^2|^{1/2} \quad \text{vs} \quad V_2 = 2|J - \Delta| \end{cases} \tag{2.70}$$

Nevertheless, we can adduce an argument to reinforce our results. The argument is the following: in the currently accepted phase diagram the critical phase persists, even in the limit $\Delta, V \to \infty$. In fact:

$$\begin{cases} \lim_{\Delta\to\infty} V_1 = \lim_{\Delta\to\infty} 2|J + \Delta| = \infty \\ \lim_{\Delta\to\infty} V_2 = \lim_{\Delta\to\infty} 2|J - \Delta| = \infty \end{cases} \tag{2.71}$$

But the quantity $|V_1 - V_2|$ remains finite as long as $J \neq 0$:

$$\lim_{\Delta\to\infty} |V_1 - V_2| = \lim_{\Delta\to\infty} 2\Big||J + \Delta| - |J - \Delta|\Big| = 4|J| \tag{2.72}$$

Of course, the same discussion can be done with the limit $J \to \infty$ because all critical surfaces are invariant under the exchange $J \iff \Delta$, but this is a non physical situation.

On the other hand, our results share the same limits for V_1 and V_2:

$$\begin{cases} \lim_{\Delta\to\infty} V_1 = \lim_{\Delta\to\infty} 2|J^2 + \Delta^2|^{1/2} = \infty \\ \lim_{\Delta\to\infty} V_2 = \lim_{\Delta\to\infty} 2|J^2 - \Delta^2|^{1/2} = \infty \end{cases} \tag{2.73}$$

But they show the correct limit for the quantity $|V_1 - V_2|$:

$$\lim_{\Delta\to\infty} |V_1 - V_2| = \lim_{\Delta\to\infty} \left| 2\Delta\sqrt{|1 + (J/\Delta)^2|} - 2\Delta\sqrt{|1 - (J/\Delta)^2|} \right| = 0 \tag{2.74}$$

In a few words the two branches in our prediction converge to the same line as we can see in the figure 2.20 (c), where the phase diagram is represented in logarithmic scale. Here we can clearly see the critical phase disappearing and, moreover, we recover the critical line $V = 2\Delta$. Instead, the currently accepted phase diagram shows a critical strip for every value of $J \neq 0$. So, in the end, we got an explicit expression for the critical surfaces that generates a new phase diagram. The new phase diagram could be proposed to solve the asymptotic problems of the currently accepted one. If supported by simulations, our results can deepen a lot the comprehension of the Aubry-André model with p-wave superconducting term.

2.6 Interacting Aubry-André model with p-wave supercoducting term

The last version of the Aubry-André model that we analyze is the most complex version with the superconducting p-wave term and the interaction. In this case cannot be done observations on the duality, because the interaction does not allow to write the single particle Hamiltonian. Moreover, applying the Fourier transform on the first-neighbor interaction, the result would be a long range interaction. This long range interaction cannot be reduced to an analogous Hamiltonian as we have done in the other cases. Nevertheless we can simulate the system setting again $J = 1$ and looking at our phase diagrams for a given initial state. We performed simulations on the $U - V$ plane for some values of Δ. In figure 2.21 we can see the phase diagram for the Neèl state and for four values of Δ. We can see that for $\Delta = 1$ (a) and $\Delta = 2$ (b) the diagram is not different respect to the $\Delta = 0$ case. On the other hand, a phase transition seems to happen for $\Delta = 5$ (c) and $\Delta = 10$ (d) because the topology of the diagrams change profoundly. In particular, emerges a localized region for small values of V. Unfortunately, we are not able to find an analytical explanation of these behaviours.

2.7 Numerical details of the simulations

For our simulations we used the pyton library qutip. This library is made on purpose of classical simulations of quantum systems. The idea behind the library is to put all phisical elements like states, eigenstates, density matrices, observables or operators in a class called `Qobj`.

Now we describe how we developed the codex to perform our simulations. Qtip is built to simulate standard quantum mechanics, so we cannot implement directly the fermionic Hamiltonians. To simuate Aubry-André like models we used the Jordan-Wigner transformations. In fact, with this method, the Hamiltonian is a sum of products of Pauli matrices that can be easily implemented in qtip. Given that, our codex starts initializing ladder operators with the relative `Qobj` given by the tensorial product of the Pauli matrices. Our library already contains the Pauli matrices as variables and the method `Qobj.tensor(args)` returns the tensor product of a given list of arguments. Provided the ladder operators, we can wrote the Hamiltonian as a `Qobj`. Then, up to the simulations we needed we used several methods. In particular, we always used the attribute `Qobj.eigenstates()` to get eigenvectors and eigenvalues of the Hamiltonian. We also plenty used the method `Qobj.sesolve()` to solve the Schrodinger equation and compute the time evolution for a given initial state. Moreover, `Qobj.sesolve()` can be used also to get the time evolution of the expectation value of a given operator. We used

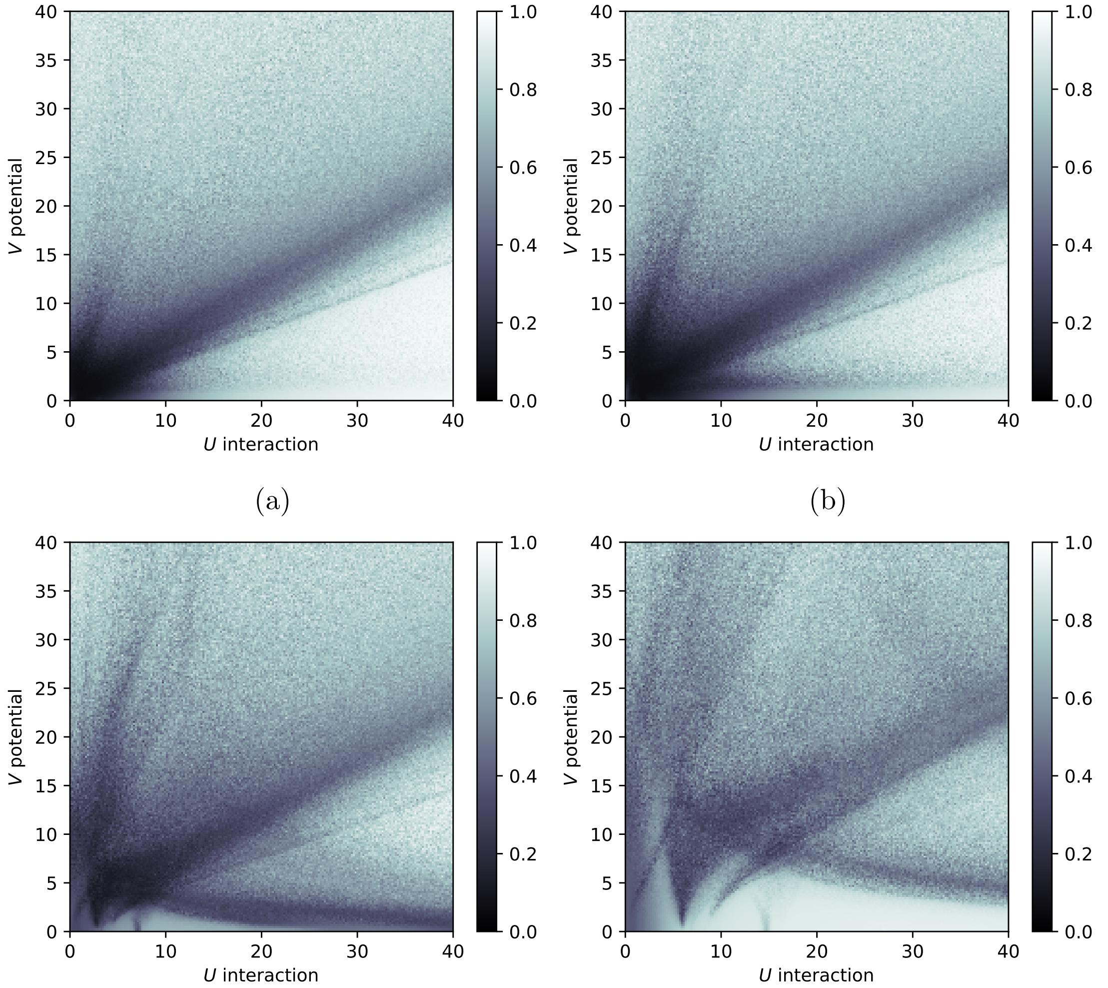

(a) (b) (c) (d)

Figure 2.21: Here we see the phase diagram of the evolved IPR of the Neèl state. The sampling strategy used is always taking 50 values in the interval between 20 and 30 time units. Moreover the mean is performed on 10 realizations of the random parameter. The pictures correspond to four different values of Δ the value of the IPR. As we can see for $\Delta = 1$ (a) and $\Delta = 2$ (b) the phase diagram is similar to the case with $\Delta = 0$ (fig 2.9). On the contrary for $\Delta = 5$ (c) and $\Delta = 10$ (d) the diagram become more chaotic and the localized phase is in the region with small values of V

abundantly this property to compute the time evolution of the imbalance. Those two methods resume the main structure of our codex. In fact, all the simulations we did were made starting from the exact diagonalization of the Hamiltonian and computing the time evolution of the quantities we evolved. As we have seen the computation we made is on an 8-site long chain with PBC. This corresponded to the diagonalization of a 256×256 matrix.

Chapter 3

The Bravy-Kitaev and Jordan-Wigner transformations

Here we describe and analyze in detail Jordan-Wigner and Bravy-Kitaev transformations. These unitary transformations allow to pass from a fermionic formulation to a spin variables formulation of the same phisical problem. We show how they are built and what are their uses and advantages. In particular we see their application to the mathematical problem of integrating the XY model and their advantage in term of resource needed to perform a simulation in the scope of quantum computing.

3.1 Jordan-Wigner transformations

In the late 20's Pascual Jordan and Eugene Wigner were trying to integrate spin chains models [32] . They found an analogy between spin $\frac{1}{2}$ variables and spinless fermions that can simplify the calculations. This analogy is suggested by the structure of the Fock space of both systems. Then, they developed unitary transformations that map fermionic excitations into spin variables.

These transformations allow us to write fermionic ladder operators f and $f^\dagger$ in terms of Pauli matrices $\sigma^x, \sigma^y, \sigma^z$. A spinless fermionic system with length L has a Fock space $\mathcal{F}_f$ of dimension 2^L because there can be only one fermionic excitation for each site. In the second quantization formalism the Fock space is built using fermionic ladder operators f and $f^\dagger$. A basis state has the form

$$|\psi\rangle_f = |n_0, n_1, ..., n_j, ...n_{L-1}\rangle = f_0^\dagger f_1^\dagger \dots f_{L-1}^\dagger |0\rangle$$

where $n_j \in \{0, 1\}$ specifies the occupation number of the jth site, f_j creates a fermion in the site j and $|0\rangle$ is the vacuum. Ladder operators are ruled by their canonical anti-commutation relations:

$$[f_i, f_j]_+ = 0, \quad [f_i^\dagger, f_j^\dagger]_+ = 0, \quad [f_i, f_j^\dagger]_+ = \delta_{i,j} \tag{3.1}$$

The effect of ladder operators on a basis state is summarized in the following equations:

$$f_j^\dagger \left| n_0, n_1, ..., 0_j, ...n_{L-1} \right\rangle = (-1)^{\sum_{k=0}^{j-1} n_j} \left| n_0, n_1, ..., 1_j, ...n_{L-1} \right\rangle \tag{3.2}$$

$$f_j^\dagger \left| n_0, n_1, ..., 1_j, ...n_{L-1} \right\rangle = 0 \tag{3.3}$$

$$f_j \left| n_0, n_1, ..., 1_j, ...n_{L-1} \right\rangle = (-1)^{\sum_{k=0}^{j-1} n_j} \left| n_0, n_1, ..., 0_j, ...n_{L-1} \right\rangle \tag{3.4}$$

$$f_j \left| n_0, n_1, ..., 0_j, ...n_{L-1} \right\rangle = 0 \tag{3.5}$$

As we can see, creating a particle in a filled site or destroying a particle in a empty site gives 0. Moreover, from (3.1), operators belonging to different sites anti-commute, so that emerges a phase:

$$\phi_j = (-1)^{\sum_{k=0}^{j-1} n_j} \tag{3.6}$$

This phase is due to the order exchange of creation operators acting on vacuum, like in the following situation:

$$f_3^\dagger \left|1, 0, 0, 0, 0\right\rangle = f_3^\dagger f_0^\dagger \left|0\right\rangle = -f_0^\dagger f_3^\dagger \left|0\right\rangle = -\left|1, 0, 0, 1, 0\right\rangle$$

Jordan and Wigner found an analogy between the Fock space of those fermions and that of spin chains and developed their tranformations. For example their dimension is the same. The unitary mapping create a combination of Pauli matrices such that it follows the canonical anti-commutation relations of the fermionic ladder operators (3.1).

In the spin chain the Fock space $\mathcal{F}_\sigma$ is built applying σ_j^+ and σ_j^-, defined as:

$$\sigma^+ = \frac{1}{2}(\sigma^x - i\sigma^y), \quad \sigma^- = \frac{1}{2}(\sigma^x + i\sigma^y) \tag{3.7}$$

to a basis state

$$\left|\psi\right\rangle_\sigma = \left|s_0, s_1, ..., s_j, ...s_{L-1}\right\rangle = \sigma_0^+ \dots \sigma_{L-1}^+ \left|-1_0, -1_1, \dots, -1_{L-1}\right\rangle$$

where $s_j \in \{-1, +1\}$ is the spin value of the site. Those operators (3.7) rise and lower the value of spin in the j-th site and $\left|-1\right\rangle$ is the vacuum. The Pauli matrices commutation and anti-commutation relation are the following:

$$\begin{aligned} [\sigma^i \sigma^j] &= 2i\epsilon^{ijk}\sigma^k \\ [\sigma^i \sigma^j]_+ &= 2\delta^{ij} \end{aligned} \tag{3.8}$$

Using (3.8) can be shown that $[\sigma_i^+, \sigma_i^+]_+ = [\sigma_i^-, \sigma_i^-]_+ = 0$ and $[\sigma_i^-, \sigma_i^+]_+ = 1$. Unfortunately, for different sites they commutes. So, σ_i^+ and σ_i^- act similarly to f_i and $f_i^\dagger$ up to the anti-commutation on different sites. In the fermionic case the anti-commutation is responsible of the arising phase ϕ (3.6).

The anti-commutation property is obtained adding a string of σ^z on all the previous sites respect to that we want to fill or empty with σ_i^+ and σ_i^- . In this way we gain a phase for each site that has spin down. Given that, the Jordan-Wigner transformations assume the mathematical expression:

$$f_i^\dagger = \sigma_i^+ \prod_{j=0}^{i-1} \sigma_j^z \qquad f_i = \sigma_i^- \prod_{j=0}^{i-1} \sigma_j^z \tag{3.9}$$

We can call *parity set* the set of indices on which we apply σ^z, that is from 0 to $i-1$. This definition will be crucial on the next part, where we discuss the Bravy-Kitaev transformations.

3.1.1 Recovering the canonical anti-commutation relations

We can directly verify the anti-commutation relations. For simplicity we can identify our terms with capital letters A,B,C,D.

$$A^\pm = \sigma_i^\pm, \quad B = \prod_{j=0}^{i-1} \sigma_j^z \quad C^\pm = \sigma_k^\pm, \quad D = \prod_{j=0}^{k-1} \sigma_j^z \tag{3.10}$$

The anti-commutation relations look like this:

$$[f_i, f_k]_+ = \left[\sigma_i^- \prod_{j=0}^{i-1} \sigma_j^z, \sigma_k^- \prod_{j=0}^{k-1} \sigma_j^z\right]_+ = \left[A^- B, C^- D\right]_+ = 0 \tag{3.11}$$

$$[f_i^\dagger, f_k^\dagger]_+ = \left[\sigma_i^+ \prod_{j=0}^{i-1} \sigma_j^z, \sigma_k^+ \prod_{j=0}^{k-1} \sigma_j^z\right]_+ = \left[A^+ B, C^+ D\right]_+ = 0 \tag{3.12}$$

$$[f_i, f_k^\dagger]_+ = \left[\sigma_i^- \prod_{j=0}^{i-1} \sigma_j^z, \sigma_k^+ \prod_{j=0}^{k-1} \sigma_j^z\right]_+ = \left[A^- B, C^+ D\right]_+ = \delta_{ik} \tag{3.13}$$

The algebra of Pauli matrices on the same site is given by (3.8) and tells us that on different sites they commute: $[\sigma_i^l, \sigma_j^m] = 0$ with $l, m \in \{x, y, z\}$ for $i \neq j$. Without loss of generality we can assume in the anti-commutator $i \leq k$. Then, we can write the commutators that are null:

$$\left[\sigma_i^\pm, \prod_{j=0}^{i-1} \sigma_j^z\right] = \left[A^\pm, B\right] = 0, \quad \left[\sigma_k^\pm, \prod_{j=0}^{k-1} \sigma_j^z\right] = \left[C^\pm, D\right] = 0 \tag{3.14}$$

$$\left[\sigma_i^\pm,\sigma_k^\pm\right]=\left[A^\pm,C^\pm\right]=0 \tag{3.15}$$

$$\left[\prod_{j=0}^{i-1}\sigma_j^z,\prod_{j=0}^{k-1}\sigma_j^z\right]=\left[B,D\right]=0 \tag{3.16}$$

$$\left[\prod_{j=0}^{i-1}\sigma_j^z,\sigma_k^\pm\right]=\left[B,C^\pm\right]=0 \tag{3.17}$$

We can see that the couples A/B and C/D commutes because in the fermionic operator the string of σ^z ends before the site on which act $\sigma^\pm$ (3.14). Then, the eq (3.15) is due to the fact that on different sites σ^+ and σ^- commute, while on the same site holds $(\sigma_i^+)^2=(\sigma_i^-)^2=0$. In eq (3.16), B and D chains commute because there are only σ^z and then their commutator is always null. In the last equation (3.17), given that $k\geq i$, B chain commutes with $\sigma_k^\pm$ because its upper extreme index is less than k. On the contrary, the anti-commutator:

$$\left[\sigma_i^\pm,\prod_{j=0}^{k-1}\sigma_j^z\right]_+=\left[A^\pm,D\right]_+=0 \tag{3.18}$$

is null because $i\leq k$ and is present σ_i^z in the D chain. In fact, being $\sigma_i^\pm$ a linear combination of σ_i^x and σ_i^y it anti-commutes with σ_i^z from (3.8). Now we can demonstrate (3.11) and (3.12). To lighten the notation we use $A=A^\pm$ and $C=C^\pm$. We have:

$$\left[AB,CD\right]_+=ABCD+CDAB \tag{3.19}$$

We can rewrite $BC^\pm$ and $DA^\pm$ such that:

$$ABCD+CDAB=A\Big(CB+\left[B,C\right]\Big)D+C\Big(\left[A,D\right]_+-AD\Big)B \tag{3.20}$$

using (3.17) and (3.18) the result is the following:

$$ABCD+CDAB=ACBD-CADB \tag{3.21}$$

Then applying the same technique to BD and CA and using the commutation rules (3.15) and (3.16) we get 0.

$$\begin{aligned}ACBD-CADB&=AC\Big(DB+\left[B,D\right]\Big)-\Big(AC-\left[A,C\right]\Big)DB=\\&=ACDB-ACDB=0\end{aligned} \tag{3.22}$$

The for last commutator (3.13) the we have to study two cases $i < k$ and $i = k$. In the first case, we have the anti-commutator equal to 0 while in the second case it is the identity. To demonstrate the first one we need to use the following null commutators:

$$\begin{aligned}\left[\sigma_i^-, \sigma_k^+\right] &= \left[A^-, C^+\right] = 0\\ \left[\sigma_i^+, \sigma_k^-\right] &= \left[A^+, C^-\right] = 0\end{aligned} \tag{3.23}$$

They vanish because we are only studying cases in which $i \neq k$. Using these commutators instead of (3.15) we can repeat all the steps from (3.19) to (3.22) and get 0. So we have demonstrated that $[f_i, f_k^\dagger]_+ = 0$ for $i \neq k$. For the last case there is a difference. Here A and D does not anti-commute anymore. On the contrary, for $i = k$ the D and B chain are equal, so both $\sigma_i^\pm$ and $\sigma_k^\pm$ commute with them. Then we have, using $A = A^\pm$ and $C = C^\mp$:

$$\left[\sigma_i^\pm, k\prod_{j=0}^{k-1}\sigma_j^z\right] = \left[A, D\right] = 0 \tag{3.24}$$

Using (3.24),(3.14) and (3.17) we can solve the anti-commutator:

$$\begin{aligned}&\left[AB, CD\right]_+ = ABCD + CDAB =\\ &A\Big(CB + \left[B, C\right]\Big)D + C\Big(\left[A, D\right] + AD\Big)B =\\ &ACBD + CADB = \left[A, C\right]_+ BD = I\end{aligned} \tag{3.25}$$

Here, $[A, C]_+$ is the identity because $\sigma^+\sigma^- = \sigma^-\sigma^+ = \frac{1}{2}I$. Also BD is the identity because we have a product like $\prod_{j=0}^{k-1}(\sigma_j^z)^2 = I^k = I$. Then we have completed the demonstration of our canonical commutation relations and we can study several cases in which the transformations are used.

3.1.2 An example: XY Chain

As we mentioned before, the Jordan-Wigner transformations were invented to find the energy spectrum of spin chains. Their use is well explained in the quantum XY model. This toy model is a generalization of the more famous Ising model. Its Hamiltonian is shown here:

$$H_\sigma = \frac{J}{2}\sum_{j=1}^{N}\left[\left(\frac{1+\gamma}{2}\right)\sigma_j^x\sigma_{j+1}^x + \left(\frac{1-\gamma}{2}\right)\sigma_j^y\sigma_{j+1}^y + h\sigma_j^z\right] \tag{3.26}$$

Here the phase diagram is parametrized by the anisotropy parameter γ capturing the relative strength of interaction in the x and y components and by the external magnetic field h, directed along the transverse z-axis. It is instructive to observe the passages that show the power of the Jordan-Wigner transformations. They are particularly useful in the diagonalization of Hamiltonian. In this case we transform the Hamiltonian of a spin chain into a sum of fermionic ladder operators using the inverse transformations:

$$\sigma_j^+ = f_j\prod_{j-1}^{i=1}(I-2f_i^\dagger f_i), \quad \sigma_j^- = f_j^\dagger\prod_{j-1}^{i=1}(I-2f_i^\dagger f_i), \quad \sigma_j^z = (I-2f_j^\dagger f_j) \tag{3.27}$$

With these transformations, spin up is mapped into an empty state and a spin down to an occupied one. After having applied the them we obtain the Hamiltonian:

$$\begin{aligned} H_f = -\frac{1}{2}\sum_{j=1}^{N-1}\big(f_j^\dagger f_{j+1}+f_{j+1}^\dagger f_j + \gamma f_{j+1}^\dagger f_j^\dagger + \gamma f_{j+1}f_j\big) + \sum_{j=1}^{N} 2hf_j^\dagger f_j - \frac{hN}{2} \\ + \frac{\mu_N^x}{2}(f_N^\dagger f_1 + f_1^\dagger f_N + \gamma f_N^\dagger f_1^\dagger + f_1^\dagger f_N^\dagger) \end{aligned} \tag{3.28}$$

where μ_N^x is given by

$$\mu_N^x = \prod_{j=1}^{N}\sigma_j^z = \prod_{j=1}^{N}(I - f_j^\dagger f_j) \tag{3.29}$$

It is the parity operator and has eigenvalues $+1$ or -1 if the number of particles is even or odd. Notice that the number operator

$$\nu_N = \sum_{j=1}^{N}\sigma_j^z = \sum_{j=1}^{N}(I - f_j^\dagger f_j) \tag{3.30}$$

does not commute with the Hamiltonian, because the number of particles is not conserved. Nevertheless, μ_N^x does because particles are created in couples and the parity is conserved. Given that, Hilbert space can be divided in two sectors labelled by the eigenvalues of μ_N^x and divided by the projectors:

$$\begin{aligned} E &= \frac{1-\mu_N^x}{2} \\ O &= \frac{1+\mu_N^x}{2} \end{aligned} \tag{3.31}$$

The two sectors are the subspace with an even number of particles and the other with odd number of particles.

$$\begin{aligned} f^{+}_{j+N} &= -f^{+}_{j} \quad for \quad \mu^x_N = +1 \\ f^{-}_{j+N} &= f^{-}_{j} \quad for \quad \mu^x_N = -1 \end{aligned} \tag{3.32}$$

Choosing the proper boundary conditions (3.32), i.e. periodic for even sector and anti-periodic for odd sector, boundary terms can be discarded. Then, we get the following Hamiltonian for both sectors:

$$H^{\pm} = -\frac{1}{2}\sum_{j=1}^{N}\left(f^\dagger_j f_{j+1} + f^\dagger_{j+1} f_j + \gamma f^\dagger_{j+1} f^\dagger_j + \gamma f_{j+1} f_j - 2h f^\dagger_j f_j\right) - \frac{hN}{2} \tag{3.33}$$

Now, starting from left, are already visible hopping term, superconductive term and the number term inside the sum. The next step to solve exactly the system is to apply a Fourier transform:

$$f^{\pm}_j = \frac{e^{i\frac{\pi}{4}}}{N}\sum_{q\in\Gamma_{\pm}} e^{i\frac{2\pi}{N}qj} f_q, \quad f^{\pm}_q = e^{-i\frac{\pi}{4}}\sum_{j=1}^{N} e^{-\frac{2\pi}{N}qj} f^{\pm}_j \tag{3.34}$$

Here $\Gamma_{\pm}$ indicates the set of momentum values belonging to the respective sector:

$$\begin{aligned} q \in \mathcal{N} + \frac{1}{2} = \frac{1}{2}, \frac{3}{2}, ...N - \frac{1}{2} \quad &\text{for Even Particle Number} \\ q \in \mathcal{N}+ = 1, 2, ...N - 1 \quad &\text{for Odd Particle Number} \end{aligned} \tag{3.35}$$

Now we have the formulation in momentum space (3.36).

$$H^{\pm} = \frac{1}{N}\sum_{q\in\Gamma_{\pm}}\left[h - cos\left(\frac{2\pi}{N}q\right)\right] f^\dagger_q f_q + \frac{\gamma}{2N}\sum_{q\in\Gamma_{\pm}} sin\left(\frac{2\pi}{N}q\right)\left\{f_q f_{-q} + f^\dagger_q f^\dagger_{-q}\right\} \tag{3.36}$$

In the end, a Bogoliubov diagonalization of the Hamiltonian written in momentum space gives a canonical Hamiltonian written in terms of Bogoliubov quasi-particles ladder operators $\chi^\dagger_q$, χ_q:

$$H^{\pm} = \frac{1}{N}\sum_{q\in\Gamma_{\pm}} \epsilon\left(\frac{2\pi}{N}q\right)\left[\chi^\dagger_q \chi_q - \frac{1}{2}\right] \tag{3.37}$$

The resulting energy spectrum is shown here:

$$\epsilon(\alpha) = \sqrt{(h - \cos(\alpha))^2 + \gamma^2 \sin^2(\alpha)} \tag{3.38}$$

In this section we have seen briefly what are able to do our transformations and how they are the mathematical formulation of a deep analogy between different kinds of physical quantum systems. Moreover we introduced some operators like the number operator and the parity operator that will be crucial in the future discussions.

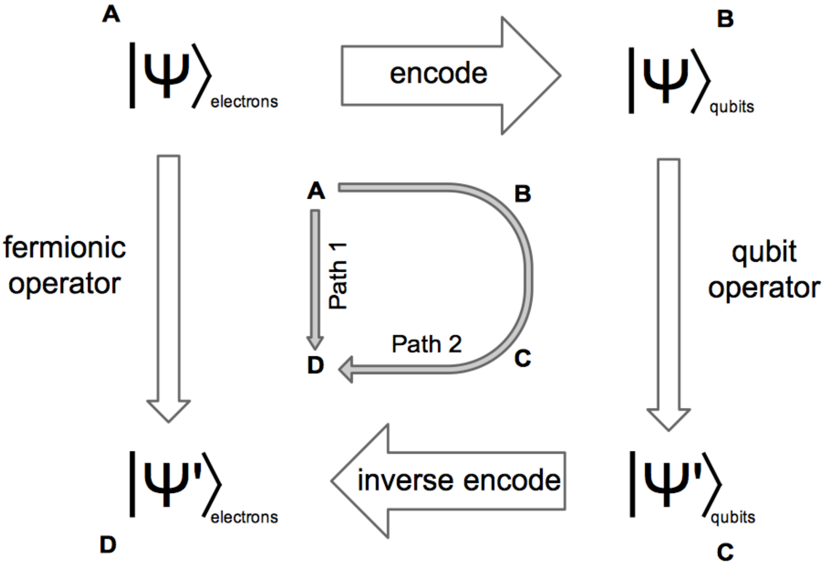

Figure 3.1: This image show the passages between the femionic and qbit languages and the embedding of the occupation basis in another. Taken from [22]

3.2 The Parity transformations

After having seen how Jordan-Wigner transformations work, it is the time to deepen the Bravy-Kitaev transformations. Those transformations were introduced in the scope of quantum computation [22]. To understand how the transformations are built we can follow the construction in [33]. For now we explore their "embedding" and only at a later time the form of the ladder fermionic operators, that we call "encoding". For "embedding" we mean a bijective map between two basis used to describe the Fock space in the same formulation, i.e. choosing one between spinless fermions or spin variables. For "encoding" instead, we mean the transformations used to pass from spins to fermions and vice-versa. Figure 3.1 shows a map of the encodings (horizontal arrows) and the embeddings (vertical arrows) of unitary maps between fermionic and spin systems.

To clarify what is an embedding, we have to take our ket vectors $|\psi\rangle = |n_0, n_1, ..., n_j, ...n_{L-1}\rangle$ and treat them as binary vectors $|\psi\rangle \longrightarrow \vec{v} = (n_{L-1}, n_{L-2}, ..., n_j, ...n_0)^T$. Notice that order is inverted. Then, an embedding is a binary isomorphism $T : \vec{v} \longrightarrow \vec{v'}$. It is important underline that T does not act on the Fock space. In fact v has dimension L and not 2^L and belongs to the modulus $\mathbb{Z}_2^L$, consequently T belongs to the space of applications $\mathcal{T} : \mathbb{Z}_2^L \longrightarrow \mathbb{Z}_2^L$. Now we examine several of those isomorphisms. First of all, it is necessary to introduce the occupation basis that is the most intuitive embedding. It is the Fock space $\mathcal{F}$ built with $f_i^\dagger$ acting on the vacuum $|0\rangle$. In this case, there is an identity between the state of the Fock basis and the binary vectors $\vec{v}$.

Another basis that can be defined is what is called "parity basis". We can create a trasformation that links the occupation basis with the parity basis. It is described by a $L \times L$ upper triangular matrix P_{ij}, made by ones if $i \leq j$ and 0 otherwise. It has the following form:

$$P = \begin{pmatrix} 1 & 1 & \cdots & 1 \\ 0 & 1 & \cdots & 1 \\ \vdots & \vdots & \ddots & \vdots \\ 0 & 0 & \cdots & 1 \end{pmatrix} \tag{3.39}$$

A generic state in the occupation basis $\vec{\psi}_O = (n_{L-1}, n_{L-2}, ..., n_j, ...n_0)^T$, with $n \in \{0, 1\}$, is written in the parity basis as $\vec{\psi}_P = (p_{L-1}, p_{L-2}, ..., p_j, ...p_0)^T$, where $p_j = \sum_{i=0}^{j} n_i$ with the sum intended $mod \equiv 2$. We can see it in an exemple:

Given the row vector: $\vec{u} = (1, 1, 0, 1)^T$

we can apply P: $\quad u \longrightarrow Pu$

$$(1_0, 1_1, 0_2, 1_3)_O \longrightarrow \Big(1_0, (1_0 + 1_1), (1_0 + 1_1 + 0_2), (1_0 + 1_1 + 0_2 + 1_3)\Big)_P = (1, 0, 0, 1)_P \tag{3.40}$$

So, if in the j-th element of the state in the parity basis is equal to 0 or 1 it means that if one count the number of particles in the occupation basis in the sites with $i \leq j$ get an even or an odd number respectively. This embedding carries a new kind of transformations based on the parity.

Those parity transformations have a chain of σ^x on the sites that come after the site j. (3.43). In fact, creating or destroying a particle change the parity on the remaining sites sites with indexes $i = j + 1, ..., L - 1$, while does not affects the previous ones. Moreover, we have to consider that the parity of the sites with index $i < j$ change the effect of σ^+ and σ^- on the site j. In fact, acting on σ^+ on the index j while the parity of the sites $i < j$ is odd does not create a particle, but destroys one. So, to establish if the role of $\sigma^\pm$ is exchanged is sufficient to check the parity of all previous sites. This can be done looking at the parity coefficient p_{j-1} that stores the parity of all the sites from 0 to $j-1$. In the formulations of the fermionic ladder operators this corresponds to add in the string of pauli matrices σ^z_{j-1}. Can be also defined projectors on the even and odd subspaces:

$$\hat{E}_{j-1} = \frac{1}{2}(I + \sigma^z_{j-1}) \quad \hat{O}_{j-1} = \frac{1}{2}(I - \sigma^z_{j-1}) \tag{3.41}$$

To define new operators that lower and rise the spin:

$$s_j^{\pm} = \sigma^{\pm}\hat{E}_{j-1} - \sigma^{\mp}\hat{O}_{j-1} = \frac{1}{2}(\sigma_{j-1}^z \sigma_j^x \pm i\sigma_j^y) \tag{3.42}$$

Then, the expression of the fermionic ladder operators is:

$$f_j^{\dagger} = s_j^{+} \prod_{i=j+1}^{L-1} \sigma_i^x \qquad f_j = s_j^{-} \prod_{i=j+1}^{L-1} \sigma_i^x \tag{3.43}$$

Analogously to what we have done in Jordan-Wigner transformations, now we can call the set of indices of the σ^x chain *update set*. This definition comes from the fact that we have to "update" the parity of the sites that come after the site j exchanging their state. Instead the index $j-1$ can be associated to a *flip set*, because in a certain sense, it "flips" the effect of σ^+ and σ^-. This behaviour is said dual respect to the Jordan-Wigner one.

3.2.1 Recovering the anti-commutation relations

We can recover the fermionic anti-commutation relations, as did in 3.1.1, also fo rthe parity transformations.we can identify our terms with capital letters A,B,C,D.

$$A^{\pm} = s_i^{\pm}, \quad B = \prod_{j=i+1}^{L-1} \sigma_j^x \quad C^{\pm} = s_k^{\pm}, \quad D = \prod_{j=k+1}^{L-1} \sigma_j^x \tag{3.44}$$

Notice that now $\sigma^{\pm}$ are replaced by $s^{\pm}$. The anti-commutation relations look like this:

$$[f_i, f_k]_+ = \left[s_i^- \prod_{j=i+1}^{L-1} \sigma_j^x, s_k^- \prod_{j=k+1}^{L-1} \sigma_j^x\right]_+ = \left[A^-B, C^-D\right]_+ = 0 \tag{3.45}$$

$$[f_i^{\dagger}, f_k^{\dagger}]_+ = \left[s_i^+ \prod_{j=i+1}^{L-1} \sigma_j^x, s_k^+ \prod_{j=k+1}^{L-1} \sigma_j^x\right]_+ = \left[A^+B, C^+D\right]_+ = 0 \tag{3.46}$$

$$[f_i, f_k^{\dagger}]_+ = \left[s_i^- \prod_{j=i+1}^{L-1} \sigma_j^x, s_k^+ \prod_{j=k+1}^{L-1} \sigma_j^x\right]_+ = \left[A^-B, C^+D\right]_+ = \delta_{ik} \tag{3.47}$$

As said before, algebra of Pauli matrices on the same site is given by (3.8), while on different sites they commute: $[\sigma_i^l, \sigma_j^m] = 0$ with $l, m \in \{x, y, z\}$ for $i \neq j$. Again we can assume in the anti-commutator $i \leq k$. Then, we can write the null commutators:

$$\left[s_i^{\pm}, \prod_{j=i+1}^{L-1} \sigma_j^x\right] = \left[A^{\pm}, B\right] = 0, \quad \left[s_k^{\pm}, \prod_{j=k+1}^{L-1} \sigma_j^x\right] = \left[C^{\pm}, D\right] = 0 \tag{3.48}$$

$$\Big[s_i^{\pm}, s_k^{\pm}\Big] = \Big[A^{\pm}, C^{\pm}\Big] = 0 \quad \text{for } i \neq k-1 \tag{3.49}$$

$$\Big[\prod_{j=i+1}^{L-1} \sigma_j^x, \prod_{j=k+1}^{L-1} \sigma_j^x\Big] = \Big[B, D\Big] = 0 \tag{3.50}$$

$$\Big[s_i^{\pm}, \prod_{j=k+1}^{L-1} \sigma_j^x\Big] = \Big[A^{\pm}, D\Big] = 0 \tag{3.51}$$

We can see that the couples A/B and C/D commutes because the string of σ^x starts after the site on which act $s^{\pm}$ (3.48). The eq (3.49) is different with respect to (3.15) because s^+ and s^- commute for every i except for $i = k-1$. On the same site holds: $(s_i^+)^2 = (s_i^-)^2 = 0$ and $(s_i^- s_i^+) = I$. This happens because in this case the in the explicit expression appear two different Pauli matrices acting to the same site:

$$\Big[s_{k-1}^{\pm}, s_k^{\pm}\Big] = \frac{1}{4}\Big[\sigma_{k-2}^z \sigma_{k-1}^x \pm i\sigma_{k-1}^y, \sigma_{k-1}^z \sigma_k^x \pm i\sigma_k^y\Big] \tag{3.52}$$

we can see that there are in both members Pauli matrices acting on the site $k-1$. In eq (3.50), B and D chains commute because there are only σ^x and then their commutator is always null. In the last equation (3.51), given that $i \leq k$, D chain commutes with $s_k^{\pm}$ because its lower extreme index is greater than i. On the contrary, the anti-commutator:

$$\Big[\prod_{j=i+1}^{L-1} \sigma_j^x, s_k^{\pm}\Big]_+ = \Big[B, C^{\pm}\Big]_+ = 0 \quad \text{for } i \neq k-1 \tag{3.53}$$

is null because $i \leq k-1$ and are present a σ_k^x and a σ_{k-1}^x in the B chain. In fact, being $s_k^{\pm} = \frac{1}{2}(\sigma_{k-1}^z \sigma_k^x \pm i\sigma_k^y)$ given the aforementioned conditions, it anti-commutes with the chain segment $\sigma_{k-1}^x \sigma_k^x$. Notice that if $i = k-1$, σ_{k-1}^x does not belong to the B chain and the anti commutation is not realized. In fact:

$$s_k^{\pm} \sigma_k^x = \frac{1}{2}(\sigma_{k-1}^z \sigma_k^x \pm i\sigma_k^y)\sigma_k^x = \sigma_k^x \frac{1}{2}(\sigma_{k-1}^z \sigma_k^x \mp i\sigma_k^y) = \sigma_k^x s_k^{\mp} \neq -\sigma_k^x s_k^{\pm} \tag{3.54}$$

Now we can demonstrate (3.45) and (3.46) for $i = j$ and $i < k-1$. To lighten the notation we use $A = A^{\pm}$ and $C = C^{\pm}$. We have:

$$\Big[AB, CD\Big]_+ = ABCD + CDAB \tag{3.55}$$

We can rewrite $BC^{\pm}$ and $DA^{\pm}$ such that:

$$ABCD + CDAB = A\Big(\Big[B, C\Big]_+ - CB\Big)D + C\Big(DA + \Big[A, D\Big]\Big)B \tag{3.56}$$

using (3.51) and (3.18) the result is the following:

$$ABCD + CDAB = CADB - ACBD \tag{3.57}$$

Then because B and D commute:

$$CADB - ACBD = \Big[C, A\Big]BD = 0 \tag{3.58}$$

Using the (3.49) we get 0. Now we have to explore the case $i = k - 1$. Here we can use the equation (3.54) to show that:

$$BC\overset{\pm}{=}C^{\mp}B \tag{3.59}$$

So that the solution is the following:

$$A^{\pm}BC^{\pm}D + C^{\pm}DA^{\pm}B = A^{\pm}C^{\mp}BD + C^{\pm}A^{\pm}BD = \Big(A^{\pm}C^{\mp} + C^{\pm}A^{\pm}\Big)BD \tag{3.60}$$

Notice that now the product BC is only σ^x_k. The last step is to show that the therm into the parenthesis in the last member is 0. To do this we write explicitly the product $C^{\pm}A^{\pm}$:

$$\begin{aligned} s^{\pm}_k s^{\pm}_{k-1} &= \frac{1}{4}\Big(\sigma^z_{k-1}\sigma^x_k \pm i\sigma^y_k\Big)\Big(\sigma^z_{k-2}\sigma^x_{k-1} \pm i\sigma^y_{k-1}\Big) = \\ &= \frac{1}{4}\Big(\sigma^z_{k-1}\sigma^x_k \pm i\sigma^y_k\Big)\Big(\sigma^z_{k-2}\sigma^x_{k-1}\Big) \pm \frac{i}{4}\Big(\sigma^z_{k-1}\sigma^x_k \pm i\sigma^y_k\Big)\Big(\sigma^y_{k-1}\Big) = \\ &= \frac{1}{4}\Big(\sigma^z_{k-2}\Big)\Big(\sigma^z_{k-1}\sigma^x_k \pm i\sigma^y_k\Big)\Big(\sigma^x_{k-1}\Big) \pm \frac{i}{4}\Big(\sigma^z_{k-1}\sigma^x_k \pm i\sigma^y_k\Big)\Big(\sigma^y_{k-1}\Big) \end{aligned}$$

A this point we have splitted s_{k-1}. Then, σ^z_{k-2} passes through s_k. In the last passages we have to care about anti commutation of Pauli matrices with index $k - 1$:

$$\begin{aligned} &\frac{1}{4}\Big(\sigma^z_{k-2}\Big)\Big(\sigma^z_{k-1}\sigma^x_k \pm i\sigma^y_k\Big)\Big(\sigma^x_{k-1}\Big) \pm \frac{i}{4}\Big(\sigma^z_{k-1}\sigma^x_k \pm i\sigma^y_k\Big)\Big(\sigma^y_{k-1}\Big) = \\ &= \frac{1}{4}\Big(\sigma^z_{k-2}\sigma^x_{k-1}\Big)\Big(-\sigma^z_{k-1}\sigma^x_k \pm i\sigma^y_k\Big) \pm \frac{i}{4}\Big(\sigma^y_{k-1}\Big)\Big(-\sigma^z_{k-1}\sigma^x_k \pm i\sigma^y_k\Big) = \\ &= \frac{1}{4}\Big(\sigma^z_{k-2}\sigma^x_{k-1} \pm i\sigma^y_{k-1}\Big)\Big(-\sigma^z_{k-1}\sigma^x_k \pm i\sigma^y_k\Big) \end{aligned}$$

Extracting a minus sign from the second factor we get:

$$\begin{aligned} \frac{1}{4}\Big(\sigma^z_{k-2}\sigma^x_{k-1}i \pm i\sigma^y_{k-1}\Big)\Big(-\sigma^z_{k-1}\sigma^x_k \pm i\sigma^y_k\Big) &= -\frac{1}{4}\Big(\sigma^z_{k-2}\sigma^x_{k-1} \pm i\sigma^y_{k-1}\Big)\Big(\sigma^z_{k-1}\sigma^x_k \mp i\sigma^y_k\Big) = \\ &= -s^{\pm}_{k-1}s^{\mp}_k \end{aligned}$$

Then for $i = k - 1$ we have:

$$C^{\pm}A^{\pm} = -A^{\pm}C^{\mp} \tag{3.61}$$

This statement concludes the demonstration of (3.45) and (3.46). The last anti-commutator (3.47) can be solved for $i < k-1$ with the same argument we used for (3.45) and (3.46). In fact in this case we have all the null commutation relations (3.48), (3.51), (3.50) plus the following one:

$$\left[s_i^-, s_k^+\right] = \left[A^-, C^+\right] = 0 \quad \text{for } i \leq k-1 \tag{3.62}$$

to use in the last passage (3.58) instead of (3.49). On the other hand when $i = k$ we have that the B and D chains disappear and the anti-commutator reduces to the identity:

$$\left[s_i^-, s_i^+\right]_+ = \left[A^-, B^+\right]_+ = I \tag{3.63}$$

The last case $i = k - 1$ is solved through the following steps:

$$A^-BC^+D + C^+DA^-B = BDA^-C^+ + BDC^-A^- = BD\Big(A^-C^+ + C^-A^-\Big) \tag{3.64}$$

Where we have used the null commutators (3.48), (3.51), (3.50) and the relation (3.59). But the parenthesis of the last product are null. In fact from (3.61) we have that $A^-C^+ = -C^-A^-$. This ends the checking of the canonical anti-commutation relations for the Parity transformations.

3.3 The Bravy-Kitaev transformations

The Bravy-Kitaev embedding is an half way between Jordan-Wigner transformations and the Parity transformations. There are some indexes in this basis that store exactly the occupation number of the site, while there are others that store the parity of a subset of sites given by the embedding. Our objective is that of writing the fermionic ladder operators in a way similar to that of Jordan-Wigner transformations or Parity transformations. We will see that the peculiar structure of Bravy-Kitaev transformations generate an expression for f and $f^\dagger$ composed by a string of σ^z belonging to a proper parity set of indices, a spin ladder operator $\sigma^\pm$ and a string of σ^x belonging to a proper update set of indices. First of all, in the Bravy-Kitaev binary vector $\vec{\psi}_B = (b_{L-1}, b_{L-2}, ..., b_j, ...b_0)^T$ the coefficients b_j are given, depending on j, by the embedding in the following way:

- If j is even the index store exactly the occupation number: $b_j = n_j$

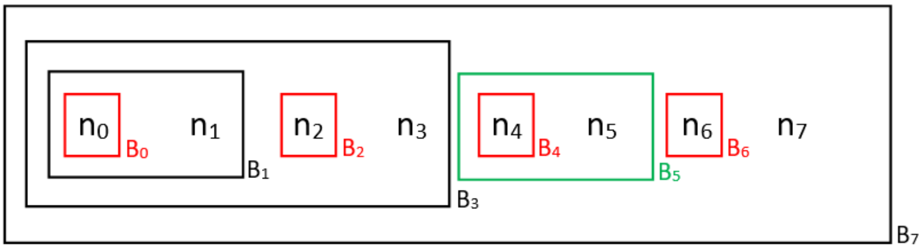

Figure 3.2: Here we can see the embedding of Bravy and Kitaev for 8 sites. Every box belong stores the parity of the sites contained in him. We can see in black the boxes with index of the form $2^k - 1$, in red the boxes with an even index and in green the box with an odd index bot not of the form $2^k - 1$.

- If j is odd but not of the form $2^k - 1$ it stores the parity of the sites j and $j-1$: $b_j = n_j + n_{j-1}$
- If j is of the form $2^k - 1$ it stores the parity of all previous sites with index $i = 0, \cdots, j$: $b_j = \sum_{k=0}^{j} n_k$

The matrix related to this coding from the occupation basis is defined in the following recursive way in:

$$\mathrm{BK}_{2^{x+1}} = \left(\begin{array}{c|cccc} & 1 & 1 & \cdots & 1 \\ & 0 & 0 & \cdots & 0 \\ \mathrm{BK}_{2^x} & \vdots & \vdots & \ddots & \vdots \\ & 0 & 0 & \cdots & 0 \\ \hline 0 & \multicolumn{4}{c}{\mathrm{BK}_{2^x}} \end{array}\right) \tag{3.65}$$

With as initial value $BK_{2^0} = 1$. With this construction is sufficient to take the $L \times L$ submatrix if the total number of sites L is not a power of two. Now we can pass to the examination of the expression of the fermionic ladder operators in terms of Pauli matrices.

3.3.1 Three set of indices

To obtain an expression for our ladder operators that looks like (3.9) or (3.43), it is necessary to define the sets of indices needed to built our transformations: the parity set, the update set and the flip set. The meaning of these three sets can be understood through the graphical representation of figure 3.2. Here we can see the embedding for 8 sites, indicated with n labeled with $j \in \{0,1,2,3,4,5,6,7\}$. Every box contains the indices whose parity is stored in. The sites occupation stored in the boxes can be summarized in the following scheme:

$$B_0 = \{n_0\} \quad B_1 = \{n_0, n_1\} \quad B_2 = \{n_2\} \quad B_3 = \{n_0, n_1, n_2, n_3\} \quad B_4 = \{n_4\}$$

$$B_5 = \{n_4, n_5\} \quad B_6 = \{n_6\} \quad B_7 = \{n_0, n_1, n_2, n_3, n_4, n_5, n_6, n_7\}$$

We can immediately see that even index boxes store only the parity of the single site, i.e. the occupation number of that site. On the other hand, the boxes with the indexes $1, 3$ and 7 store the parity of all the previous sites. In the end index 5 store their parity and that of the previous site respectively. Then, we have to define our sets.

The parity set, $P(j)$ is the set of indexes that contain the parity in the j-th site. Roughly speaking we have to count the parity of the number of filled sites from $i = 0$ to $i = j - 1$. For Jordan-Wigner is composed by all the indexes that run from 0 to $j - 1$, while for the Parity transformations is always the empty set. To recover it we have to look at the index of all the higher level boxes that are included at its left. For Bravy-Kitaev is not necessary to take the entire string, because there are some boxes B_j that contains the parity of a larger set of sites.

For example, for the parity in the site 5, we have to remove the box B_5 because it not ends before n_5, then at its left there are B_3 and B_4. So the parity set indexes of b_5 are 3 and 4 (fig 3.3).

So, if we want to know the parity of the j-th site we have only to check the parity of the Bravy-Kitaev coefficients b_i whose index belong to the parity set of the index j. We can summarize the result for the 8-sites chain in the following scheme:

$$P(0) = \{\} \quad P(1) = \{b_0\} \quad P(2) = \{b_1\} \quad P(3) = \{b_1, b_2\}$$

$$P(4) = \{b_3\} \quad P(5) = \{b_3, b_4\} \quad P(6) = \{b_3, b_5\} \quad P(7) = \{b_3, b_5, b_6\}$$

The update set, $U(j)$ is the set of sites that have to be updated after changing the value in the j-th site. In case of Jordan-Wigner is always the empty set, while for Parity transformations is made by all the indexes between $j + 1$ and $L - 1$. Now we have to update only the sites that store the occupation of our j-th site. Graphically it can be done looking at the box of n_j and see in which others it is contained. The Bravy-Kitaev embedding guarantees that we have only update a small amount of indexes because only the boxes b_j with $j = 2^k - 1$ store the parity of all the previous sites. Notice that their number grows logarithmically with L.

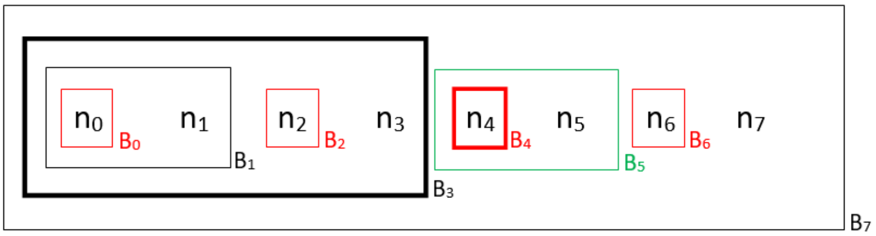

Figure 3.3: Here we can see the definition of the parity set for b_5. To emphasize the boxes at left of n_5 they are thickened respect to others. We do not care about the other boxes contained in the red box B_3 because only the higher index matters. Moreover, we can clearly see that the boxes of B_5 itself and B_7 cannot be counted because they do not end strictly before the site n_5, so they cannot considered at left of it. In the end the entire parity of the coefficient b_5 is contained in B_3 and B_4, so that the indexes of the parity set are 3 and 4.

For example, if we look at n_0 box it is contained in that of n_1, n_3 and n_7 and so on for all n_j (fig 3.4).

Now if we change the occupation of the j-th site we have only to update the Bravy-Kitaev coefficients b_i whose index i belongs to the update set of indices of the site j. We can summarize the update set for our chain in the following way.

$$U(0) = \{b_1, b_3, b_7\} \quad U(1) = \{b_3, b_7\} \quad U(2) = \{b_3, b_7\} \quad U(3) = \{b_7\}$$

$$U(4) = \{b_5, b_7\} \quad U(5) = \{b_7\} \quad U(6) = \{b_7\} \quad U(7) = \{\}$$

The flip set, $F(j)$ is the set that indicates if creating or destroying a particle in the site j we have to act with σ_j^+ or σ_j^- or vice versa. Graphically, can be recovered just looking at the box that contain n_j and see the greatest index contained in each of the other boxes contained in the same box of n_j, except n_j.

For example, for n_3, we see that it contains the boxes of n_2 and n_1. Obviously, there is the index 2 and the higher index between 1 and 0 (fig 3.5). For even indexes it is the empty set because they store their occupation only, so that to fill or empty these indexes correspond to act with σ^+ and σ^- respectively.

So if we want to change the occupation of the site j, we have to act with σ^+ or σ^- up to the parity of a subset of Bravy-Kitaev coefficients defined by the flip

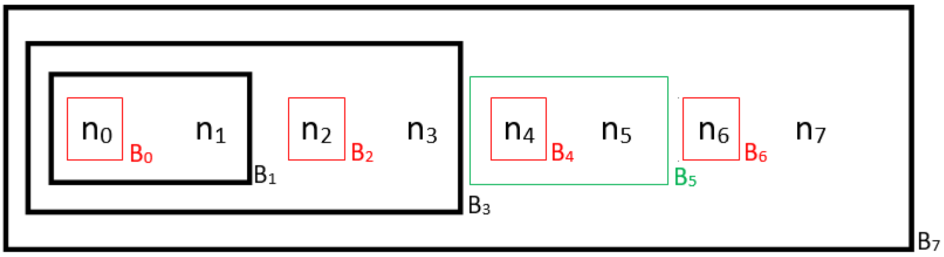

Figure 3.4: Here we can see the definition of the update set for the first Bravy-Kitaev coefficient b_0. We have to look at what boxes contain the occupation n_0. To emphasize those boxes, we thickened them with respect to others. We can easily see that n_0 is contained in the boxes with indexes 1,3 and 7.

set. We can summarize the update set for our chain in the following way.

$$F(0) = \{\} \quad F(1) = \{b_0\} \quad F(2) = \{\} \quad F(3) = \{b_1, b_2\}$$

$$F(4) = \{\} \quad F(5) = \{b_4\} \quad F(6) = \{\} \quad F(7) = \{b_3, b_5, b_6\}$$

With the same graphical representation, we can also recover the Jordan-Wigner and the Parity transformations. In fact, in the figure 3.6 are represented with N_i and P_i the boxes that contains the occupation of the sites according to Jordan-Winger and Parity embeddings. Here we can build again for each index a parity set, an update set and a flip set. The final results coincide with what we have already seen in the definitions of the fermionic ladder operators in the equations (3.9) and (3.43). Using these definitions we can write the three sets of indices for every site. As we will see they are crucial to write the explicit expressions of the transformations.

3.3.2 The complete expression

Now we can explicitly write our transformations. We can write the ladder fermionic operator f_j, $f_j^\dagger$ using the product of three terms. The first one is a string of σ^z to take in account the parity. Then, $\sigma^\pm$ to create or destroy the particle. In the end, a string of σ^x to update the remaining sites. Differently from J-W and Parity

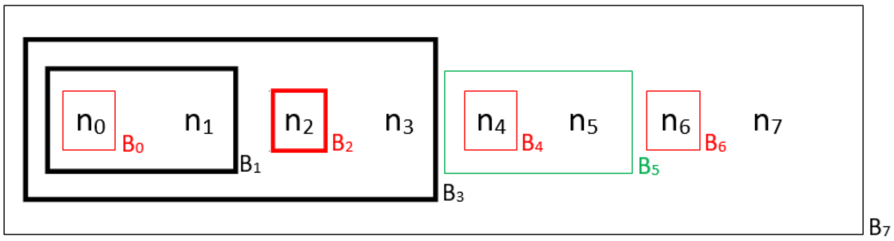

Figure 3.5: Here we can see the definition of the flip set for the Bravy-Kitaev coefficient b_3. To emphasize those boxes that are contained in the box B_3 they are thickened respect to others. We can see that it contains only the box B_1 and the red box of B_2. We do not care about the box of B_0 because we have to take only the higher indexes between the sites occupation stored in the B_3 box. So, the two indexes belonging to the flip set of B_3 are the index 1 and 2.

transformations, here the the indexes of σ^z and σ^x are taken by the parity and update set. For the sites with an even index, the transformations have the form:

$$f_i^\dagger = (\prod_{j\in P(i)} \sigma_j^z) \quad \sigma_i^+ \quad (\prod_{j\in U(i)} \sigma_j^x) \qquad f_i = (\prod_{j\in P(i)} \sigma_j^z) \quad \sigma_i^- \quad (\prod_{j\in U(i)} \sigma_j^x) \quad \text{for } i \text{ Even} \tag{3.66}$$

Here $P(i)$ and $U(i)$ are the parity set and the update set for the index i. The previous formula is valid for even indexes only, because they stores the occupation of the site. In case of j odd, the index stores the parity of a subset of sites. So, applying $f_i^\dagger$ not always means acting with σ_i^+ and the same for f_i and σ_i^-. It is up to the parity of the flip set of the index j. It is useful define the projectors on the even and odd Hilbert subspaces:

$$\hat{E} = \frac{1}{2}\left(I + \prod_{j=0}^{n-1} \sigma_j^z\right) \qquad \hat{O} = \frac{1}{2}\left(I - \prod_{j=0}^{n-1} \sigma_j^z\right) \tag{3.67}$$

Now we can define the correct operators that rise and lower the spin taking in account the parity of the flip set:

$$s_i^\pm = \sigma_i^\pm \hat{E}_{F(i)} - \sigma_i^\mp \hat{O}_{F(i)} = \frac{1}{2}(\sigma_i^x \prod_{F(i)} \sigma^z \pm \sigma^y) \tag{3.68}$$

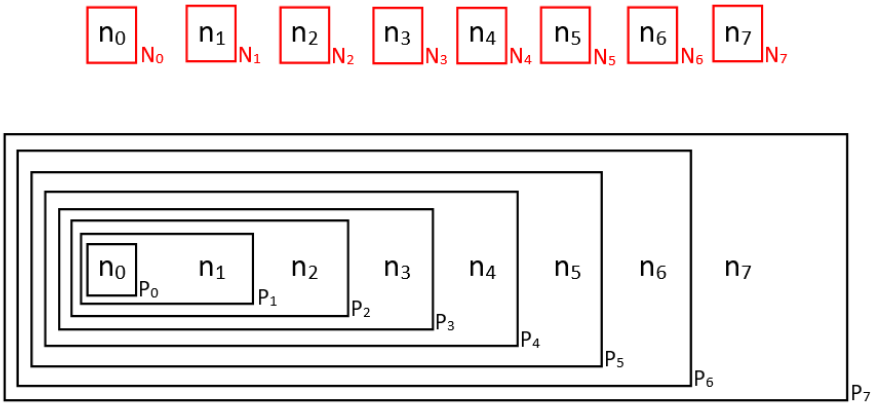

Figure 3.6: Here we can see graphical representation of the Jordan-Wigner embedding (top) and the Parity embedding (bottom). As we can see in the first case each box stores only the occupation of the corresponding site, while in the parity case each box contains the occupation of all the previous ones. Using graphical methods is simple to recover that the parity set for Jordan-Wigner is represented by all the indexes less than j, because at left of site j there is one box for every site. On the contrary while the flip set and the update set are empty. As far is concerned the Parity basis is clear that the update set is made by all the index greater than j because each box is contained in all the following ones. For the parity set and the flip set they are completely equivalent because the box j stores the parity of all the sites between 0 and j. Notice that this is not true in general for the Bravy-Kitaev basis, but only for the indexes of the form $2^k - 1$.

Notice that the projectors are built directly from the flip set $F(i)$. In fact, if we are on an even site $F(i) = 0$ and we recover the previous case with $s_i^{\pm} = \sigma_i^{\pm}$. Substituting $\sigma^{\pm}$ with $s^{\pm}$ we obtain the transformations for both j odd and even:

$$f_i^{\dagger} = (\prod_{j \in R(i)} \sigma_j^z) s_i^+ (\prod_{j \in U(i)} \sigma_j^x) \quad f_i = (\prod_{j \in R(i)} \sigma_j^z) s_i^- (\prod_{j \in U(i)} \sigma_j^x) \quad \text{for } i \text{ Even and Odd} \tag{3.69}$$

where $R(i) = P(i) \setminus F(i)$ is the difference set between parity set and flip set. Now we have written an explicit form for the Bravy-Kitaev transformations.

3.4 Quantum Computing

At this point, we must discuss a little on quantum computation and the role of our transformations in this subject. In 1982 Richard Feynman started the debate about the simulation of quantum systems. The problem on which Feynman focused on was try to prevent the exponential growth of resources needed to simulate quantum systems on classical computers [34]. To give an example of this behaviour we can look at an ensemble of L two-states quantum systems. The Fock $\mathcal{F}_L$ space turn out to be the tensorial product of the two-dimensional Hilbert space $\mathcal{H}_2$ of single subsystems. Its dimension is 2^L. Analogously, the vector state is made by 2^L complex numbers. On a classical computer, every single complex number occupy $2 *$ `sizeof(double)` bytes. This happens because one double stores the real part while the other the imaginary part. The total amount of memory needed for a system is $2^{n+1} *$`sizeof(double)`. In this way with 36 subsystems we reach already $1TB$ and with 43 sites are necessary around $140TB$ for every state. This make impossible to simulate anything to most of classical computers. The answer that Feynman gave to its question was to simulate quantum systems directly on other quantum systems, i.e. on quantum computers. A quantum computer is itself a quantum system that has some particular features:

- The computer is made up of a certain number of cells. These cells are quantum systems with a low dimensional Hilbert space. In case dimension $d = 2$ they are called qubits.

- It must be possible to act on a subset of cells at a time. Every operation on those cells is described by an unitary operator U. U is the tensor product of the operators acting on the different cells and the identity on the rest of the system

- All the cells are identical systems, so that every operator can by classified by their action on a generic set of cells

In this framework the classical logical gates are replaced by a proper set of unitary operators called quantum gates. The advantage of quantum computers is that the complexity class of some computational problems, like the aforementioned simulation problem, is lowered respect to classical ones. The complexity class of a computational problem is the request of resource in terms of space and time to solve it increasing the length of the input. As we have seen, the simulation of a quantum systems on a classical computer requires an amount of resources that grows exponentially with the system length L. So that, this problem belong to the complexity class $O(\exp(L))$. On the other hand, to simulate a quantum system on a quantum computer become a computational problem belonging to the polynomial complexity class $O(L^k)$, for some power k. After this general description of the quantum computing framework, it is the time to explore more deeply the physical principles on which it is based on.

3.4.1 Quantum bits and quantum gates

As we said before, a qubit is a two level quantum system whose states are a linear combination of the "off" state $|0\rangle$ and the "on" state $|1\rangle$ expressed in the following way:

$$|\psi\rangle = \alpha\,|0\rangle + \beta\,|1\rangle \tag{3.70}$$

where α and β respect the relation:

$$|\alpha|^2 + |\beta|^2 = 1 \tag{3.71}$$

The basis $|0\rangle$, $|1\rangle$ we used is also called computational basis of the qubit Hilbert space $\mathcal{H}_q$. The equation (3.71) describes a sphere of unitary radius in the complex variables $|\alpha|$ and $|\beta|$. It follows that can be parametrized by two angular coordinates θ and ϕ. This construction is made up to a global phase that does not matters because cannot be measured. Using the spherical coordinates the (3.71) can be written as:

$$|\psi\rangle = \cos\left(\theta/2\right)|0\rangle + \exp\left(i\phi\right)\sin\left(\theta/2\right)|1\rangle \tag{3.72}$$

Using this parametrization also can be done a graphical representation called "Block sphere" 3.7, in which every point on that sphere corresponds to a certain state of our qbit.

As far is concerned operators on a quantum computer, are tensorial products of Pauli matrices belonging to different qubits. Among all possible operators of a L-qubits quantum computer, only a small subset of them is necessary to perform a quantum simulation. This subset is called a universal set of quantum gates. It is not unique and the number of its components can also vary. It is simply a basis

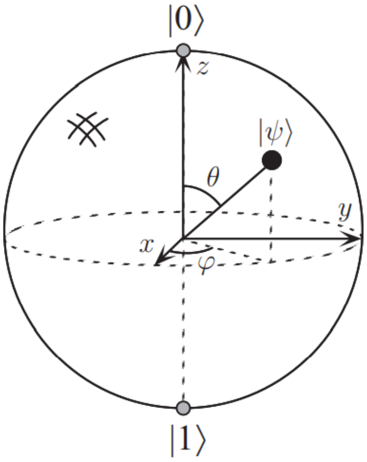

Figure 3.7: Here we can see the Bloch sphere with the two angular coordinates that identify uniquely the state. Picture taken from [35]

of operators that allows to write all the others operators as their composition, but not exactly. In fact, every operator can be written as their composition with arbitrary great precision. The effective choice of the universal set actually depends on the architecture of the quantum computer. In fact, qubits can be obtined from different phisical systems, for example from polarized photons, from two level atoms or from spin $\frac{1}{2}$ particles like electrons. Up to the kind of phisical system used can be simpler to apply a quantum gate rather than another. The most single-qbit common gates used in quantum computing are the Pauli matrices:

$$\sigma_x = \begin{pmatrix} 0 & 1 \\ 1 & 0 \end{pmatrix} \quad \sigma_y = \begin{pmatrix} 0 & -i \\ i & 0 \end{pmatrix} \quad \sigma_z = \begin{pmatrix} 1 & 0 \\ 0 & -1 \end{pmatrix} \tag{3.73}$$

The action of σ^x is that of changing the state of the qubit, σ^y do the same adding a phase $\pm i$ up to the initial state of the qbit while σ^z add a phase leaving unchanged the state of the qbit. Over these three gates there are three others commonly used:

$$H = \frac{1}{\sqrt{2}} \begin{pmatrix} 1 & 1 \\ 1 & 1 \end{pmatrix} \quad S = \begin{pmatrix} 1 & 0 \\ 0 & i \end{pmatrix} \quad T = \begin{pmatrix} 1 & 0 \\ 0 & \exp\left(\frac{i\pi}{4}\right) \end{pmatrix} \tag{3.74}$$

The first gate is called Hadamard gate and has the porperty to pass from the basis of σ^z to that of σ^x. The other two gates add a phase on the qbit if it is on the state $|0\rangle$. In the end the last three operators used are those defined in this way: $R_x(\theta) = \exp\left(-i\theta\sigma^x/2\right)$, $R_y(\theta) = \exp\left(-i\theta\sigma^y/2\right)$ and $R_z(\theta) = \exp\left(-i\theta\sigma^z/2\right)$. These are nothing but the respective complex rotations around the three axis of the unitary block sphere. As far is concerned the two qbits gates we can mention the following two gates:

$$\text{CNOT} = \begin{pmatrix} 1 & 0 & 0 & 0 \\ 0 & 1 & 0 & 0 \\ 0 & 0 & 0 & 1 \\ 0 & 0 & 1 & 0 \end{pmatrix} \quad \text{SWAP} = \begin{pmatrix} 1 & 0 & 0 & 0 \\ 0 & 0 & 1 & 0 \\ 0 & 1 & 0 & 0 \\ 0 & 0 & 0 & 1 \end{pmatrix} \tag{3.75}$$

Their effect can be summarized in the following way: CNOT stays for Controlled NOT and exchange the state of the second qbit if the second is set to $|0\rangle$, while the swap gate exchange the state of the two qbits. The CNOT gate belong to the greater set of controlled gates and can be generalized to the controlled application of every unitary gate.

3.4.2 Quantum simulations of fermionic systems

Coming back to fermionic systems, we must pass necessarily through our transformations to write fermionic operators in terms of quantum gates. In fact, simulations performed on a quantum computer are divided in two kinds: "analogic" and "digital". The first kind is referred to simulations of a two state systems like the computer itself. The second, instead, is referred to all the others quantum systems and needs a coding to be simulated. In this scope the role of our transformations is relevant. Roughly speaking, performing a digital quantum simulation means taking a quantum system and transform it such that its operators, is written in terms of quantum gates. One use, for example, is that of performing a time evolution of our fermionic system. In this case, the steps to follow are these:

- Apply Jordan-Wigner or Bravy-Kitaev transformations to our fermionic Hamiltonian. After that our Hamiltonian will be a sum of string of Pauli matrices
- Approximate the time evolution operator. It that has the form $\hat{U} = e^{\frac{-i\hat{H}t}{\hbar}}$, and some problems can arise because most of times our Hamiltonian contains terms that not commute. To avoid this is used the Trotter formula, an approximation of the exact exponential. Given two non commuting terms $\hat{A}$ and $\hat{B}$, the formula turn out to be that written in (3.76).

  $$\hat{U}(t) = e^{i(\hat{A}+\hat{B})t} = \lim_{n\to+\infty}\left(e^{i\frac{\hat{A}t}{n}}e^{i\frac{\hat{B}t}{n}}\right)^n \tag{3.76}$$

  This formula allows to approximate the entire evolution in the time interval $[0,t]$ iterating the same term n times to obtain an arbitrary precision.
- The last task is to compute explicitly the exponential of the single term of the Trotter evolution. The result of this step give us the corresponding part

of quantum circuit. In this last part is crucial the set of universal quantum gates we want to use, because the result have to be expressed only using those specific quantum gates.

3.4.3 Comparison between Bravy-Kitaev and Jordan-Wigner

Now, knowing how the quantum simulation works, we can talk about our transformations in terms of computational efficiency. Nowadays, the computational power of quantum computers is very low respect to their potentiality. Especially, there are problems with decoerences and also an order of magnitude of $\sim 10^2$ gates can be difficult to implement. To exploit them at maximum, every means can be useful. One of them is the coding between fermionic ladder operators and Pauli matrices. It is so, because a less number of Pauli matrices in the Hamiltonian means immediately a less number of quantum gates. So we can make a count of the complexity class of this problem up to our different algorithms:

- Jordan-Wigner transformations: as we have seen there is a chain of σ^z plus a $\sigma^{\pm}$. Potentially, the total chain can be long n if i have to act on the last site, so it belongs to $O(n)$. This is due to the fact that while the occupation is stored locally, the parity is not

- Parity transformations: in these transformations there is exactly the opposite situation, the parity is stored locally while the occupation not. The chain of σ^x needed to update the parity makes these transformations belong to $O(n)$ too.

- Bravy-Kitaev transformations: here the situation is different because the length of both the update and parity set scale as $O(log(n))$. This is mathematically shown in [22]. The difference is that, respect to Jordan-Wigner, the occupation of sites up to site j is no longer stored in a single qubit and we no longer need to check the parity of all the qubits with index less than j, but only those that store the parity of the site j. On the contrary, respect to Parity transformations, the parity of occupied sites up to site j is no longer stored in a single qubit and we no longer need to update all the qubits with index greater than j, but only those that store partial sums which include occupation number j

As we have seen, the quantum simulation needs tools like Bravy-Kitaev transformations to be implemented, especially if we refer to the efficiency of the transformations in terms of quantum circuits length. The discussion can be deepened, for example applying it in the computing of the value of the ground state energy of atomic orbitals. In [23] is done an explicit comparison between Barvy-Kitaev and

Jordan-Wigner in terms of number quantum gates used in the quantum circuit and is shown that the first kind of transformations generally outperforms the second one.

Conclusions

Conclusions and outlook

In this work we study an extension of the Aubry-André model with a superconducting term. We derive a duality transformation that allows us to obtain an analytic form of the phase transition lines. Another consistent part of our original work is based on numerical simulations. We detect the many-body localization by computing physical quantities such as the imbalance, the fidelity and the IPR. Moreover, we propose a weighted IPR as a new indicator for the many-body localization.

The topics of our work that can be studied more deeply are the following. Firstly, the critical lines that we obtained by using the duality transformations could be tested by implementing numerical simulations that probe the physics in the thermodynamic limit. Then, we can study the origin of the discrepancy between the weighted IPR and the evolved IPR to establish the validity of our quantity as a detector of localization.

Bibliography

[1] R. Nandkishore and D. A. Huse, Many-Body Localization and Thermalization in Quantum Statistical Mechanics, *Annual Review of Condensed Matter Physics* **6** 15 (2015).

[2] E. Altman and R. Vosk, Universal Dynamics and Renormalization in Many-Body-Localized Systems, *Annual Review of Condensed Matter Physics* **6** 383 (2015).

[3] D. A. Abanin and Z. Papić, Recent progress in many-body localization, *Annalen der Physik* **529** 1700169 (2017).

[4] F. Alet and N. Laflorencie, Many-body localization: An introduction and selected topics, *Comptes Rendus Physique* **19** 498 (2018).

[5] M. Srednicki, Chaos and quantum thermalization, *Phys. Rev. E* **50** 888 (1994).

[6] T. Kinoshita, T. Wenger, and D. S. Weiss, A quantum Newton's cradle, *Nature* **440** 900 (2006).

[7] M. Rigol, V. Dunjko, and M. Olshanii, Thermalization and its mechanism for generic isolated quantum systems, *Nature* **452** 854 (2008).

[8] J. Biddle and S. Das Sarma, Predicted Mobility Edges in One-Dimensional Incommensurate Optical Lattices: An Exactly Solvable Model of Anderson Localization, *Physical Review Letters* **104** (2010).

[9] P. W. Anderson, Absence of Diffusion in Certain Random Lattices, *Phys. Rev.* **109** 1492 (1958).

[10] S. Das Sarma, A. Kobayashi, and R. E. Prange, Proposed Experimental Realization of Anderson Localization in Random and Incommensurate Artificially Layered Systems, *Phys. Rev. Lett.* **56** 1280 (1986).

[11] M. Schreiber, S. S. Hodgman, P. Bordia, H. P. Lüschen, M. H. Fischer, R. Vosk, E. Altman, U. Schneider, and I. Bloch, Observation of many-body localization of interacting fermions in a quasirandom optical lattice, *Science* **349** 842 (2015).

[12] J. Smith, A. Lee, P. Richerme, B. Neyenhuis, P. W. Hess, P. Hauke, M. Heyl, D. A. Huse, and C. Monroe, Many-body localization in a quantum simulator with programmable random disorder, *Nature Physics* **12** 907 (2016).

[13] B. Bauer and C. Nayak, Area laws in a many-body localized state and its implications for topological order, *Journal of Statistical Mechanics: Theory and Experiment* **2013** P09005 (2013).

[14] S. Choi, N. Y. Yao, S. Gopalakrishnan, and M. D. Lukin, *Quantum Control of Many-body Localized States*, 2015, arXiv: `1508.06992 [quant-ph]`.

[15] B. Bauer and C. Nayak, Analyzing Many-Body Localization with a Quantum Computer, *Physical Review X* **4** (2014).

[16] K. Agarwal, S. Gopalakrishnan, M. Knap, M. Müller, and E. Demler, Anomalous Diffusion and Griffiths Effects Near the Many-Body Localization Transition, *Physical Review Letters* **114** (2015).

[17] A. C. Potter and R. Vasseur, Symmetry constraints on many-body localization, *Physical Review B* **94** (2016).

[18] J. Wang, X.-J. Liu, G. Xianlong, and H. Hu, Phase diagram of a non-Abelian Aubry-André-Harper model withp-wave superfluidity, *Physical Review B* **93** (2016).

[19] Y. Bar Lev, G. Cohen, and D. R. Reichman, Absence of Diffusion in an Interacting System of Spinless Fermions on a One-Dimensional Disordered Lattice, *Physical Review Letters* **114** (2015).

[20] S. Aubry and G. Andrè, Analyticity breaking and Anderson localization in incommensurate lattices, *Ann. Israel Phys. Soc.* **3** 133 (1980).

[21] J. Biddle, D. J. Priour, B. Wang, and S. Das Sarma, Localization in one-dimensional lattices with non-nearest-neighbor hopping: Generalized Anderson and Aubry-André models, *Physical Review B* **83** (2011).

[22] S. B. Bravyi and A. Y. Kitaev, Fermionic Quantum Computation, *Annals of Physics* **298** 210 (2002).

[23] A. Tranter, P. J. Love, F. Mintert, and P. V. Coveney, A Comparison of the Bravyi–Kitaev and Jordan–Wigner Transformations for the Quantum Simulation of Quantum Chemistry, *Journal of Chemical Theory and Computation* **14** 5617 (2018).

[24] P. Bordia, H. Lüschen, U. Schneider, M. Knap, and I. Bloch, Periodically Driving a Many-Body Localized Quantum System, *Nature Physics* **13** (2016).

[25] D. Basko, I. Aleiner, and B. Altshuler, Metal–insulator transition in a weakly interacting many-electron system with localized single-particle states, *Annals of Physics* **321** 1126 (2006).

[26] S. M. Girvin and K. Yang. Modern Condensed Matter Physics. (Cambridge University Press, 2019).

[27] E. J. Heller, Bound-State Eigenfunctions of Classically Chaotic Hamiltonian Systems: Scars of Periodic Orbits, *Phys. Rev. Lett.* **53** 1515 (1984).

[28] C. J. Turner, A. A. Michailidis, D. A. Abanin, M. Serbyn, and Z. Papić, Quantum scarred eigenstates in a Rydberg atom chain: Entanglement, breakdown of thermalization, and stability to perturbations, *Physical Review B* **98** (2018).

[29] X. Tong, Y.-M. Meng, X. Jiang, C. Lee, G. D. d. M. Neto, and G. Xianlong, Dynamics of a quantum phase transition in the Aubry-André-Harper model with p -wave superconductivity, *Physical Review B* **103** (2021).

[30] X. Cai, L.-J. Lang, S. Chen, and Y. Wang, Topological superconductor to Anderson localization transition in one-dimensional incommensurate lattices, *Physical review letters* **110** 176403 (2013).

[31] X. Cai, L.-J. Lang, S. Chen, and Y. Wang, Topological Superconductor to Anderson Localization Transition in One-Dimensional Incommensurate Lattices, *Physical Review Letters* **110** (2013).

[32] P. Jordan and E. Wigner, Über das Paulische Äquivalenzverbot, *Zeitschrift für Physik* **47** 631 (1928).

[33] J. T. Seeley, M. J. Richard, and P. J. Love, The Bravyi-Kitaev transformation for quantum computation of electronic structure, *The Journal of Chemical Physics* **137** 224109 (2012).

[34] R. P. Feynman, Simulating physics with computers, *International journal of theoretical physics* **21** 467 (1982).

[35] M. A. Nielsen and I. L. Chuang. Quantum Computation and Quantum Information: 10th Anniversary Edition. 10th, (Cambridge University Press, USA, 2011).